

Study on Vibration Acceleration Distribution Inside Micro/Nano Satellites for Environment Test Standardization

| | |
|--------|---|
| 著者 | Amgalanbat Batsuren |
| year | 2014 |
| 学位授与年度 | 平成26年度 |
| 学位授与番号 | 17104甲工第373号 |
| URL | http://hdl.handle.net/10228/5317 |

DISSERTATION

STUDY ON VIBRATION ACCELERATION DISTRIBUTION INSIDE
MICRO/NANO SATELLITES FOR ENVIRONMENT TEST STANDARDIZATION

SUBMITTED

IN PARTIAL FULFILLMENT OF THE REQUIREMENTS

FOR THE DEGREE OF
DOCTOR OF ENGINEERING

BY

AMGALANBAT BATSUREN

SUPERVISED BY

PROFESSOR MENGU CHO

DEPARTMENT OF APPLIED SCIENCE FOR INTEGRATED SYSTEM
ENGINEERING

KYUSHU INSTITUTE OF TECHNOLOGY

2014

STUDY ON VIBRATION ACCELERATION DISTRIBUTION INSIDE
MICRO/NANO SATELLITES FOR ENVIRONMENT TEST STANDARDIZATION

By

Amgalanbat Batsuren

(Student Number: 11590906)

Supervisor:

Professor Mengu Cho

Member of Dissertation committee:

Professor Mengu Cho

Professor Yasuhiro Akahoshi

Professor Kazuhiro Toyoda

Professor Keiichi Okuyama

Professor Kenichi Asami

Kyushu Institute of Technology

Department of Applied Science and Integrated System Engineering

TABLE OF CONTENTS

| | |
|---|------------|
| <i>Contents</i> | <i>i</i> |
| <i>Nomenclature</i> | <i>iii</i> |
| <i>Abbreviations</i> | <i>iv</i> |
| <i>List of Figures</i> | <i>v</i> |
| <i>List of Tables</i> | <i>vii</i> |
| <i>Executive Summary</i> | <i>x</i> |
| <i>Acknowledgements</i> | <i>xv</i> |
| | |
| 1. Introduction | 1 |
| 1.1 Background of Study | 1 |
| 1.2 Literature review | 3 |
| 1.2.1 Prediction techniques and analysis | 3 |
| 1.2.2 Vibration acceleration distribution | 6 |
| 1.3 Purpose of the study | 7 |
| 1.4 Scope of thesis | 8 |
| 2. Experiment | 9 |
| 2.1 Test articles | 9 |
| 2.2 Test settings | 13 |
| 2.3 Test procedure | 15 |

| | |
|--|-----------|
| 2.4 Experimental results and discussion | 19 |
| 2.4.1 Experiment data statistics | 24 |
| 2.4.2 Derivation of Unit QT based on the experiment results | 30 |
| 3. Analysis | 39 |
| 3.1 Analysis model | 40 |
| 3.2 Analysis modelling and settings | 44 |
| 4. Results and Discussion | 49 |
| 4.1 Analysis results and discussion | 49 |
| 4.1.1 Analysis results of dummy satellite | 49 |
| 4.1.2 Comparison between experiment and analytical results | 52 |
| 4.1.3 Analysis results of other types of satellites and their statistics | 57 |
| 4.2 Derivation of unit QT conditions | 65 |
| 5. Conclusions and Future work | 70 |
| 5.1 Conclusions | 70 |
| 5.2 Future work | 72 |
| References | 73 |
| Appendix | 75 |

Nomenclature

| | |
|-------------|--------------------|
| f : | base frequency |
| f_0 : | resonant frequency |
| ζ : | damping rate |
| n : | sample number |
| κ : | frequency rate |
| s_y : | standard deviation |
| t : | transmittance |
| \bar{y} : | average of sample |
| Q : | Q factor |

Abbreviations

| | |
|----------------|---|
| AT : | Acceptance test |
| DM: | Dummy mass |
| DOF(s): | Degree(s) of freedom |
| OBC: | On Board Computer |
| PAF: | Payload Adapter Fitting |
| PCU: | Power Control Unit |
| PFT: | Proto-Flight Test |
| PSD: | Power Spectral Density |
| RF: | Radio Frequency |
| RMS: | Root Mean Square |
| MEE: | Maximum Expected Environment |
| NTL: | Normal Tolerance Limit |
| NETS: | Nano satellite Environment Test Standardization |
| QT: | Qualification Test |

List of Figures

Figure 1.2.1: Simplified structure of analysis process

Figure 1.2.2: Flight test data of twelve measured points

Figure 2.1.1: Structure of the dummy satellite bus.

Figure 2.1.2: Photo of Hodoyoshi-3 satellite and internal panel structure

Figure 2.1.3: Picture of other satellites

Figure 2.2.1: Overview of the units and accelerometer positions on the dummy satellite (+X internal panel).

Figure 2.2.2: The test equipment diagram.

Figure. 2.2.3: Mounting position of base accelerometers on the jig.

Figure 2.3.1: Vibration profile of dummy satellite

Figure 2.3.2: Vibration profile of Hodoyoshi-3

Figure 2.3.3: The view of attachment of the accelerometers

Figure 2.4.1: PSD Waveform of the dummy satellite

Figure 2.4.2: Peak amplification factor comparison.

Figure 2.4.3: Vibration response at internal panel

Figure 2.4.4: Probability distribution (normal).

Figure 2.4.5: Transmittance (τ) against frequency ratio (κ).

Figure 2.4.6: The amplification factor and resonance frequency range for unit
QT test level (20-2000Hz).

Figure 2.4.7: Unit QT level (20-2000Hz).

Figure 3.1.1: Basic types of micro/nano satellite structures.

Figure 3.1.2: Center of Gravity of dummy satellite model

Figure 3.1.3: Center of Gravity of Pi type model

Figure 3.1.4: Center of Gravity of T type model

Figure 3.2.1: Finite element model of the dummy satellite

Figure 3.2.2: Main structure view

Figure 3.2.3: Finite element model of the PAF and Jig.

Figure 3.2.4: Virtual sensor position

Figure 4.1.1: Example of test and analysis result comparison(1Grms, horizontal)

Figure 4.1.2: Peak amplification factor and resonant frequency (T-type, horizontal1)

Figure 4.1.3: Peak amplification factor and resonant frequency (T-type, horizontal2)

Figure 4.1.4: Peak amplification factor and resonant frequency (T-type, vertical)

Figure 4.1.5: Peak amplification factor and resonant frequency (Pi-type, horizontal1)

Figure 4.1.6: Peak amplification factor and resonant frequency (Pi-type, horizontal2)

Figure 4.1.7: Peak amplification factor and resonant frequency (Pi-type, vertical)

List of Tables

Table 2.3.1: Vibration testing system specification

Table 2.4.1: Resonant frequency statistics (dummy satellite, 300-1000Hz).

Table 2.4.2: Peak value of amplification factor (dummy satellite, 300- 1000Hz).

Table 2.4.3: Resonant frequency range (dummy satellite, 300-1000Hz).

Table 2.4.4: Normal tolerance limit of amplification factor in logarithm of the
dummy satellite in the range: 300-1000Hz (real values are
shown in bracket).

Table 2.4.5: Resonant frequency range (dummy satellite, 1000-2000Hz).

Table 2.4.6: Normal tolerance limit of amplification factor in logarithm of the
dummy satellite in the range: 1000-2000Hz (real values are
shown in bracket).

Table 2.4.7: Resonant frequency range (Hodoyoshi-3, 300-1000Hz).

Table 2.4.8: Normal tolerance limit of amplification factor in logarithm of the
Hodoyoshi-3 satellite in the range: 300-1000Hz (real values are shown
in bracket).

Table 2.4.9: Resonant frequency range (Hodoyoshi-3, 1000-2000Hz).

Table 2.4.10: Normal tolerance limit of amplification factor in logarithm of the
Hodoyoshi-3 satellite in the range: 1000-2000Hz (real values are shown
in bracket).

Table 2.4.11: Resonant frequency range (dummy satellite, 20-300Hz).

Table 2.4.12: Normal tolerance limit of amplification factor in logarithm of the dummy satellite in the range: 20-300Hz.

Table 2.4.13: Resonant frequency of each satellite (20-300Hz).

Table 2.4.14: Amplification factor of each satellite (20-300Hz).

Table 2.4.15: Resonant frequency range (20-300Hz).

Table 2.4.16: Normal tolerance limit of amplification factor in logarithm in the range:
20-300Hz (real values are shown in bracket).

Table 3.2.1: Summary of the dummy satellite FE model.

Table 3.2.2: Summary of the T-type structure FE model.

Table 3.2.3: Summary of the Pi-type structure FE model.

Table 4.1.1: Peak Amplification factor and resonant frequency statistics of Dummy
satellite (horizontal1)

Table 4.1.2: Peak Amplification factor and resonant frequency statistics of Dummy
satellite(horizontal2)

Table 4.1.3 Peak Amplification factor and Resonant frequency statistics of Dummy
satellite(vertical)

Table 4.1.4: Comparison of Amplification factor and resonant frequency
(20-100Hz)

Table 4.1.5: Comparison of Amplification factor and resonant frequency
(100-200Hz).

Table 4.1.6: Comparison of Amplification factor and resonant frequency

(200-300Hz)

Table 4.1.7: Peak Amplification factor and Resonant frequency statistics of T-type

structure (horizontal1)

Table 4.1.8: Peak Amplification factor and Resonant frequency statistics of T-type

structure (horizontal2).

Table 4.1.9: Peak Amplification factor and Resonant frequency statistics of T-type

structure (vertical)

Table 4.1.10: Peak Amplification factor and Resonant frequency statistics of Pi-type

structure (horizontal1)

Table 4.1.11: Peak Amplification factor and Resonant frequency statistics of Pi-type

structure (horizontal2)

Table 4.1.13: Peak amplification factor and resonant frequency of top sensor

Table 4.2.1: Resonant frequency range of T-type (20-300Hz).

Table 4.2.2: Normal tolerance limit of amplification factor of T type (20-300Hz).

Table 4.2.3: Resonant frequency range of Pi-type.(20-300Hz)

Table 4.2.4: Normal tolerance limit of amplification factor of Pi type.(20-300Hz)

Table 4.2.5: Resonant frequency range of Pi type (20-300Hz)

Table 4.2.6: Normal tolerance limit of amplification factor of Pi type (20-300Hz)

Table 4.2.7: Overall statistics of experiment and analysis

Executive Summary

The thesis is composed of five chapters. The first chapter introduces background and literature survey. The second chapter describes the experiment. The third part describes the analysis, the fourth chapter describes results and discussion and in the last the chapter overall research was concluded.

Chapter 1: Introduction

In Chapter 1 of this thesis, it is reviewing about research background and literature research about vibration testing. At present, a large level of acceleration is applied to satellite units during the test, which has been derived by taking into account various safety margins. The bases of the margins are not always clear. At the same time, there are many COTS-based units in the market, which are claimed to be good for micro/nano satellites. Those products often however lack of test history under which they are qualified for the space use. Satellite developers are caught in the middle whether they choose an expensive and long-delivery product weighing more emphasis on the reliability or choose the COTS-based product taking the risk of having a product that may not work in space. Currently there is no such standard for micro/nano satellite units. In this regard, there is need to define the qualification test (QT) level the units have to pass to be sold as products for space use.

Based on the literature study and identification of the problems associated with micro/nano satellite vibration testing, the authors set the aim of the thesis to define unit

Qualification test (QT) level for micro/nano satellites and to extrapolate the findings to other types of small satellites using a Finite element method. Two major issues are addressed in this thesis: vibration acceleration distribution analysis based on experiment and finite element method. These two parts of the work determine the Unit QT level identification of the micro/nano satellite environment testing standard.

Chapter 2: Experiment

Chapter 2 addresses the experiment. Series of random vibration tests using different acceleration ranges up to 9.0Grms with frequencies in the range of 20 to 2000Hz were conducted. The author used experimental results of two satellites, dummy satellite and Hodoyoshi-3 satellite to obtain the acceleration distribution inside the satellites. The dummy satellite is a copy of 50kg-50cm nano-satellite that was previously developed for remote sensing purpose. The dummy satellite was made of basic satellite functions such as RF transmitter, PCU, battery and computer. The other units are made by dummy mass with heater inside the units. Hodoyoshi-3 is also an Earth remote sensing satellite of 50cm/50kg class. The test article used in the present research is its engineering model. Therefore, many of the internal units are still dummy mass. The satellites were fixed to the vibration machine using a mock-up of payload adaptor fitting (PAF) and a jig.

For the dummy satellite, the author measured at 18 points at dummy masses/units that were placed on internal panels. For the whole satellite modes, the vibration test data of six other satellites were used. Those satellites are in the range of 50cm/50kg class.

The resonant frequencies and the amplification factors were identified between 20 and 2,000Hz. Statistically estimating the interval of the resonant frequency range, and

normal tolerance limits (NTL) were derived on the amplification factor. In order to compute a normal tolerance limit, the author followed the same methodology as the NASA standard. Before this the author also examined whether the tested data followed normal or lognormal distributions. After evaluating χ^2 (Chi squared) testing, the lognormal was chosen as the distribution of amplification factor.

The author deduced the vibration test level in the frequency range, 20-300Hz, 300-1,000Hz and 1,000-2,000Hz. Finally the results of three frequency ranges were merged and the unit QT level between 20 and 2000Hz has been derived.

Chapter 3: Analysis

In the Chapter 3, the author has presented about extrapolation to other structures using Finite element Analysis (FEA). The purpose of this analysis was to extend and extrapolate these experimental results for other types of satellite structure by using FEA without laboratory testing. This chapter presents a review of general steps of finite element analysis of vibration acceleration distribution of the dummy satellite structures. The chapter also includes how to divide a satellite body and panels into finite elements and how to select the type of finite elements to represent the overall structure and also details modeling of loading and boundary conditions applied to the satellite structure.

Three basic structure types of 50kg class satellites were modeled and analyzed such as Yojo-han, T-type and Pi-type structure. These three types are mostly used for micro/nano satellite nowadays. A random vibration analysis was carried out for the satellite models. The solid model was created with a mesh size of 10 mm on the internal panels of the satellite structure while the PAF and Jig use a mesh size of 20 mm. The

structures were modelled using shell/mid-surface and beam elements and concentrated masses.

Chapter 4: Results and Discussion

Chapter 4 compares the resonant frequency range and peak amplification factors applied to Simulated and Experimental data. The author made qualitative and quantitative comparison between the experimental results and analysis results of resonant frequencies and amplification in the range 20-300Hz at the certain positions of the satellites and models to check the validity of the dummy satellite's analysis. The comparison carried out shows excellent agreement for 20-100Hz of dummy satellite and good agreement 100-200Hz. The accuracy decreases with increasing frequency beyond 200Hz. Finally the unit QT level is derived.

Chapter 5: Conclusion

This research was concluded in Chapter 5. The author found that there are several vibration modes for micro/nano satellites depending on entire structures and internal panel structure arrangements. Other important achievements obtained in this study are also summarized. Based on the experiment and analysis results, the following specific conclusions can be drawn:

1. The experimental and numerical analyses of this work have both indicated that there are several vibration modes for the satellites, mainly associated with the internal panel structure of the satellites.

2. The finite element modal analysis of the simplified model based on the original CAD drawings of the dummy satellite has introduced amplification peaks and resonant frequencies, both of which are close to the experimental ones. That is expected, the Unit QT level derived from the experiment results is applicable, especially at lower frequency modes. However, the FEA modal analysis may introduce errors if it is used to investigate vibration acceleration response and resonant frequencies associated with local vibration modes beyond 200Hz.

3. Based on the agreement between the analysis and the experiment, the unit QT level for the minimum assurance against random vibration was proposed. As the proposed random vibration amplification factor at frequencies is close to unity at frequencies higher than 200 Hz, the effects associated with the analysis error is minimal.

4. The information gained from the finite element modal analysis and the vibration-waveforms generated both by experiment and analysis can be used to guide small satellite structure developers to the vibration acceleration distribution inside the micro/nano satellites.

5. Knowing the problem at resonant frequencies that can cause higher acceleration at specific points at internal panels where units or components are mounted to the micro/nano satellites, it may become possible to propose a solution to avoid the resonance in satellites by introducing vibration distribution study of the tested and analyzed structures.

Acknowledgement

First of all, I'm deeply grateful to my advisor Prof. Mengu Cho for the continuous support of my PhD study and research during these past three years. I would like to thank you for encouraging my research and for allowing me to grow as a research scientist. To work with you has been a real pleasure to me. I would also thank my thesis committee members, Prof. Yasuhiro Akahoshi, Prof. Kazuhiro Toyoda, Prof. Keiichi Okuyama and Prof. Kenichi Asami for serving as my committee members and for your brilliant comments and suggestions. I would especially like to thank academic and technical staff, Assistant Prof. Hirokazu Masui, Assistant Prof. John Polansky, Assistant Prof. Md. Arifur Khan, Toru Hatamura, Seiji Kawano, Kumiko Shirakawa and Kanae Iyama for their helpful advices, suggestions and all kind of assistance during my study. I'm grateful for the following satellite projects for providing the satellites vibration test data: HODOYOSHI, UNIFORM , RISESAT, RISING2, QSAT-EOS and TSUBAME projects. My sincere thanks also goes to Prof. Kuniaki Shiraki for his encouragement and support and the members of NETS committee for their valuable comments. I'm also indebted to my fellow labmates, DNST and PNST students I had the pleasure to work with. Special thanks to my family: my parents Batkhuu Batsuren, Burentugs Saranchimeg and my younger sisters B.Amgalanchimeg and B.Bayarchimeg for all of the sacrifices that you've made on my behalf. At the end I would like express my deepest appreciation to my beloved wife Gombojav Delgermaa who spent sleepless nights with and was always my support in the moments when there was no one to answer my queries. I would also like to thank my wonderful kids A.Margad, A.Anar and A.Erkhes. I love them so much, and I would not have made this far without them.

Chapter 1: Introduction

1.1 Background of the study

Until now there have been suitable environment test standards for large and medium sized satellites. Besides that taking into consideration of small satellite rapid development trend especially for new comers development of proper environment test standard is essential for micro/nano satellites.

As the uses of micro/nano satellites proliferate all over the world, there is an increasing need of improving their reliability [1]. As the reliability expected for micro/nano satellites are different from that of the large/medium satellites, however, the test level, duration and precision may not be the same as those applied to the testing of large/medium satellites. The existing standards are not suitable for micro/nano satellites that achieve low-cost and fast-delivery by using non-space qualified, Commercial-Off-The-Shelf (COTS) components extensively. The reliability expected for micro/nano satellites is different from that of the large/medium satellites. There is a need of test standard to improve the reliability while keeping the nature of low-cost and fast-delivery. Currently there are confusion about testing approach among developers and customers about how the environment tests should be implemented for micro/nano satellites and their units.

The word “micro/nano-satellite” in this thesis is used for satellites that are mostly made of COTS units. Their weight and size is, but not limited to, typically less than 50kg and 50cm, respectively.

In the present research, the author deals with unit vibration test. At present, a large level of acceleration is applied to satellite units during the test, which has been derived by taking into account various safety margins. The bases of the margins are not always clear.

At the same time, there are many COTS-based units in the market, which are claimed to be good for micro/nano satellites. Those products often however lack of test history under which they are qualified for the space use. Satellite developers are caught in the middle whether they choose an expensive and long-delivery product weighing more emphasis on the reliability or choose the COTS-based product taking the risk of having a product that may not work in space. If the COTS-based product already passed a certain level of testing defined in a standard, the satellite developer may choose the COTS-based units with more confidence. Currently there is no such standard for micro/nano satellite units. One of the purposes of the research is to define the qualification test (QT) level the units have to pass before being sold as products for space use.

The unit QT proposing in the research does not include proper margin against the maximum predicted environment stress, which depends on each satellite. The satellite developers who procure the unit may carry out another QT using a dedicated test model. As long as the unit uses COTS parts, there is a little guarantee that the test model is the same as the flight model. They may carry out PFT using a flight model or only AT taking the risk of little margin. The satellite developer shall provide the test levels and duration of the additional QT, AT or PFT.

1.2 Literature Review

This section gives a concise introduction to existing methods for vibration testing standards, vibration acceleration distribution and analysis for large/medium sized satellites and it provides a list of only most important references.

1.2.1 Prediction techniques and analysis

In recent years, the Finite element method analysis is widely used for prediction of dynamic resonance and model validation for space crafts and vehicles. Finite element analysis used from 1950s and 1960s in aircraft industry [2].

Since 1990s, as the computer performance has been continuously developed, the FEM analysis is widely used predict vibration acceleration distribution inside a satellite. The development of fast digital computers, numerical simulation techniques and measurement technology has led to an increase of these procedures in last decades..

One of the powerful analytical software is Nastran which is originally developed by NASA and commonly used for discrete analyzing of satellite structure nowadays.

There are several methods used for prediction of vibration acceleration. The most commonly-used modelling technique for prediction of the dynamic properties of structures (natural frequencies and mode shapes) and of their response characteristics is that of Finite Element Analysis [3],[4],[5],[6],[7].

A traditional process of predicting the dynamic response from the Payload design stage to final production is shown in Figure 1.2.1.

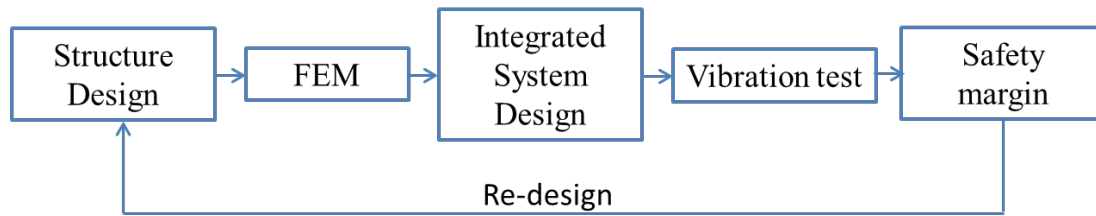


Figure 1.2.1: Simplified structure of analysis process

It can be seen from the Figure 1.2.1 that first initial design of a spacecraft is made, Finite element analysis including dynamic effects is performed and the first prototype is built.

Generally, for the prediction of high frequency response the following procedures are commonly used [8]:

1. Normal Mode Analysis
2. Statistical Energy Analysis (SEA)
3. Finite Element Method (FEM)
4. Extrapolation techniques
5. Direct measurement

From the above procedures, the Finite element method (FEM) and statistical energy analysis method (SEA) have been used for predicting the random vibration loads . The FEM is generally used to compute loads for low frequencies and SEA is used for the high frequency region [9].

FEM analysis is widely used for predicting vibration response up to the frequency of about 50th normal mode. If the structure is precisely modeled or has sufficient number of Degree of freedom, it might be higher.

Information about the prediction of random vibration loads for payload using FEM analysis can be found in the works of Chung et al [10]. They carried out Finite element analysis using MSC/Nastran for vibration prediction for a large aerospace vehicle up to about 150Hz. The random vibration analysis is executed from 0 to 150 Hz at a frequency resolution of 1Hz. The random vibration loads predicted by the finite element approach are compared with those computed by Miles equation. They have found that for the analyzed payloads investigated, the finite element results for random vibration rms acceleration are less than those predicted by Mile's Equation.

There are numerous papers discussed in the open literature FEM analysis has been used for random vibration analysis in a variety of satellite structures. One of the latest example is that Michael et al [9] have studied maximum principal stress from Random analysis based on satellite structure model. They have analyzed up to 400Hz using random input excitation with 3.6Grms. They have compared PSD and Transient response and concluded that matches was good.

Comparison between FEM analysis and direct measurement data is known as "correlation" process. Direct measurement is one of the predictions way and mostly using data attached to a flight vehicle. The prediction techniques and data analyzing is described in [11] and [12].

Condos et al [11] and Piersol [12], are example of works which show vibration response distribution as introduced in next section.

1.2.2 Vibration acceleration distribution

There are test standards on the satellite environment test, those were aimed at traditional large/medium class satellite that demands very high reliability. Test standards always determine maximum expected environment for large/medium sized satellites. Piersol et al [12] have studied vibration acceleration distribution and described maximum structural responses based on the flight data at 12 measurement points. They assumed that for adding some factor to the measured vibration test levels that become Maximum expected environment. These maximum expected environment level makes up point-to-point (spatial) and flight-to-flight variations. This prediction is very conservative relative to the flight environment. They also noted that this maximum expected environment is usually described for acceleration.

They have found that to arrive at a conservative limit is to compute a normal tolerance limit for the predicted spectra. Normal tolerance limits apply only to normally distributed random variables. They also stated that spatial variation of structural responses to stationary, nonstationary, and transient dynamic loads is not normally distributed.

Barrett [13] and Anon [14] have considered about the statistical distribution of vibration data and suggested the distribution for the structural response spectral values in a specific frequency resolution bandwidth fits a lognormal distribution.

The result of these researches [12],[13],[14] were used for NASA standard [8] for the computation of maximum expected environment as shown in Figure 1.2.2.

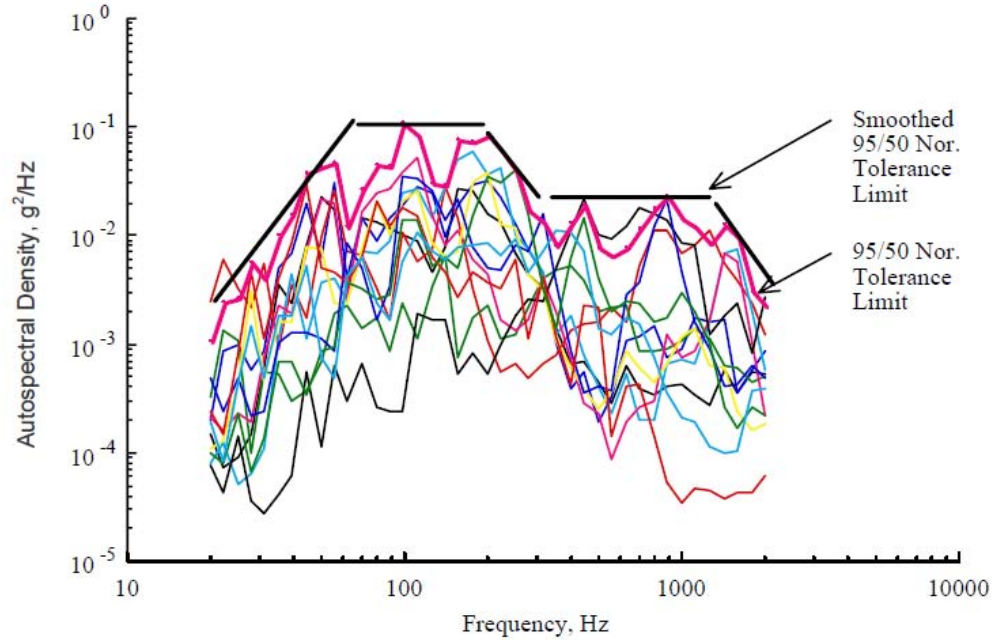


Figure 1.2.2: Flight test data of twelve measured points

(source: Piersol, A. NASA- HDBK-7005 [8])

Based on the above mentioned literature study and identification of the problems associated with micro/nano satellite testing and analysis, the authors set the aim of the thesis to define unit Qualification test (QT) test level for micro/nano satellites and to extrapolate the Unit QT to other types of small satellites using Finite element method.

1.3 Purpose of the study

The author set the aim of the thesis to define unit Qualification test (QT) test level for micro/nano satellites and to extrapolate the findings to other types of small satellites using a Finite element method. Two major issues are addressed in this thesis: vibration

acceleration distribution analysis based on experiment and finite element method. These two parts of the work determine the Unit QT level identification of the micro/nano satellite environment testing standard.

1.4 Scope of the thesis

The existing testing standard is not suitable for micro/nano satellites that achieve low-cost and fast-delivery by using COTS (Commercial off-the-shelf) components extensively. There is no doubt that small satellite industry is an active user of COTS components. These COTS components have no testing history. Therefore, there is a need of basic research to provide the physical basis of the test conditions to be defined in the new micro/nano satellite environment testing standard. The basic research is needed for establishing the qualification test (QT) level a unit has to pass to be sold as a product for space usage.

In order to reach these goals the following needs to be done and forms the basis of research in this thesis. It is necessary to define the minimum test level for micro/nano satellites carrying out the followings:

- 1) The vibration testing system in the Kyushu Institute of Technology is used and that has full capability of testing micro/nano satellites.
- 2) We will conduct series of tests of the 50 cm class dummy satellite to get amplification at various position of the satellite.
- 3) The vibration test data of Engineering Model of Hodoyoshi-3 satellite is used for updating testing results of the dummy satellite.

- 4) In order to cover satellite to satellite variation, we need to carry out computer simulation such as Finite element method. In the research, 3 different simple models are used.
- 5) Finally the Unit QT level to be derived based on the real experiment data of micro satellites and updated with the analysis result of other types of structures.

2. Experiment

2.1 Test article

In this chapter the tested satellites and their data were used in the research are introduced. Two micro/nano satellites were used for the experimental results, Dummy satellite and Hodoyoshi-3 satellite as shown in Fig. 2.1.1 and Fig. 2.1.2 respectively to obtain the acceleration distribution inside the satellites. For the whole satellite modes, we used seven satellites data. The satellites vibration test data used in the research are HODOYOSHI-2&3, UNIFORM, RISESAT, RISING2, QSAT-EOS and TSUBAME as shown in Fig.2.1.3.

The internal structure of the dummy satellite body is made of four panels with two third the width of the satellite body cross linked forming a “Yojo-han (four half tatami)” when viewed from the top, it can be seen as the popular layout of tatamis, Japanese traditional carpet. There is a square column made by the four panels at the center. The internal and external panels are made of Aluminum (alloy:5052). The dummy satellite is a copy of 50kg-50cm nano-satellite that was previously developed for remote sensing purpose as illustrated in Figure 2.1.1 The dummy satellite was made of basic satellite functions such as RF transmitter, PCU, battery and computer. The other units are made by dummy mass with heater inside. The components mentioned above and the satellite structure are of flight quality. The advantage of the Yojo-han satellite is its easiness to install and access the components. Because the structural style is composed of four internal panels and five external panels fixed to each with bolts, however, it may cause

more mechanical stress than other structural styles with a center cylinder and panels. There are more than 100 connection points within the dummy satellite.

Hodoyoshi-3 is also an Earth remote sensing satellite of 50cm/50kg class. The test article used in the research is its engineering model. Therefore, many of the internal units are still dummy mass. The basic structure of Hodoyoshi-3 satellite is a cube, to which two internal panels are fixed look like T shape from the top to mount different components as illustrated in Figure 2.1.2. Two deployable solar panels attached to the satellite by a simple and reliable hold-release mechanism i.e. latch-able hinge. In the present research, the test data are obtained during its random vibration test was used.

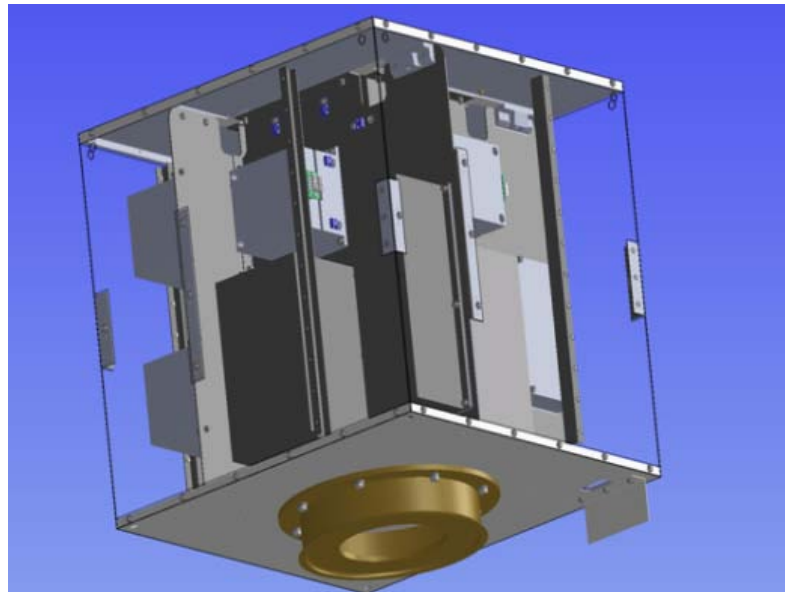


Figure 2.1.1: Structure of the dummy satellite bus.

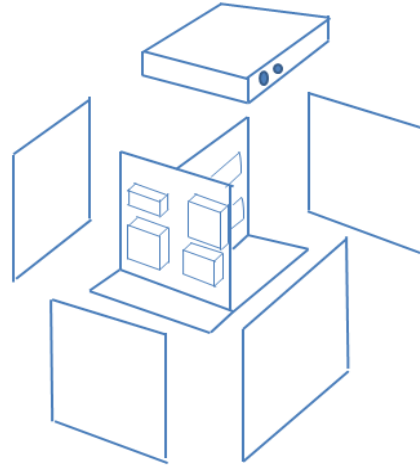
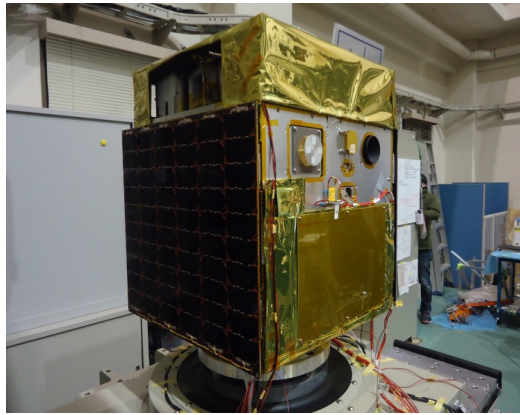


Figure 2.1.2: Photo of Hodoyoshi-3 satellite and internal panel structure.

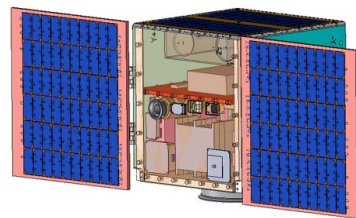
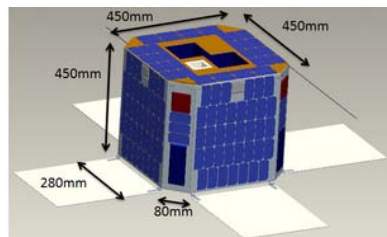
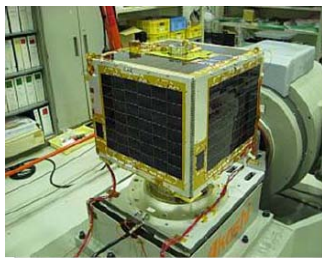
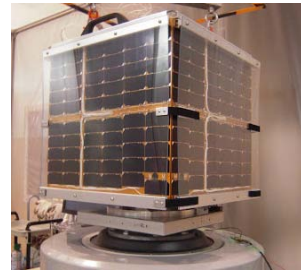
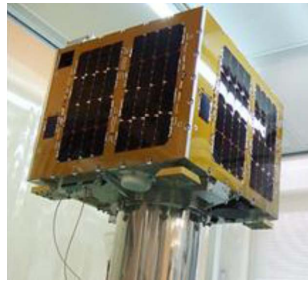
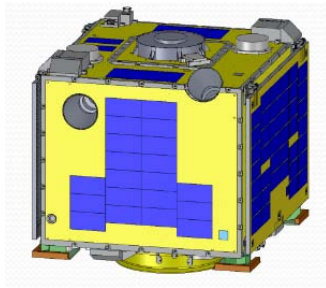


Figure 2.1.3: Picture of other satellites.

2.2 Test settings

Accelerometers were attached inside the satellite and studied the distribution of mechanical stress inside the satellite. The satellite was fixed to the vibration machine using a mock-up of payload adaptor fitting (PAF) and a jig. The experiment was conducted by a shaker machine capable of 28kN rms random vibrations. For the dummy satellite, totally 46 points were measured in the experiment. Among the 46 points, 18 points were at dummy masses/units that were placed on internal panels. Figure 2.2.1 shows some of the accelerometer positions. The accelerometers were attached to the internal panels of the satellite rather than the unit boxes. It is because the acceleration used for reference in the unit vibration test should be the ones of the base plate, i.e. the satellite internal panel. For Hodoyoshi-3 satellite, the accelerometers data at 8 positions were used of inside panels. The measurement and analyzing philosophy of the Hodoyoshi-3 is similar to the dummy satellite.

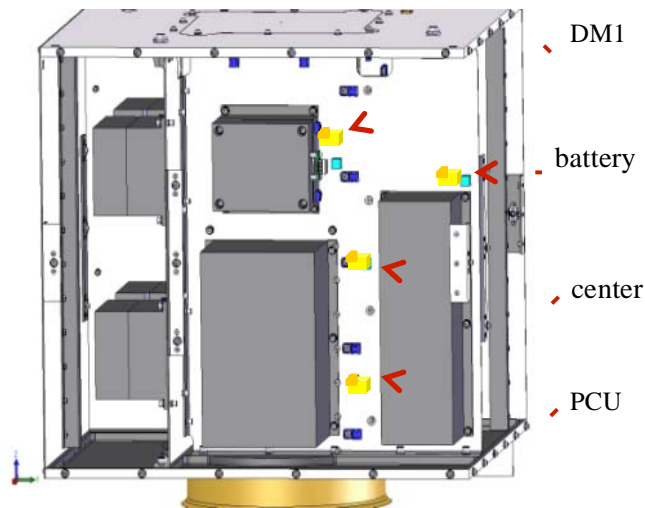


Figure 2.2.1: Overview of the units and accelerometer positions on the dummy satellite (+X internal panel).

The maximum of 24 channels of the analog signal with the range of $\pm 10V$ from the charge amplifier was taken simultaneously and converted to digital signal at 16 bit DAQ (5000 samples). Fast Fourier Transform (FFT) was applied by a standard desktop PC using Labview as shown in Figure 2.2.2.

Each accelerometer (manufacturer: EMIC Corp., model: 710-C) was connected to a charge amplifier (manufacturer: SHOWA SOKKI Corp., model: Showa 4035). The data was taken through DAQ (manufacturer: National Instruments, model: NI CDAQ-9178) to a PC with USB cable.

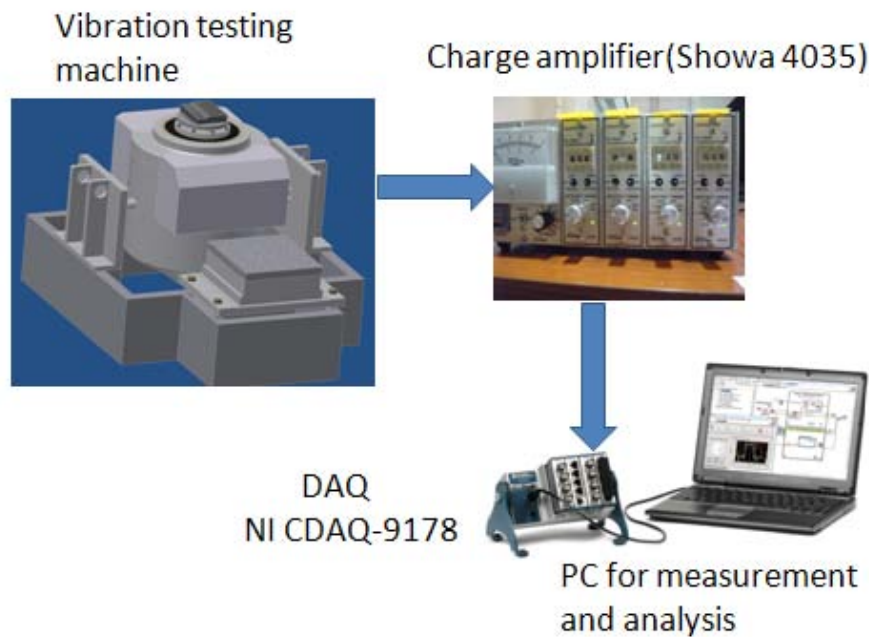


Figure 2.2.2: The test equipment diagram.

In the test, the vibration level was controlled by monitoring the average of two mono-axial accelerometers (control accelerometer) attached rigidly on the jig aligned with the axis of applied vibration to check the input signal and taking the average of them (Figure

2.2.3). Base accelerometers (ch23, ch24) for calculating amplification ratio were mounted besides the control accelerometers.

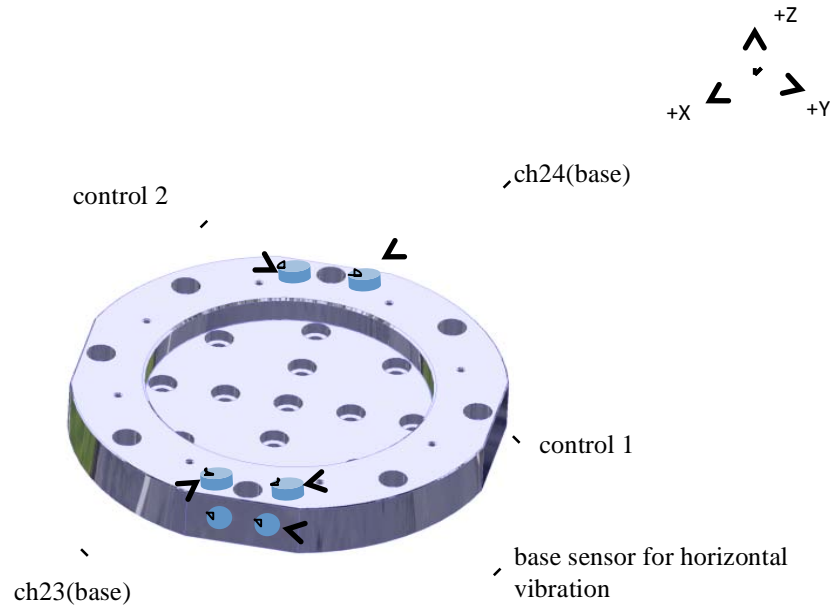


Figure. 2.2.3: Mounting position of base accelerometers on the jig.

2.3 Test procedure

Vibration tests were performed along the X, Y and Z satellite axes. Testing along the Z axis (parallel to the launcher axis) was performed mounting the satellite on the shaker using the jig. The same shaker and support, connected to the horizontal vibration table, were used for the X and Y axes vibration test (transverse vibration).

The base acceleration levels are shown in Figs. 2.3.1 and 2.3.2. For the Dummy satellite, the shape of input level comes from the Space and Missile Systems Center Standard (SMC) [15]. Using the same shape as shown in Fig. 2.3.1, the level was shifted

so that we could test 5 levels, i.e. 0.3 Grms, 1 Grms, 3 Grms, 6 Grms and 9 Grms. The test started from 0.3 Grms toward 1.0Grms and 9.0Grms at the end. Each vibration was applied for 50 seconds. For Hodoyoshi-3, the base acceleration is based on the system QT level of 6.2 Grms specified by a launch provider as shown in Fig. 2.3.2. Each vibration test was also applied for 50 seconds.

In order to derive the vibration response at each point in the satellites, the author selected random vibration, instead of sinusoidal sweep due to two reasons. The first one is that the random vibration contains all the frequencies. Therefore, it is easy to derive the frequency response after carrying out the Fourier transform. The second is that the unit QT test to be carried out is random vibration test rather than sinusoidal sweep test.

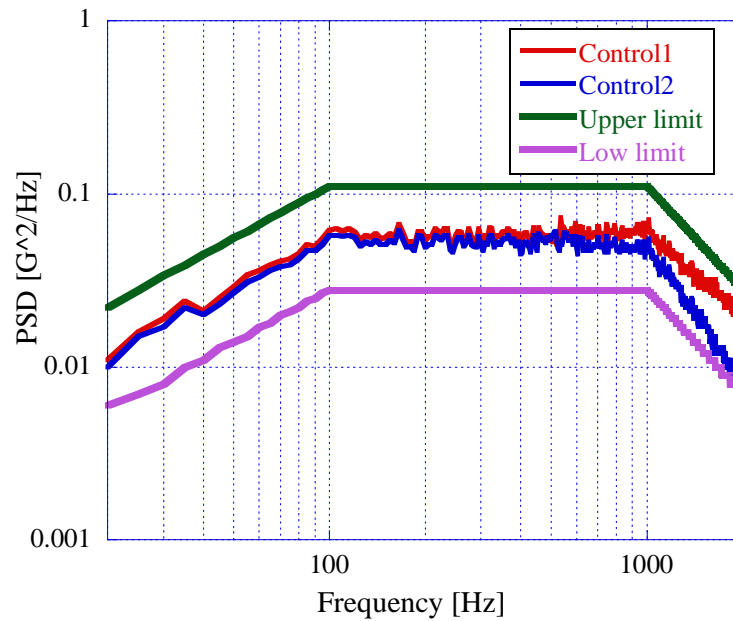


Figure 2.3.1: Vibration profile of dummy satellite.

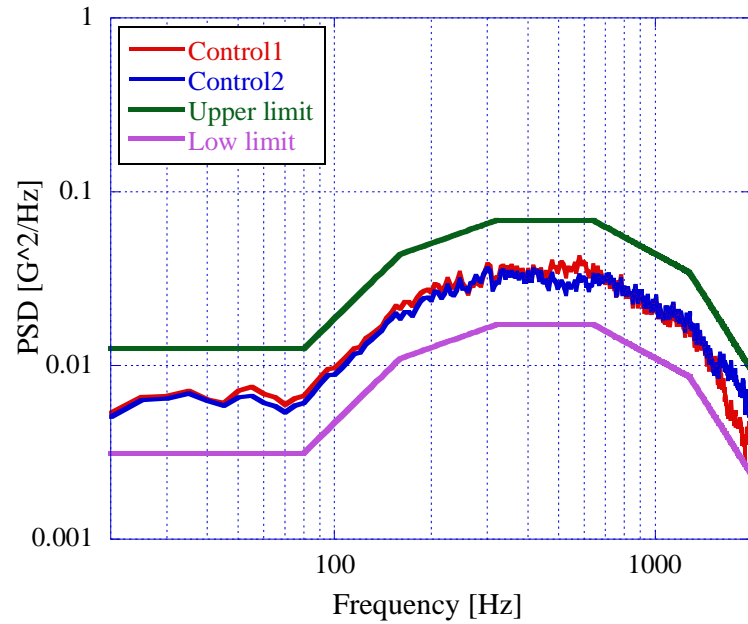


Figure 2.3.2: Vibration profile of Hodoyoshi-3.

After each vibration, the author checked the characteristic changes by performing a low level random, i.e. 0.3Grms to check if there are no changes for natural frequency etc.

Table 2.3.1: Vibration testing system specification.

| No. | Items | Specification | | |
|-----|---------------------------------|--------------------------------|-------|--------------------|
| 1 | Type | F-35000BD/LA36AP(made by EMIC) | | |
| 2 | Exciting Force | Sine | | 35.0kN |
| | | Random | | 28.0kN |
| | | Shock | | 87.5kN |
| 3 | No-load maximum acceleration | Vertical | Sine | 1060.0 m/s^2 |
| | | | Shock | 1470.0 m/s^2 (0-p) |
| | | Horizontal | Sine | 460.5m/s^2 |
| | | | Shock | 1151.3 m/s^2 (0-p) |
| 4 | Maximum loading mass | Vertical | | 400kg |
| | | Horizontal | | 500kg |
| 5 | Horizontal vibration table size | 50cm x 50 cm | | |
| 6 | Power | 49.0kVA | | |



Figure 2.3.3: The view of attachment of the accelerometers.

One axis accelerometers attached to a glass epoxy cube for each vibration direction respectively and attached to the units with Aron alpha adhesive as shown in Figure 2.3.3.

Data analysis is carried out simultaneously with the test by a PC. 20 accelerometers are connected to Showa charge amplifier, 4 accelerometers are connected to Emic Charge Amplifier. The data is taken through DAQ to a PC with USB cable. The maximum of 24 channels of the analog signal with the range of $\pm 10V$ from the charge amplifier was taken simultaneously and converted to digital signal at 16 bit DAQ (5,000 samples) for 60 seconds (for modal and random test) and the Fast Fourier Transform (FFT) was applied by a PC using Labview programming. Totally 250,000 sampled discrete data are measured using 5000sample/sec rate in 50 sec for a measurement. In order to analyze frequency, FFT is used to convert from time domain to frequency domain. Number of FFT point is 1024. The frequency resolution was chosen as 4.88Hz in order to ensure smoother PSD [16].

2.4 Experimental results and discussion

Figure 2.4.1 shows PSD waveform for the vibration in z-direction as an example. The PSD values in the figure were measured from accelerometers to measure z axial acceleration attached to DM1, PCU and Battery that are placed at +x internal panel for the 0.3Grms input level. Random vibration tests were conducted using different acceleration ranges up to 9.0Grms with frequencies in the range of 20 to 2,000Hz. Accelerometers inside satellites measured the distribution of mechanical stress.

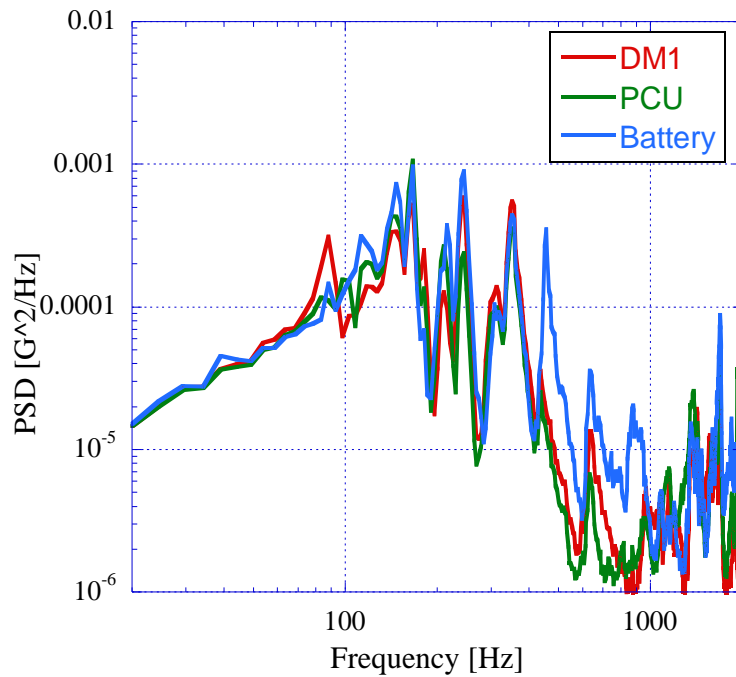


Figure 2.4.1: PSD Waveform of the dummy satellite.

The resonant frequencies and the maximum amplification factor were calculated in the X, Y and Z vibration axes. The vibration was divided to three categories depending on the frequency ranges. The range between 20 and 300Hz is called “*whole satellite*

mode”, because the vibration has strong signature associated with the resonance of the whole satellite body. The signature appears commonly among accelerometers at different locations. The ranges between 300 to 1,000Hz and 1,000 to 2,000Hz are called “*local vibration mode*”, because they are associated with resonance of individual structural components, such as an internal panel. The signature differs depending on the location of each accelerometer. Ref. 17 dealt with whole satellite modes of six different micro satellites whose size and weight were mostly 50cm cube and 50kg. In the present research, the author deals with local vibration modes of two satellites. Combining the results with the ones of Ref. 17, the resonant frequencies and the amplification factors were finally identified between 20 and 2000Hz. The amplification factor is defined as the square root of the ratio of the measured PSD value at a given point by the base level as:

$$AF = \sqrt{\frac{PSD_m}{PSD_b}} \quad \text{Eq. 2.1}$$

where AF is the Amplification factor, PSD_m is the measured PSD value, and the base PSD level is referred as PSD_b . The amplification factor was calculated by using Eq. (2.1) for each measured points. Peak amplification factors were derived among the amplification factors corresponding to resonant frequency of each channel of measurement. Figure 2.4.2 shows the maximum of the peak amplification factors for the various test level from 0.3 Grms to 9 Grms. Here, the maximum and minimum of peak amplification factors mean the maximum and minimum values among all the measurement points and the sensors of the same direction as excitation. The figure shows

that peaks of amplification factor decreases with the increased base vibration level. (For more detail refer to Ref. 16)

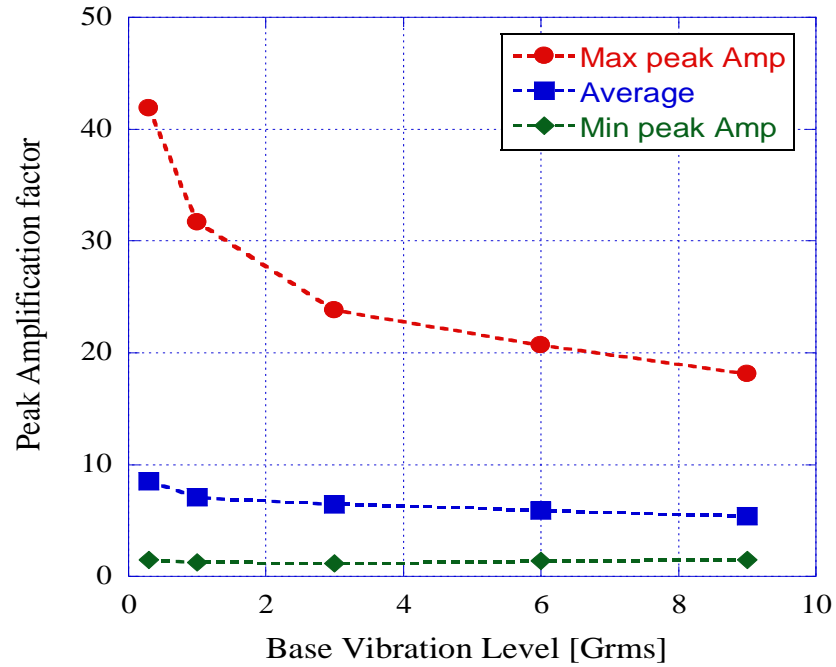


Figure 2.4.2: Peak amplification factor comparison.

0.6Grms data were used to do the statistical analysis to avoid non-linear effect of higher level. On the other hand, only maximum amplification factors were used for the statistical analysis to derive the unit QT level.

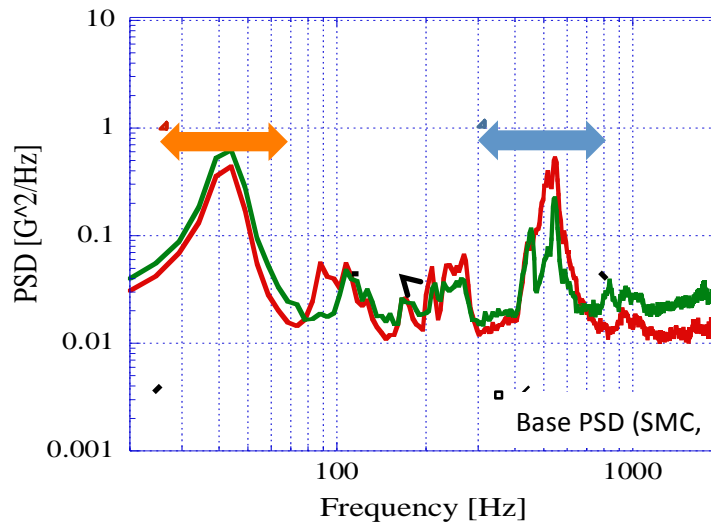


Figure 2.4.3: Vibration response at internal panel

Figure 2.4.3 shows the example of PSD waveform when the base vibration is given in the direction parallel to the axis. Peaks at low frequencies are typically less than 300Hz. Those peaks originated from the resonance of entire satellite structures to the vibration. That is why it is called “Whole satellite mode”. The whole satellite mode of various 50cm-class micro satellites was analyzed in Ref.17. The resonances appeared between 29 and 70Hz for the vibration perpendicular to the thrust axis and 144 to 208Hz for the vibration parallel to the thrust axis. The results are updated in this research to derive the unit QT test level. The peaks at frequencies higher than 300Hz (although the value 300Hz is rather arbitrary) are originated from the resonance of satellite internal structure. They depend on various factors, such as how the internal structure is arranged, direction, thickness, material of the internal panel and the sensor location and it is called “Local vibration mode”. Internal units are exposed to those modes inside a satellite. To establish the standard test level, the author needed to investigate the ranges of the whole satellite mode and local vibration mode in terms of the amplification factor at the resonant

frequencies. The ranges of the amplification factor were calculated. In the local vibration mode, the data was collected in the frequency range 300 to 2,000Hz. The local vibration mode (300-2,000Hz) was divided into 2 groups: 300-1,000Hz and 1,000Hz-2,000Hz. It was noticed that in most of the PSD waveform there are several resonant frequencies from 300Hz to 2,000Hz as seen in Figure 2.4.3. The peak PSD of resonant frequencies were found of all channels in each frequency group. Tables 2.4.1 and 2.4.2 list the resonant frequency and the peak value of the amplification factor respectively observed at each measurement point inside the dummy satellite between 300 and 1,000Hz. From these tables, normal tolerance limits were deduced using the same method as Ref. 12.

Table 2.4.1: Resonant frequency statistics (dummy satellite, 300-1,000Hz).

| | Resonant frequency[Hz] | | |
|-----------|-------------------------------|-------------------------------|--------------------|
| | Perpendicular to the axial(x) | Perpendicular to the axial(y) | Axial direction(z) |
| DM1 | 566.4 | 546.9 | 322.3 |
| PCU | 820.3 | 517.6 | 317.4 |
| BATTERY | 463.9 | 546.9 | 463.9 |
| +X CENTER | 566.4 | 546.9 | 336.9 |
| DM6 | 546.9 | 927.7 | 302.7 |
| OBC | 561.5 | 302.7 | 341.8 |
| RF | 546.9 | 493.2 | 307.6 |
| +Y CENTER | 561.5 | 483.4 | 302.7 |
| DM4 | 551.8 | 542.0 | 302.7 |
| DM2 | 571.3 | 498.1 | 302.7 |
| DM5 | 561.5 | 546.9 | 302.7 |
| -X CENTER | 532.2 | 498.1 | 302.7 |
| DM3 | 571.3 | 498.1 | 302.7 |
| DM9 | 537.1 | 996.1 | 302.7 |
| DM7 | 566.4 | 961.9 | 302.7 |
| DM10 | 537.1 | 493.2 | 356.5 |
| -Y CENTER | 566.4 | 498.1 | 302.7 |
| DM8 | 566.4 | 659.2 | 302.7 |

Table 2.4.2: Peak value of amplification factor (dummy satellite, 300- 1,000Hz).

| | Amplification factor | | |
|-----------|-------------------------------|-------------------------------|--------------------|
| | Perpendicular to the axial(x) | Perpendicular to the axial(y) | Axial direction(z) |
| DM1 | 1.35 | 2.83 | 1.69 |
| PCU | 2.50 | 5.97 | 1.54 |
| BATTERY | 4.31 | 1.85 | 2.18 |
| +X CENTER | 2.80 | 3.69 | 1.70 |
| DM6 | 2.40 | 2.31 | 1.00 |
| OBC | 5.50 | 9.86 | 0.72 |
| RF | 3.07 | 8.48 | 1.41 |
| +Y CENTER | 3.98 | 3.66 | 1.21 |
| DM4 | 1.80 | 0.99 | 1.16 |
| DM2 | 2.50 | 4.35 | 1.22 |
| DM5 | 2.38 | 1.05 | 1.52 |
| -X CENTER | 3.55 | 4.80 | 1.29 |
| DM3 | 2.41 | 5.13 | 2.03 |
| DM9 | 1.04 | 1.79 | 1.33 |
| DM7 | 2.73 | 2.54 | 1.34 |
| DM10 | 1.02 | 1.80 | 1.42 |
| -Y CENTER | 1.97 | 4.01 | 1.43 |
| DM8 | 3.35 | 2.21 | 1.50 |

The statistics in the range 20-300Hz of the dummy satellite and statistics of Hodoyoshi-3 and shown in Appendix.

2.4.1 Experiment data statistics

In order to compute a normal tolerance limit, we follow the same methodology as the Ref. 5. Statistically estimating the interval of the resonant frequency range, normal tolerance limits (NTL) on the amplification factor were derived.

The normality of the tested data was examined whether tested data follow normal or lognormal distributions. The probability plots of the normal and lognormal distribution

are shown in Figures. 2.4.4 and 2.4.5 respectively. When the data follows a straight line on the probability plot, the data follows a normal distribution.

It is difficult to judge whether lognormal is better than the normal from these probability plot. In this regard, χ^2 (Chi squared) goodness of fit statistics [18] was used to check the normality of the test data distribution.

Normal and lognormal both looked good but lognormal was slightly better than normal.

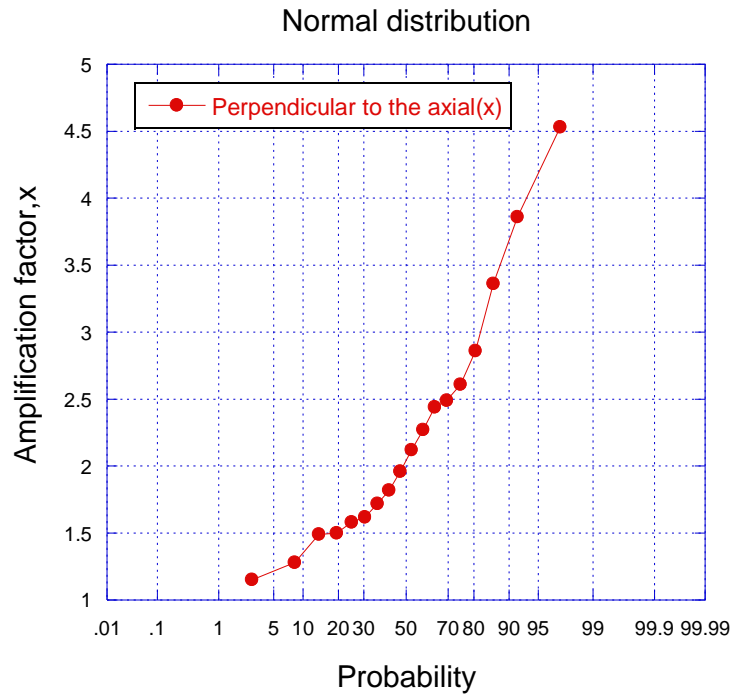


Figure 2.4.4: Probability distribution (normal).

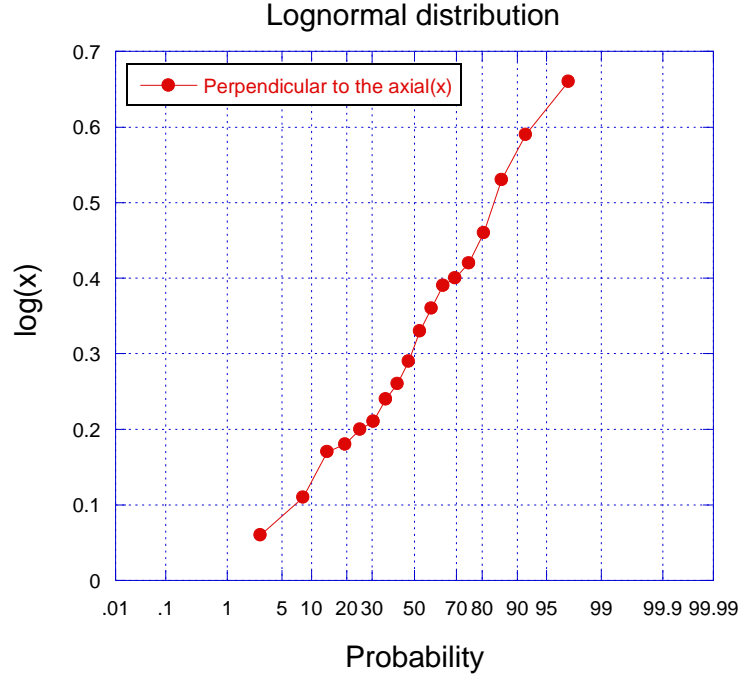


Figure 2.4.5: Probability distribution (lognormal).

After evaluating χ^2 (Chi squared) testing, the lognormal was chosen as the distribution of amplification factor. In order to evaluate, the p -value approach was used for both normal and lognormal distributions. The p -value is the probability of observing a sample statistic as extreme as the test statistic i.e. Chi-squared. On the other hand p -value is larger if the null hypothesis is true. The null hypothesis implies that the underlying distribution is normal and also that the population mean and the population standard deviation equal their estimates. In most cases, p -values of the lognormal distributions are more than normal distribution. In the example shown in Figure 2.4.5, p -value was 0.91 in lognormal while it was 0.62 in normal distribution as shown in Figure 2.4.4. For the resonant frequency normal distribution was chosen.

A Normal tolerance limits of the peak amplification factors are computed for the transformed predictions using Eq. 2.2. The Normal tolerance limit of the peak

amplification factor is defined as that value y that will exceed at least β portion of all possible values of y with a confidence coefficient of γ , and is given by Eq. 2.3. [12]

$$y = \log_{10} x \quad \text{Eq. 2.2}$$

$$\text{NTL}_y(n, \beta, \gamma) = \bar{y} \pm k_{n,\beta,\gamma} s_y \quad \text{Eq. 2.3}$$

This methodology is used only for the peak amplification factor limits calculation and the author followed normal distribution for the frequency range estimation.

In Eq. 2.3, the term $k_{n,\beta,\gamma}$ is called the normal tolerance factor, and is a tabulated value which depends on the values of n , β and γ . The peak amplification factors and resonant frequencies were gathered related to each peak PSD value measured at 18 points located inside the dummy satellite. n is 18 and $k_{n,\beta,\gamma}$ is 1.67 for the dummy satellite while $n=15$ and $k_{n,\beta,\gamma}=1.68$ for Hodoyoshi-3 data to calculate Normal tolerance limit using Eq. 2.2 and Eq. 2.3. Normal tolerance limit was chosen as 95/50 limit ($\beta=0.95$, $\gamma=0.50$) for both satellites data estimation.

Table 2.4.3: Resonant frequency range (dummy satellite, 300-1,000Hz).

| | Resonant frequency[Hz] | | |
|--------------------|-------------------------------|-------------------------------|-----------------|
| | Perpendicular to the axial(x) | Perpendicular to the axial(y) | Axial direction |
| Average | 566.4 | 586.5 | 320.9 |
| Standard deviation | 281.0 | 760.4 | 161.0 |
| Lower value | 97.3 | -683 | 51.1 |
| Upper value | 1035.7 | 1856.4 | 589.8 |

Table 2.4.4: Normal tolerance limit of amplification factor in logarithm of the dummy satellite in the range: 300-1,000Hz (real values are shown in bracket).

| | Amplification factor | | |
|--------------------|-------------------------------|-------------------------------|---------------------|
| | Perpendicular to the axial(x) | Perpendicular to the axial(y) | Axial direction (z) |
| Average | 0.39(2.4) | 0.49(3.1) | 0.14(1.4) |
| Standard deviation | 0.20(1.6) | 0.28(3.1) | 0.11(1.3) |
| NTL (Min) | 0.06(1.15) | 0.02 (1.05) | 0.04(1.1) |
| NTL (Max) | 0.72(5.25) | 0.96 (9.12) | 0.32(2.09) |

Table 2.4.5: Resonant frequency range (dummy satellite, 1,000-2,000Hz).

| | Resonant frequency[Hz] | | |
|--------------------|-------------------------------|-------------------------------|-----------------|
| | Perpendicular to the axial(x) | Perpendicular to the axial(y) | Axial direction |
| Average | 1798.2 | 1798.2 | 1694.1 |
| Standard deviation | 864.7 | 1746.1 | 601.1 |
| Lower value | 354.1 | -1117.8 | 690.3 |
| Upper value | 3242.2 | 4714.2 | 2697.9 |

Table 2.4.6: Normal tolerance limit of amplification factor in logarithm of the dummy satellite in the range: 1,000-2,000Hz (real values are shown in bracket).

| | Amplification factor | | |
|--------------------|-------------------------------|-------------------------------|-----------------|
| | Perpendicular to the axial(x) | Perpendicular to the axial(y) | Axial direction |
| Average | 0.33(2.1) | 0.32(2.1) | 0.29(1.9) |
| Standard deviation | 0.68(4.8) | 0.70(5.0) | 0.47(2.9) |
| NTL (Min) | -0.81 (0.15) | -0.85 (0.14) | -0.49 (0.32) |
| NTL (Max) | 1.47(29.5) | 1.49 (30.9) | 1.07 (11.75) |

Table 2.4.7: Resonant frequency range (Hodoyoshi-3, 300-1,000Hz).

| | Resonant frequency[Hz] | | |
|--------------------|-------------------------------|-------------------------------|-----------------|
| | Perpendicular to the axial(x) | Perpendicular to the axial(y) | Axial direction |
| Average | 576 | 464 | 501 |
| Standard deviation | 208 | 227 | 220 |
| Lower value | 206 | 60 | 109 |
| Upper value | 946 | 868 | 893 |

Table 2.4.8: Normal tolerance limit of amplification factor in logarithm of the Hodoyoshi-3 satellite in the range: 300-1,000Hz (real values are shown in bracket).

| | Amplification factor | | |
|--------------------|-------------------------------|-------------------------------|-----------------|
| | Perpendicular to the axial(x) | Perpendicular to the axial(y) | Axial direction |
| Average | 0.16(1.26) | -0.52(0.32) | -0.16(0.65) |
| Standard deviation | 0.66(4.57) | 0.67(4.68) | 0.32(2.09) |
| NTL (Min) | -1.07(0.08) | -1.67(0.02) | -0.7(0.19) |
| NTL (Max) | 1.2(15.85) | 0.6(4.74) | 0.3(2.01) |

Table 2.4.9: Resonant frequency range (Hodoyoshi-3, 1,000-2,000Hz).

| | Resonant frequency[Hz] | | |
|--------------------|-------------------------------|-------------------------------|-----------------|
| | Perpendicular to the axial(x) | Perpendicular to the axial(y) | Axial direction |
| Average | 1437 | 1689 | 1663 |
| Standard deviation | 345 | 380 | 326 |
| Lower value | 823 | 1013 | 1083 |
| Upper value | 2051 | 2365 | 2243 |

Table 2.4.10: Normal tolerance limit of amplification factor in logarithm of the Hodoyoshi-3 satellite in the range: 1,000-2,000Hz (real values are shown in bracket).

| | Amplification factor | | |
|--------------------|-------------------------------|-------------------------------|--------------------|
| | Perpendicular to the axial(x) | Perpendicular to the axial(y) | Axial direction(z) |
| Average | -0.28(0.52) | -0.79(0.16) | -0.34(0.45) |
| Standard deviation | 0.44(2.75) | 0.56(3.63) | 0.37(2.34) |
| NTL (Min) | -1.02(0.09) | -1.73(0.02) | -0.96(0.11) |
| NTL (Max) | 0.46(2.88) | 0.15(1.41) | 0.28(1.91) |

The interval of the resonant frequency of the dummy satellite in the frequency range 300-1,000Hz and 1,000-2,000Hz are listed in Table 2.4.3 and Table 2.4.5 respectively and the normal tolerance limit of the amplification factor of the dummy satellite are listed in Tables 2.4.4 and 2.4.6, respectively. The data statistics of the Hodoyoshi-3 are shown in Tables 2.4.7- 2.4.10.

Table 2.4.11: Resonant frequency range (dummy satellite, 20-300Hz).

| | Resonant frequency [Hz] | | |
|--------------------|-------------------------------|-------------------------------|---------------------|
| | Perpendicular to the axial(x) | Perpendicular to the axial(y) | Axial direction (z) |
| Average | 47.0 | 40.2 | 142.1 |
| Standard deviation | 85.9 | 41.3 | 321.7 |
| NTL (Min) | 4.2 | 19.6 | -17.9 |
| NTL (Max) | 89.7 | 60.7 | 302.1 |

Table 2.4.12: Normal tolerance limit of amplification factor in logarithm of the dummy satellite in the range: 20-300Hz (real values are shown in bracket).

| | Amplification factor | | |
|--------------------|-------------------------------|-------------------------------|---------------------|
| | Perpendicular to the axial(x) | Perpendicular to the axial(y) | Axial direction (z) |
| Average | 0.73(5.37) | 0.73(5.37) | 0.53(3.39) |
| Standard deviation | 0.19(1.55) | 0.16(1.44) | 0.08(1.2) |
| NTL (Min) | 0.41(2.57) | 0.46(2.88) | 0.39(2.45) |
| NTL (Max) | 1.05(11.2) | 0.99(9.77) | 0.66(4.57) |

Table 2.4.11 and Table 2.4.12 show statistics of the dummy satellite in the range 20-300Hz.

2.4.2 Derivation of Unit QT based on the experiment results

In this part, the unit QT test level is proposed with the estimated values. Total of six (6) cases were studied for the dummy satellite based on the local vibration mode using three (3) axes of the vibration direction namely; perpendicular to the axial direction(x), perpendicular to the axial direction(y) and axial direction (z) in particular for frequency ranges of 300-1,000Hz and also for 1,000-2,000Hz.

In the frequency range 300-1,000Hz, the amplification factor of 1.15 is chosen as the unit QT test level in the local vibration mode. 1.15 is the maximum number among the

three values in the low tolerance limit as listed in Table 2.4.4. The author chooses this maximum number at the low limit, because the test level to propose is to guarantee the minimum level of assurance. Unit manufacturers have no way of knowing in which direction their products will be mounted in the satellite. It could be on the plane perpendicular to the thrust axis or on the plane parallel to the thrust axis. At least it is possible that the product will undergo vibration amplified by a factor of 1.15 in one direction.

After determining the amplification factor for 300-1,000Hz, amplification factor and resonance frequency range for 1,000-2,000Hz interval are determined. From the estimated values in Tables 2.4.5 and 2.4.6 the minimum tolerance limit of the amplification factors were 0.15, 0.14, 0.32 for directions perpendicular to the axial (x), (y) and axial (z) respectively. The author simply takes the amplification is uniform at unity between 1,000 and 2,000 Hz.

The above mentioned numbers were examined taking into account the result of Hodosyohi-3. Using the same logic, the maximum of low limit of the amplification factor is 0.19 between 300 and 1,000 Hz and 0.11 between 1,000 and 2,000Hz. The value of 0.19 is smaller than 1.15 derived from the dummy satellite result. Therefore, the author keeps 1.15 in the 300-1,000Hz range. The amplification factor stays 1 between 1000 and 2000Hz.

270Hz was selected as the upper frequency range in the 20-300Hz frequency range which is the maximum value in the resonant frequency range estimated from the statistics of normal distribution of the resonant frequency in the range as listed in Table 2.4.13. The

vibration transmittance calculated apart from the resonance frequency ranges i.e. from 270Hz. Transmittance τ is described with damping rate ζ and frequency rate κ as shown in Eq. 2.4 and Figure 2.4.5. We approximate the vibration by a single-degree-of-freedom vibration system. In addition, frequency rate κ is described with excited frequency of the base f and resonance frequency f_0 as shown in Eq. 2.5 [17].

Damping rate ζ has the relation with Q factor (Amplification factor) as shown in Eq. 2.6. The quantity Q is a measure of the sharpness of resonance of a resonant vibratory system having a single degree of freedom. In a mechanical system, this quantity is equal to one-half the reciprocal of the damping ratio as shown in Eq. 2.6. It is commonly used only with reference to a lightly damped system and is then approximately equal to Transmittance or Transmissibility at resonance. Transmittance is the ratio of the response amplitude of a system in steady-state forced vibration to the excitation amplitude. In our case, transmittance is equal to the amplification factor. Vibration transmittance at the outside of resonance frequency, i.e. from 270Hz, was calculated with resonance frequency f_0 and Q factor at boundary conditions. For calculating the gradient value from 270Hz to higher, we extrapolated the amplification factor and frequency until the amplification factor became 1.15 using Eq. 2.4. The amplification became 1.15 at 390Hz. ζ is assumed 0.1.

$$\tau = \sqrt{\frac{1 + (2\zeta\kappa)^2}{(1 - \kappa^2)^2 + (2\zeta\kappa)^2}} \quad \text{Eq. 2.4}$$

$$\kappa = \frac{f}{f_o} \quad \text{Eq. 2.5}$$

$$Q \approx \frac{1}{2\xi} \quad \text{Eq. 2.6}$$

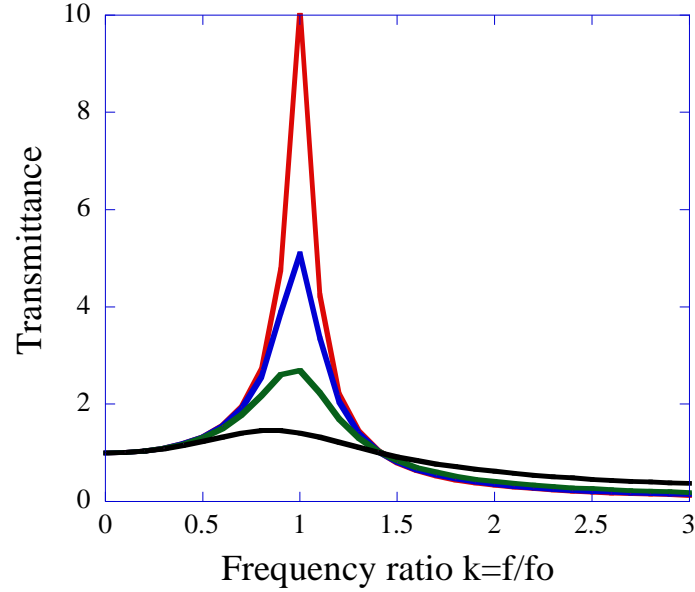


Figure 2.4.5: Transmittance (τ) against frequency ratio (κ).

The amplification factor for whole satellite mode (20-300Hz) was calculated according to those procedures used in local vibration mode. Table 2.4.13 and Table 2.4.14 show the statistics of resonant frequency and amplification factor of whole satellite vibration modes of each satellite, respectively. The data were taken from the measurement point at either the top corner of the cubic satellites or the center of the panel facing the excited direction except the satellite-G. In the whole satellite mode, HODOYOSHI-2 & 3, UNIFORM, RISESAT, RISING2, QSAT-EOS, TSUBAME satellites' random vibration data were used, which are listed as Satellite A-G in Tables 2.4.13 and 2.4.14.

Table 2.4.13: Resonant frequency of each satellite (20-300Hz).

| Satellite name | Resonant frequency[Hz] | | |
|----------------|--|--|-----------------|
| | Perpendicular to the axial direction 1 | Perpendicular to the axial direction 2 | Axial direction |
| Satellite-A | 62 | 59 | 165 |
| Satellite-B | 56.3 | 43.8 | 165.6 |
| Satellite-C | 48.8 | 44.6 | 186 |
| Satellite-D | 44.6 | 40.9 | 144 |
| Satellite-E | 61 | 61 | 208 |
| Satellite-F | 32.3 | 29.3 | 144 |
| Satellite-G | 70 | 65 | 190 |

The data was taken from the result of QT random vibration test. As the satellite-G did not have accelerometers at neither the top corner nor the center of the panel, only the resonant frequencies are shown. There are three whole satellite vibration modes against three axis of the satellite.

Table 2.4.14: Amplification factor of each satellite (20-300Hz).

| Satellite name | Amplification factor | | |
|----------------|--|--|-----------------|
| | Perpendicular to the axial direction 1 | Perpendicular to the axial direction 2 | Axial direction |
| Satellite-A | 8.2 | 10.4 | 8.0 |
| Satellite-B | 4.21 | 5.18 | 5.86 |
| Satellite-C | 6.52 | 5.75 | 7.56 |
| Satellite-D | 7.31 | 7.27 | 5.05 |
| Satellite-E | 5.73 | 6.92 | 3.39 |
| Satellite-F | 6.78 | 5.19 | 3.27 |
| Satellite-G | - | - | - |

With these results, interval of the resonant frequency and the normal tolerance limit of the amplification factor were estimated using same method as the one used for local vibration mode. The average of sample, low limit value and high limit value have also been estimated as listed in Tables 2.4.15 and 2.4.16.

Table 2.4.15: Resonant frequency range (20-300Hz).

| | Resonant frequency [Hz] | | |
|--------------------|--|--|-----------------|
| | Perpendicular to the axial direction 1 | Perpendicular to the axial direction 2 | Axial direction |
| Average | 54 | 49 | 172 |
| Standard deviation | 27 | 28 | 56 |
| Lower value | 6.7 | 0 | 74 |
| Upper value | 101.2 | 98 | 270 |

Table 2.4.16.: Normal tolerance limit of amplification factor in logarithm in the range: 20-300Hz (real values are shown in bracket).

| | Amplification factor | | |
|--------------------|--|--|-----------------|
| | Perpendicular to the axial direction 1 | Perpendicular to the axial direction 2 | Axial direction |
| Average | 0.80 (6.3) | 0.82(6.6) | 0.72(5.2) |
| Standard deviation | 0.10 (1.2) | 0.12(1.3) | 0.17(1.5) |
| NTL (Min) | 0.62 (4.2) | 0.61 (4.1) | 0.42 (2.6) |
| NTL (Max) | 0.97 (9.3) | 1.03 (10.7) | 1.0 (10) |

4.2 is chosen as the unit QT level between 20Hz and 101Hz while the unit QT level was chosen as 2.6 in the 101Hz and 270Hz range. The author chooses this maximum number 4.2 from two perpendiculars to the axial direction estimated values, because the test level proposing in this research is to guarantee the minimum level of assurance. Unit manufacturers have no way of knowing in which direction their products (units) will be mounted in a satellite. It could be on any vibration axis. Level 4.2 is keeping until 101Hz according to the estimation and beyond 101Hz, minimum amplification level is 2.6 until 270Hz as listed in Table 2.4.13. The amplification factor at 270Hz is extrapolated to higher frequencies using Eq. 2.4, assuming $\zeta = 0.1$. Finally the results of three frequency ranges were merged and the amplification factor of unit QT level between 20 and 2,000Hz is shown in Figure 2.4.6.

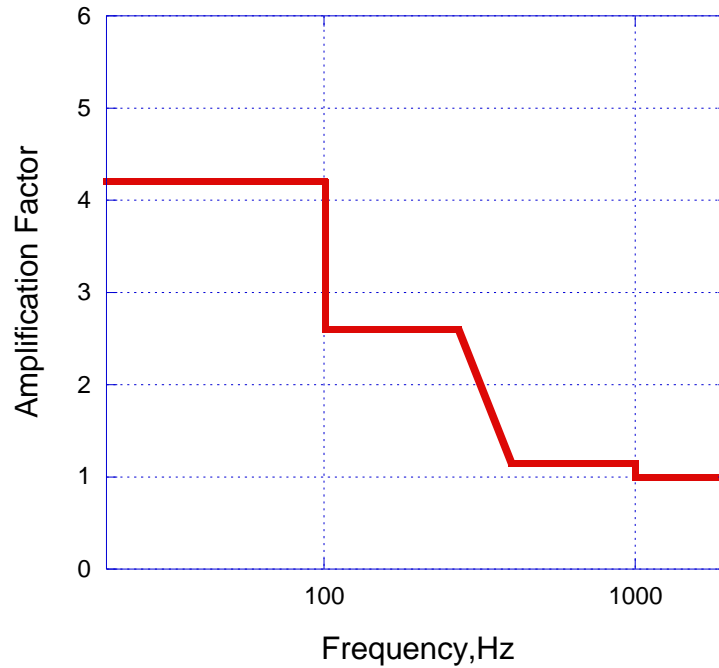


Figure 2.4.6: The amplification factor and resonance frequency range for unit QT test level (20-2,000Hz).

The base vibration level of the unit QT is given in terms of PSD. PSD of AT level of random vibration for various rockets in the frequency range of 20-2,000Hz is multiplied by the square of the amplification factor shown in Figure 2.4.6. The result is shown as the unit QT level in Figure 2.4.7. The unit QT level shown in blue corresponds to the Rocket A which is used for unit QT level. It has an RMS value of 11.8Grms. The green and orange curves correspond to AT level of different rockets. The green curve gives an RMS value of 8.4Grms, while the green curve gives 7.0Grms.

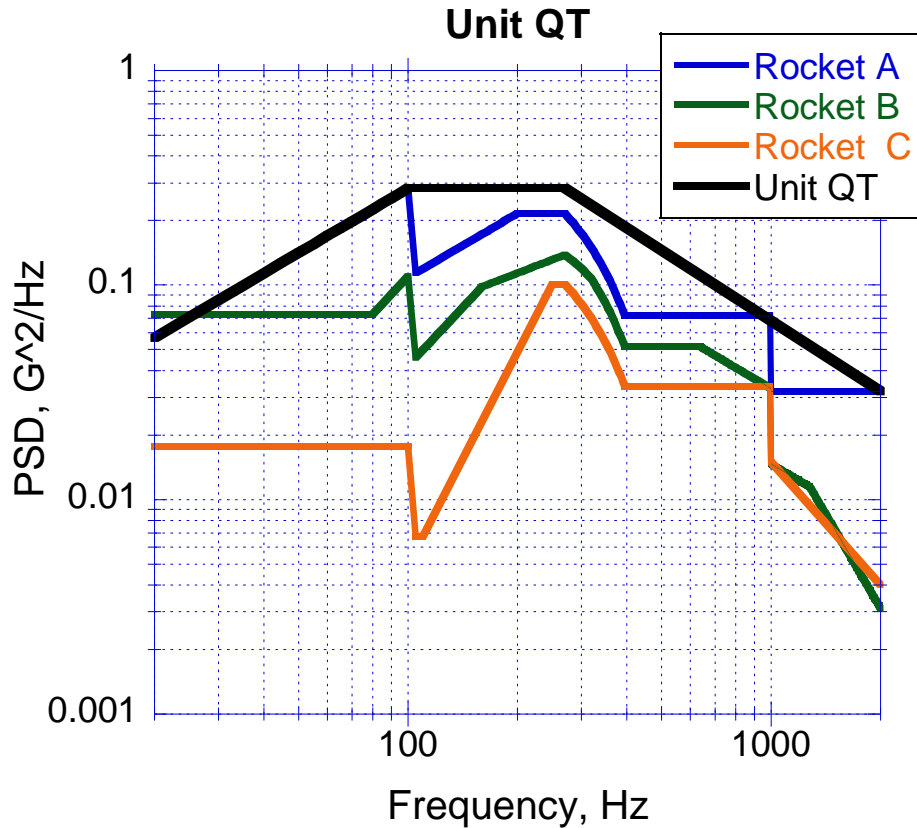


Figure 2.4.7: Unit QT level (20-2,000Hz).

The level extracted from the rocket A was chosen as Unit QT level. Basically the blue curve could be kept as Unit QT level, but practically this level is complicated for the test facilities because of the steps. In this reason, the curves should be smoothed by straight lines. The author proposes straight line as shown as black lines in Figure 2.4.7 keeps rising from 20Hz to 100Hz and keeps the level until 270Hz and going down smoothly up to 2000Hz.

It should be emphasized that the unit QT level shown in Figure 2.4.7 is the only minimum level for each test article to obtain the minimum assurance that the product may survive the launch environment. Therefore, it does not contain any margin. This Unit QT

level is performed by manufacturer to certify their products (satellite units) is good for space. If a satellite system integrator, the buyer of the product, wants to set margin, they have to choose the test level by themselves based on the specifics of their satellites.

The QT level also do not account for any flight-to-flight variation. The level accounts for satellite-to-satellite variation among 6 satellites at frequencies less than 300Hz and 2 satellites at frequencies higher than 300Hz. The flight-to-flight variation is needed if maximum limit considered. But in the research the author is proposing the minimum limit. If the variation is added to the minimum number, the level will become very low.

3. Analysis

The purpose of this chapter is to extend and extrapolate the experimental results by Finite Element Analysis. On the other hand, the author tries to accumulate more data of other satellites to improve the satellite-to-satellite variation or gather the data based on numerical analysis.

Laboratory testing can be done to investigate the vibration acceleration distribution of various small satellite structures but they are commonly complex and very expensive. The most commonly-used modelling technique for prediction of the dynamic properties of structures (natural frequencies and mode shapes) and of their response characteristics is that of Finite Element Analysis and it is one of several numerical methods that can be used to solve complex problems and is the key method nowadays.

The Finite Element Method is based on discretization of the structural geometry domain into separate elements which are used to create global mass, stiffness and damping matrices. Finite Element Analysis of vibration acceleration distribution allows us to extrapolate the findings derived from the experiment without using expensive laboratory testing for other typical micro/nano satellite structures.

Design and application of small satellite is becoming widely popular, partly due to a significant development in integrated component manufacturing, growing need for vibration acceleration analysis and simulation of the environment stress of the different type of small satellite structures.

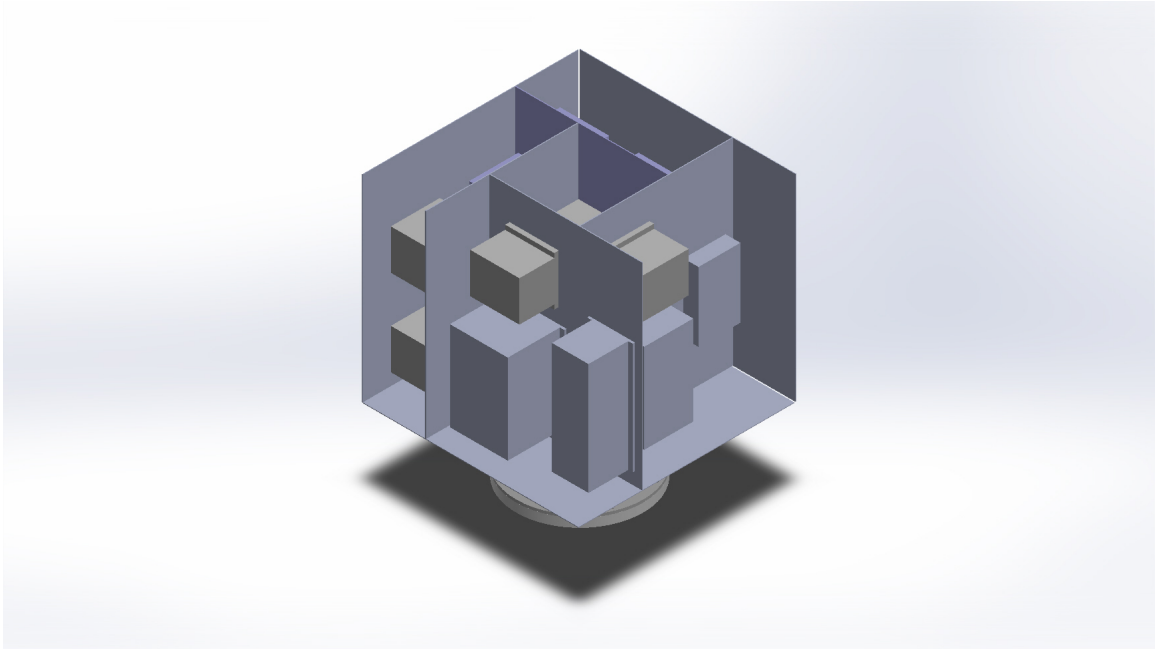
This chapter presents review of steps of finite element analysis of vibration acceleration distribution of the dummy satellite structures and other types of 50cm class satellite models such as T-type and Pi type. The chapter also includes the method to divide satellite body and panels into finite elements and selection of the types of finite elements to represent the overall structure and also details modeling of loading and boundary conditions applied to the satellite structure. The author used finite element modeling using software or finite element package, e.g., NASTRAN, FEMAP and Solidworks in finite element modeling.

3.1 Analysis models

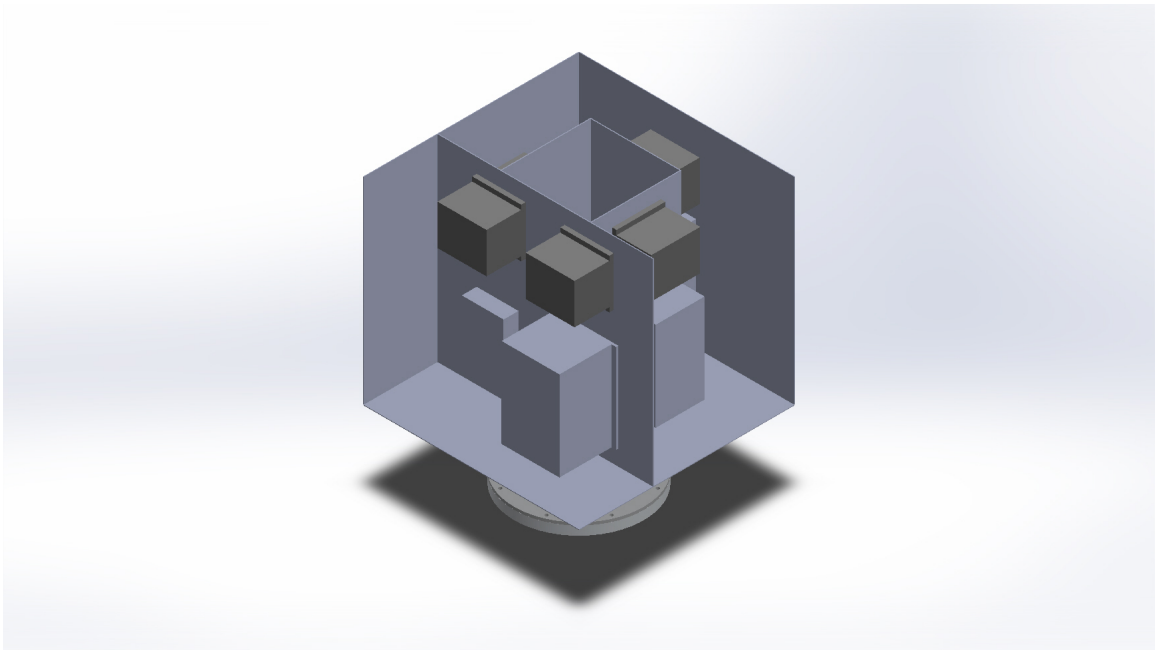
Three basic types of 50kg class satellites are analyzed in this study, which are Yojo-han, T-type and Pi-type structure. A linear random vibration analysis was done on those three satellites models. The dummy satellite model was created based on the actual dummy satellite with flight quality components. But the analyzed model is simplified one. Unnecessary small parts were simplified which might not be harmful for the analysis results as shown in Figure 3.1.1(a). All the size including thickness of the dummy satellite was modelled similarly as dummy satellite. As mentioned earlier, the dummy satellite is a copy of real satellite that is used for remote sensing purpose before in Japan.

The author also created two other unique satellite models to extrapolate the Unit QT to other types of structure. The similar structures to these models are commonly used for micro/nano satellite for scientific and remote sensing purpose. The internal and outer panel structures are similar to the real 50cm class satellites. The simple unique models

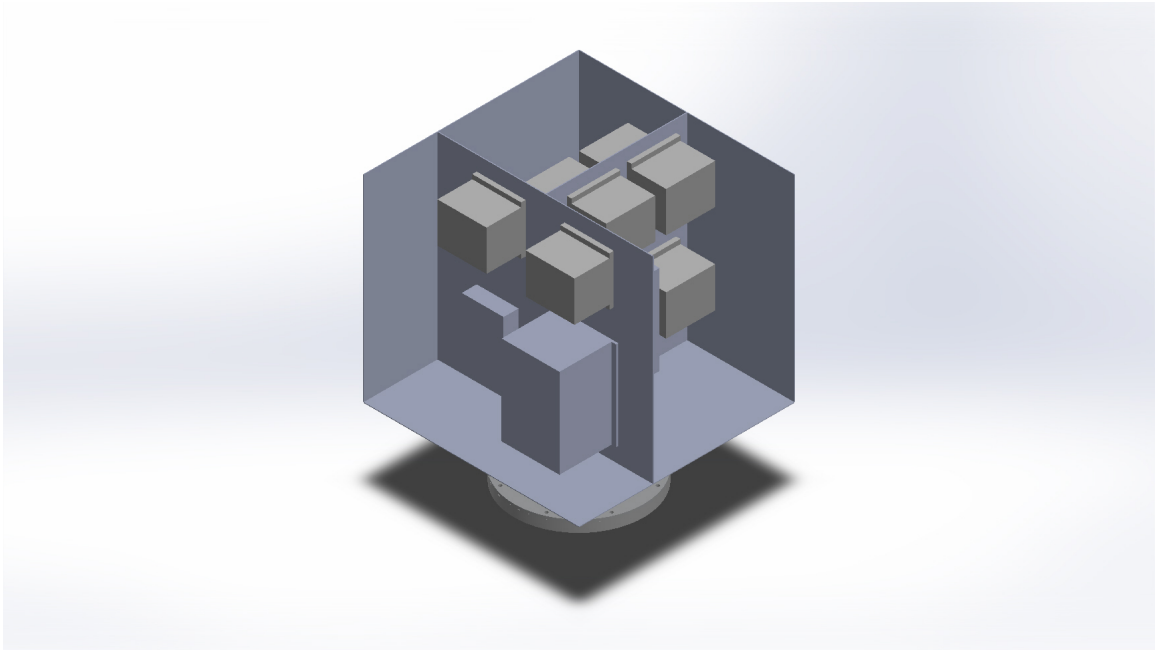
were created which are so called T and Pi type structure. When viewed from the top it can be seen as T and Pi as shown in Figure 3.1.1 (b, c).



a. Yojo-han structure .



b. Pi type structure.



c. T-type structure.

Figure 3.1.1: Basic types of micro/nano satellite structures.

The center of gravity of entire model is important. The author checked the center of gravity for each satellite structure and corrected some dummy masses to ensure the center of gravity to be located at the center of entire structure. Figures 3.1.2-3.1.4 illustrates the center of gravity of three types of structures.

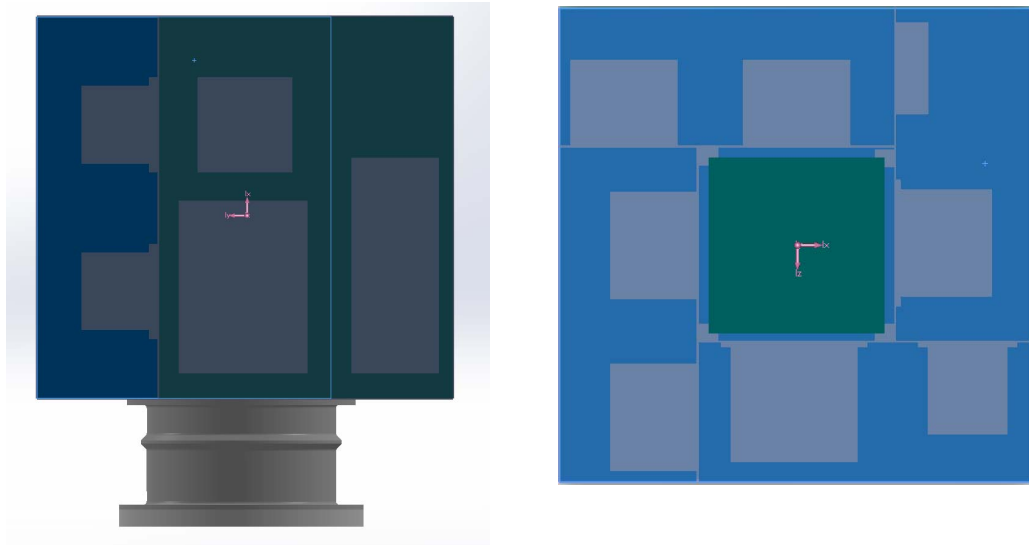


Figure 3.1.2: Center of Gravity of dummy satellite model.

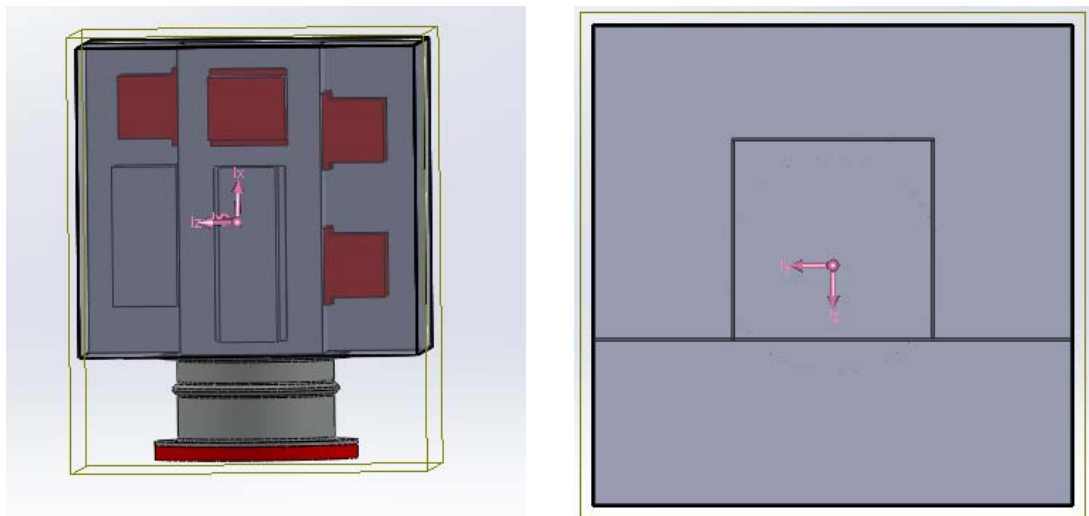


Figure 3.1.3: Center of Gravity of Pi type model.

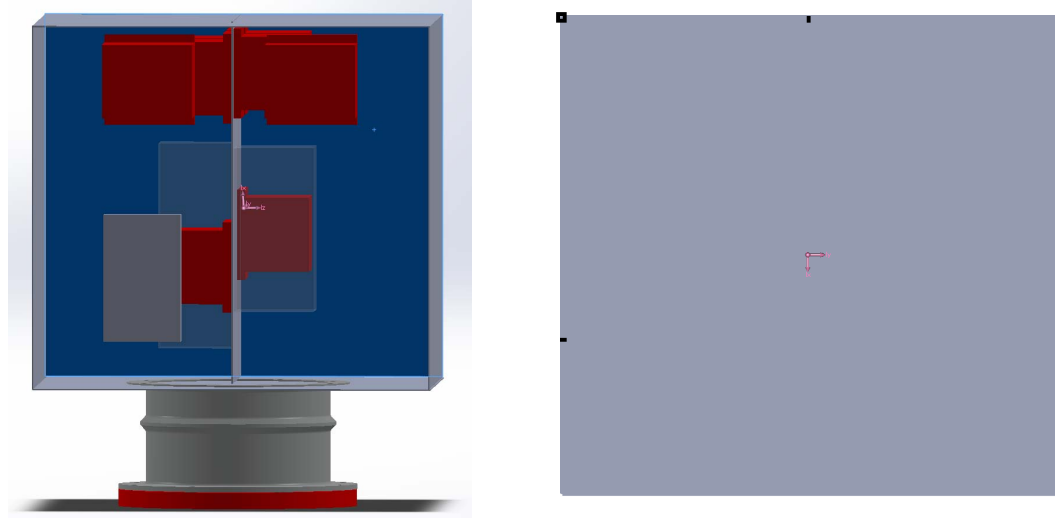


Figure 3.1.4: Center of Gravity of T type model.

3.2 Analysis modelling and settings

Nastran was used for the analysis which is the latest solver that providing results for the satellites FEA models. Four linear solvers (PCGLSS, PSS, VSS and VIS) are included in the Nastran and the author used PSS solver which is fast parallel direct solver and is highly scalable for multi CPU/core processors. The Windows based pre- and post-processor Femap was used to model the structures and processes which is tightly integrated with NEi Nastran solver.

On finite element modeling of aluminum structures of the satellite panels and details the choice of element type and mesh size were decided for the models that can accurately simulate the complicated behavior of different Aluminum structural elements.

The satellite models were created using beam and plate elements. These elements are suitable for the linear dynamic analysis.

The material and property were defined for the meshing process for the internal and external panels. The author defined the material by selecting a standard material from the Femap material library.

The solid model was created with a mesh size of 10 mm on the internal panels of the satellite structure. A finite element model of the dummy satellite used in the FE analysis is constructed, as shown in Figure 3.2.1 while the PAF and Jig use a mesh size of 20 mm, and the rest of the outer panel uses much larger elements, automatically sized using NASTRAN.

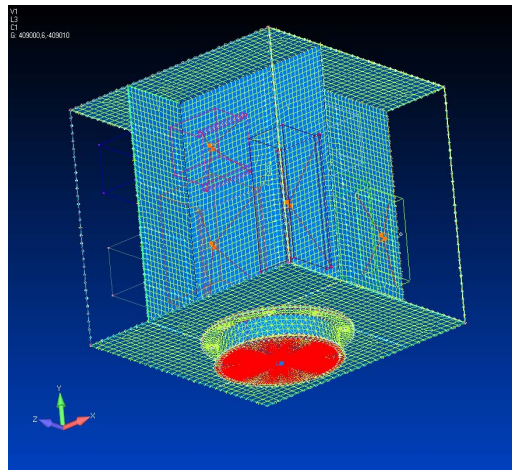


Figure 3.2.1: Finite element model of the dummy satellite.

The inside and outside panels are meshed with four-node tetrahedral element, which supplies the real stiffness of the total model. The other components are meshed with hexahedron mesh. The total number of elements and nodes of the dummy satellite finite element model are 48,381 and 80,051 respectively while 40,176 and 64,684 for T-type and 44,199 and 74,518 for Pi type models. One element is defined for presenting components mechanical information called as “Mass element” is assigned to the

interfaces between each components and panels. For the connections between main body, the PAF and a jig, the bolts are modeled as connecting element so called “Bar element” with diameter of 6 mm.

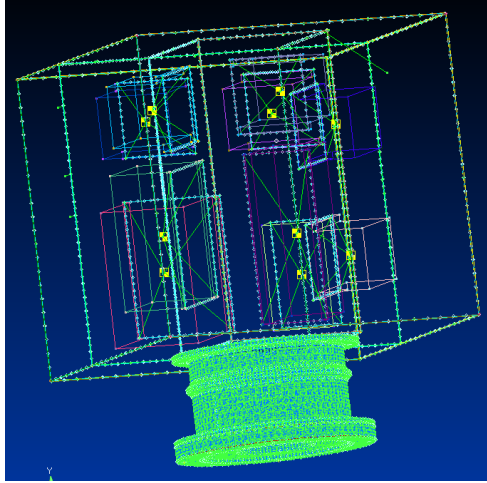


Figure 3.2.2: Main structure view.

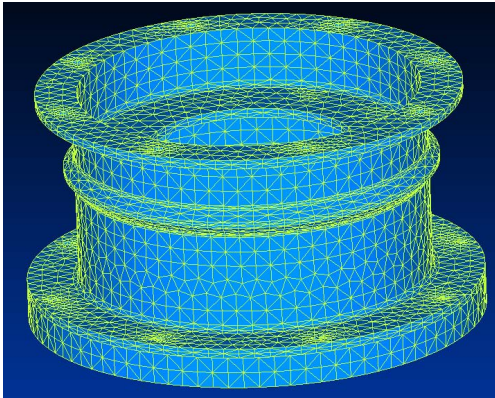


Figure 3.2.3: Finite element model of the PAF and Jig.

The Jig and PAF of the satellite are meshed using an eight-node hexahedral solid mesh as shown in Figure 3.2.3.

Material properties of the main body, PAF and Jig were defined. The analyzed satellite model is made of aluminum with Alloy number of 5052 while PAF and Jig's alloy is AL2024. These materials are same as the material of the dummy satellite used for the experiment.

Random vibration loads are directly applied to the cylinder shaped Jig and PAF. The PAF and Jig were pre-tightened with bolt of M6. The author used low level input load in order to avoid nonlinear material behavior can be efficiently and correctly modeled. Frequency increment of 5Hz was chosen in order to conserve computational time and effort and to compare experimental data also in the frequency range 20-300Hz. Another reason of choosing 5Hz is to easily compare analysis data to the experiment data where 4.88Hz frequency increment is used for the derivation of the Unit QT. Table 3.2.1-3.2.3 show the summary of the dummy satellite, T type and Pi type model respectively after meshing.

Table 3.2.1: Summary of the dummy satellite FE model.

| | |
|--------------------|----------------|
| Dimension | 50cmx50cmx50cm |
| Total weight | 48.8kg |
| Number of nodes | 80,051 |
| Number of elements | 48,381 |

Table 3.2.2: Summary of the T-type structure FE model.

| | |
|--------------------|----------------|
| Dimension | 50cmx50cmx50cm |
| Total weight | 45.7kg |
| Number of nodes | 64,684 |
| Number of elements | 40,176 |

Table 3.2.3: Summary of the Pi-type structure FE model.

| | |
|--------------------|----------------|
| Dimension | 50cmx50cmx50cm |
| Total weight | 47kg |
| Number of nodes | 74,518 |
| Number of elements | 44,199 |

18 virtual sensors were used to gather vibration acceleration response at different position of internal panels of the dummy satellite while 8 virtual sensors were used for T and Pi types structures. The virtual sensor positions are exactly same both for experiment and analysis for the dummy satellite. Figure 3.2.4 shows the virtual sensor position of Pi type structure as an example. The black circles indicate the position of virtual sensors. One single node selected as a virtual sensor near component.

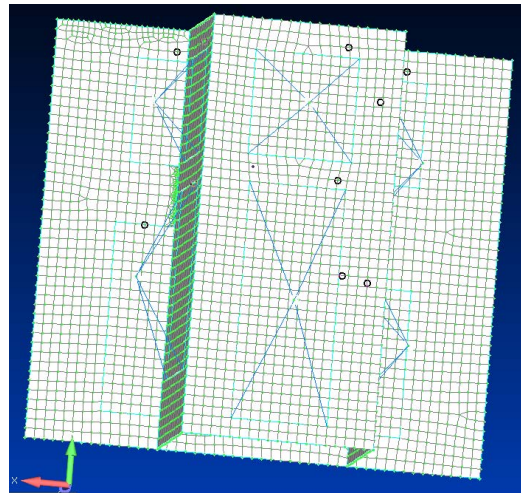


Figure 3.2.4: Virtual sensor position

In the analysis same shape as experiment i.e. SMC shape shown in Fig.2.3.1 was used for input random vibration acceleration load.

4. Result and Discussions

This chapter describes analysis results, their statistics, comparison of test and analysis data and the Unit QT conditions.

4.1 Analysis results and discussion

4.1.1 Analysis results of dummy satellite

The part details the finite element analysis results obtained. The results are discussed to show the significance of the finite element models in predicting the structural response of different small satellite types. The analysis was carried out only in the frequency range from 20 to 300Hz. Analysis results are compared with those achieved using a random vibration data under excitation induced by shakers. Table 4.1.1-Table 4.1.3 show statistics of the maximum peak amplification factors and the resonant frequencies correspond to the maximum peak amplification derived from the analysis data of the dummy satellite model. The analysis result shows that there are several peaks within the frequency range. Therefore, the author has divided the frequency into 3 groups: 20-100Hz, 100-200Hz and 200-300Hz. If we focus on whole frequency range without dividing into some groups, it is always seen the similar peaks in lower frequency i.e 45Hz etc. But these peaks are associated with whole satellite mode. If we look for the peaks associated with the local vibration mode, we have to focus on beyond 100Hz.

Table 4.1.1: Peak Amplification factor and resonant frequency statistics of Dummy satellite (horizontal1).

| | 20-100Hz | | 100-200Hz | | 200-300Hz | |
|------|----------|-------------------------|-----------|-------------------------|-----------|-------------------------|
| | AF | Resonant frequency[Hz] | AF | Resonant frequency[Hz] | AF | Resonant frequency[Hz] |
| DM1 | 6.53 | 45 | 1.14 | 105 | 0.94 | 280 |
| PCU | 2.89 | 45 | 0.6 | 140 | 1.56 | 300 |
| BAT | 8.16 | 45 | 0.61 | 105 | 0.75 | 300 |
| +X | 6.22 | 45 | 0.71 | 105 | 1.01 | 250 |
| DM6 | 6.15 | 45 | 2.65 | 110 | 1.66 | 215 |
| OBC | 2.85 | 40 | 2.18 | 195 | 4.97 | 260 |
| RF | 7.50 | 45 | 3.77 | 170 | 2.85 | 245 |
| +Y | 3.78 | 40 | 1.36 | 200 | 1.57 | 245 |
| DM4 | 6.39 | 40 | 0.84 | 200 | 0.78 | 235 |
| DM2 | 2.99 | 40 | 0.68 | 105 | 0.94 | 250 |
| DM5 | 6.06 | 45 | 0.84 | 160 | 1.4 | 250 |
| -X | 3.91 | 40 | 0.47 | 190 | 1.13 | 255 |
| DM3 | 3.81 | 40 | 0.92 | 195 | 1.21 | 265 |
| DM9 | 7.36 | 45 | 2.71 | 140 | 0.91 | 285 |
| DM7 | 4.46 | 40 | 1.83 | 105 | 0.87 | 265 |
| DM10 | 7.06 | 40 | 4.87 | 105 | 1.5 | 210 |
| -Y | 4.05 | 40 | 0.73 | 200 | 0.78 | 205 |
| DM8 | 4.10 | 45 | 3.1 | 200 | 2.85 | 200 |

Table 4.1.2: Peak Amplification factor and resonant frequency statistics of Dummy satellite (horizontal2).

| | 20-100Hz | | 100-200Hz | | 200-300Hz | |
|------|----------|---------------------------|-----------|---------------------------|-----------|------------------------|
| | AF | Resonant frequency[Hz] | AF | Resonant frequency[Hz] | AF | Resonant frequency[|
| DM1 | 5.43 | 45 | 3.74 | 195 | 2.91 | 205 |
| PCU | 4.05 | 45 | 6.88 | 200 | 5.48 | 205 |
| BAT | 5.6 | 45 | 2.82 | 195 | 5.27 | 260 |
| +X | 3.48 | 45 | 2.5 | 200 | 2.14 | 205 |
| DM6 | 5.09 | 45 | 1.02 | 190 | 0.6 | 205 |
| OBC | 3.18 | 40 | 1.24 | 200 | 1.3 | 260 |
| RF | 4.98 | 45 | 0.65 | 115 | 0.47 | 255 |
| +Y | 4.48 | 45 | 0.69 | 115 | 0.49 | 210 |
| DM4 | 6.55 | 40 | 3.52 | 180 | 2.76 | 205 |
| DM2 | 5.08 | 40 | 8.76 | 110 | 1.56 | 250 |
| DM5 | 6.76 | 40 | 6.29 | 120 | 3.01 | 205 |
| -X | 4.19 | 40 | 1.01 | 175 | 0.82 | 205 |
| DM3 | 4.3 | 40 | 3.3 | 105 | 3.27 | 205 |
| DM9 | 5.58 | 40 | 0.82 | 120 | 0.49 | 235 |
| DM7 | 5.6 | 40 | 1.02 | 150 | 1.05 | 275 |
| DM10 | 5.91 | 40 | 1.06 | 115 | 0.57 | 235 |
| -Y | 4.35 | 40 | 0.57 | 105 | 0.87 | 260 |
| DM8 | 3.82 | 40 | 0.79 | 145 | 1.87 | 240 |

Table 4.1.3 Peak Amplification factor and Resonant frequency statistics of Dummy satellite (vertical).

| | 20-100Hz | | 100-200Hz | | 200-300Hz | |
|------|----------|----------------------|-----------|------------------------|-----------|---------------------|
| | AF | Resonant frequency[H | AF | Resonant frequency[Hz] | AF | Resonant frequency[|
| DM1 | 2.03 | 90 | 3.08 | 125 | 2.00 | 245 |
| PCU | 1.57 | 90 | 3.25 | 145 | 1.51 | 215 |
| BAT | 1.53 | 95 | 3.72 | 140 | 2.25 | 250 |
| +X | 1.51 | 90 | 3.24 | 140 | 2.32 | 245 |
| DM6 | 2.68 | 90 | 2.6 | 125 | 1.26 | 230 |
| OBC | 2.21 | 90 | 2.9 | 125 | 1.65 | 230 |
| RF | 2.35 | 90 | 3.03 | 155 | 1.59 | 215 |
| +Y | 2.19 | 90 | 2.73 | 155 | 1.62 | 230 |
| DM4 | 1.92 | 90 | 3.48 | 140 | 1.24 | 260 |
| DM2 | 2.61 | 85 | 3.6 | 140 | 1.23 | 260 |
| DM5 | 1.9 | 90 | 3.83 | 140 | 1.43 | 260 |
| -X | 2.07 | 85 | 3.36 | 140 | 1.33 | 260 |
| DM3 | 2.21 | 90 | 3.51 | 140 | 1.88 | 250 |
| DM9 | 2.41 | 95 | 3.34 | 125 | 1.27 | 265 |
| DM7 | 2.38 | 80 | 3.44 | 125 | 1.27 | 225 |
| DM10 | 2.31 | 95 | 2.82 | 130 | 1.28 | 230 |
| -Y | 1.93 | 80 | 3.48 | 125 | 1.31 | 260 |
| DM8 | 1.99 | 95 | 3.88 | 125 | 1.03 | 270 |

4.1.2 Comparison between experiment and analytical results

To check the validity of the dummy satellite's analysis, comparisons are made with the experiment results. The comparison is shown in Table 4.1.4-4.1.6. The comparison carried out in this table shows excellent agreement for 20-100Hz of dummy satellite and good agreement 100-200Hz. The accuracy decreases with increasing frequency beyond 200Hz. Figure 4.1.1 illustrates one of the best agreement in quantitative comparison. At the first stage, analysis result was not good agreement with the experimental data result. So we needed to improve model and analysis settings. In order to get good match, the

dummy satellite was updated by refining the mesh which is standard function of Nastran and connected dummy PAF and a Jig which is same model as the experiment.

Comparisons at all the internal points are shown in Appendix.

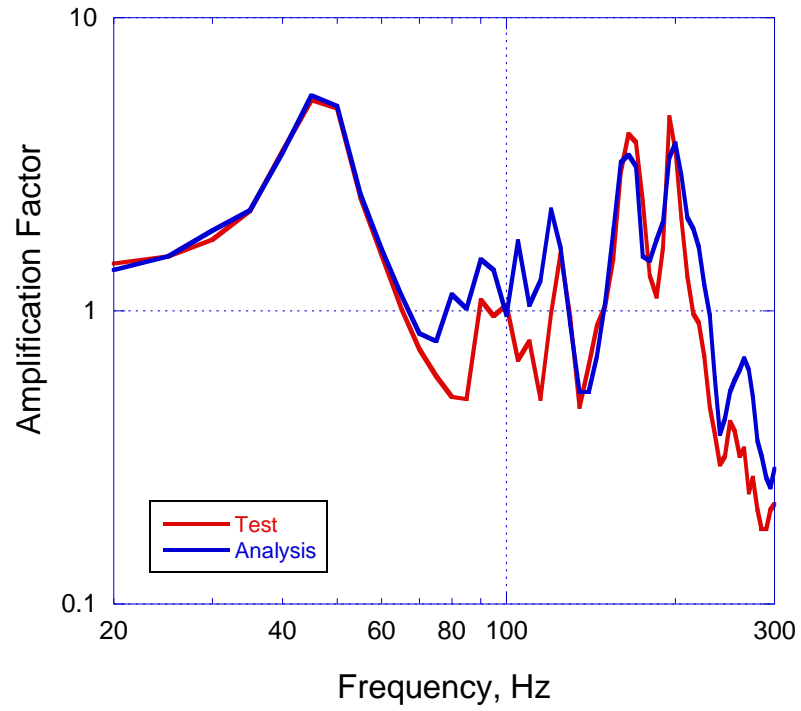


Figure 4.1.1: Example of test and analysis result comparison (horizontal direction).

Table 4.1.4: Comparison of Amplification factor and resonant frequency (20-100Hz).

| Units | Experiment | | Analysis | | Difference | |
|-----------|------------|--------------------|----------|--------------------|------------|--------------------|
| | AF | Resonant Frequency | AF | Resonant frequency | AF | Resonant frequency |
| DM1 | 6.3 | 45 | 6.5 | 45 | -0.2 | 0 |
| PCU | 2.6 | 45 | 2.9 | 45 | -0.3 | 0 |
| Battery | 7.6 | 45 | 8.2 | 45 | -0.6 | 0 |
| +x center | 5.2 | 45 | 6.2 | 45 | -1 | 0 |
| DM6 | 7.4 | 40 | 6.2 | 45 | 1.2 | -5 |
| OBC | 2.1 | 40 | 2.9 | 40 | -0.8 | 0 |
| RF | 5.9 | 40 | 7.5 | 45 | -1.6 | -5 |
| +y center | 4.3 | 40 | 3.8 | 40 | 0.5 | 0 |
| DM4 | 7.7 | 40 | 6.4 | 40 | 1.3 | 0 |
| DM2 | 3.6 | 40 | 3.0 | 40 | 0.6 | 0 |
| DM5 | 7.9 | 40 | 6.1 | 45 | 1.8 | -5 |
| -x center | 4.3 | 40 | 3.9 | 40 | 0.4 | 0 |
| DM3 | 4.2 | 40 | 3.8 | 40 | 0.4 | 0 |
| DM9 | 9.3 | 40 | 7.4 | 45 | 1.9 | -5 |
| DM7 | 9.6 | 40 | 6.6 | 40 | 3 | 0 |
| DM10 | 9.1 | 40 | 7.1 | 40 | 2 | 0 |
| -y center | 4.8 | 40 | 4.1 | 40 | 0.7 | 0 |
| DM8 | 4.0 | 40 | 4.1 | 45 | -0.1 | -5 |

Table 4.1.5: Comparison of Amplification factor and resonant frequency(100-200Hz).

| Units | Experiment | | Analysis | | Difference | |
|-----------|------------|--------------------|----------|--------------------|------------|--------------------|
| | AF | Resonant Frequency | AF | Resonant frequency | AF | Resonant frequency |
| DM1 | 1.9 | 105 | 1.1 | 105 | 0.8 | 0 |
| PCU | 0.8 | 105 | 0.6 | 140 | 0.2 | -35 |
| Battery | 1.0 | 105 | 0.6 | 105 | 0.4 | 0 |
| +x center | 1.2 | 105 | 0.7 | 110 | 0.5 | 5 |
| DM6 | 4.9 | 105 | 2.7 | 110 | 2.2 | -5 |
| OBC | 2.3 | 195 | 2.2 | 195 | 0.1 | 0 |
| RF | 2.5 | 195 | 3.8 | 170 | -1.3 | 25 |
| +y center | 1.3 | 200 | 1.4 | 200 | -0.1 | 0 |
| DM4 | 1.0 | 185 | 0.8 | 200 | 0.2 | -15 |
| DM2 | 0.9 | 105 | 0.7 | 105 | 0.2 | 0 |
| DM5 | 1.3 | 185 | 0.8 | 160 | 0.5 | 25 |
| -x center | 0.7 | 190 | 0.5 | 190 | 0.2 | 0 |
| DM3 | 1.1 | 195 | 0.9 | 200 | 0.2 | -5 |
| DM9 | 5.1 | 105 | 2.7 | 140 | 2.4 | -35 |
| DM7 | 3.1 | 105 | 1.8 | 110 | 1.3 | -5 |
| DM10 | 9.2 | 105 | 4.9 | 110 | 4.3 | -5 |
| -y center | 0.6 | 195 | 0.7 | 200 | -0.1 | -5 |
| DM8 | 3.8 | 195 | 3.1 | 200 | 0.7 | -5 |

Table 4.1.6: Comparison of Amplification factor and resonant frequency(200-300Hz).

| Units | Experiment | | Analysis | | Difference | |
|-----------|------------|--------------------|----------|--------------------|------------|--------------------|
| | AF | Resonant Frequency | AF | Resonant frequency | AF | Resonant frequency |
| DM1 | 1.3 | 280 | 0.9 | 275 | 0.4 | 5 |
| PCU | 1.4 | 275 | 1.6 | 300 | -0.2 | -25 |
| Battery | 0.9 | 280 | 0.8 | 300 | 0.1 | -20 |
| +x center | 1.5 | 250 | 1.0 | 260 | 0.5 | -10 |
| DM6 | 2.1 | 215 | 1.7 | 220 | 0.4 | -5 |
| OBC | 9.3 | 300 | 5.0 | 260 | 4.3 | 40 |
| RF | 5.5 | 240 | 2.9 | 245 | 2.6 | -5 |
| +y center | 2.8 | 240 | 1.6 | 255 | 1.2 | -15 |
| DM4 | 1.2 | 230 | 0.8 | 235 | 0.4 | -5 |
| DM2 | 1.0 | 250 | 0.9 | 225 | 0.1 | 25 |
| DM5 | 1.6 | 230 | 1.4 | 245 | 0.2 | -15 |
| -x center | 1.3 | 295 | 1.1 | 225 | 0.2 | 70 |
| DM3 | 1.3 | 245 | 1.2 | 240 | 0.1 | 5 |
| DM9 | 1.3 | 250 | 0.9 | 255 | 0.4 | -5 |
| DM7 | 1.2 | 245 | 0.9 | 255 | 0.3 | -10 |
| DM10 | 2.3 | 260 | 1.5 | 280 | 0.8 | -20 |
| -y center | 0.5 | 280 | 0.8 | 250 | -0.3 | 30 |
| DM8 | 4.7 | 205 | 2.9 | 220 | 1.8 | -15 |

FFT was used to calculate the corresponding frequency wave forms. The analysis results show that the most significant peak frequency is 40 Hz in the 20-100Hz range. The highest amplitude of the frequency waveform occurs around 40-45Hz. It was found that the FEM model generated peak amplification at 40Hz and 45Hz that is very similar to that generated by the experiment. The analysis results were consistent with the results of the experiment . This means that the setting of FEM of a dummy satellite analysis can provide for other types of structures.

4.1.3 Analysis results of other types of satellites and their statistics

In this part results of Finite element analysis of other satellite models are discussed. Table 4.1.7-Table 4.1.9 shows the analysis result data of T-type structure of horizontal and vertical vibration direction and plotted in Figure 4.1.2 - 4.1.3 respectively.

Table 4.1.7: Peak Amplification factor and Resonant frequency statistics of
T-type structure (horizontal1).

| | 20-100Hz | | 100-200Hz | | 200-300Hz | |
|---------|----------|------------------------|-----------|------------------------|-----------|------------------------|
| | AF | Resonant frequency[Hz] | AF | Resonant frequency[Hz] | AF | Resonant frequency[Hz] |
| SENSOR1 | 3.86 | 50 | 0.97 | 160 | 1.42 | 290 |
| SENSOR2 | 3.04 | 50 | 0.53 | 185 | 0.68 | 300 |
| SENSOR3 | 4.47 | 50 | 0.59 | 125 | 0.35 | 270 |
| SENSOR4 | 2.41 | 50 | 1.2 | 160 | 1.58 | 260 |
| SENSOR5 | 3.87 | 50 | 0.52 | 125 | 0.71 | 295 |
| SENSOR6 | 6.2 | 50 | 0.97 | 125 | 0.28 | 285 |
| SENSOR7 | 3.44 | 50 | 1.66 | 150 | 2 | 270 |
| SENSOR8 | 2.36 | 55 | 1.76 | 160 | 3.86 | 290 |

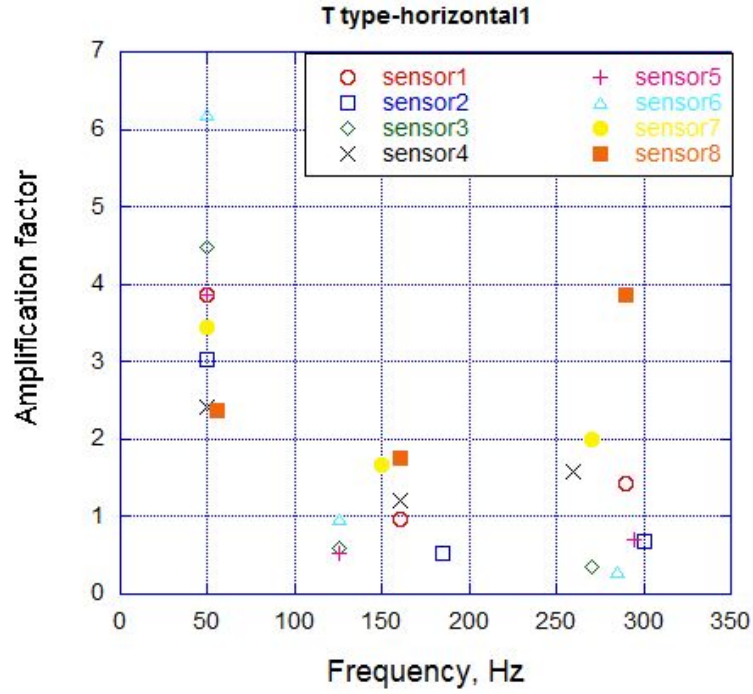


Figure 4.1.2: Peak amplification factor and resonant frequency (T-type, horizontal1).

Table 4.1.8: Peak Amplification factor and Resonant frequency statistics of T-type structure (horizontal2).

| | 20-100Hz | | 100-200Hz | | 200-300Hz | |
|---------|----------|------------------------|-----------|------------------------|-----------|------------------------|
| | AF | Resonant frequency[Hz] | AF | Resonant frequency[Hz] | AF | Resonant frequency[Hz] |
| SENSOR1 | 2.34 | 50 | 1.04 | 180 | 1.9 | 300 |
| SENSOR2 | 2.03 | 50 | 1.62 | 200 | 1.91 | 205 |
| SENSOR3 | 3.07 | 50 | 1.06 | 200 | 1.99 | 275 |
| SENSOR4 | 1.24 | 50 | 1 | 180 | 1.66 | 300 |
| SENSOR5 | 3.42 | 55 | 2.05 | 200 | 2.33 | 205 |
| SENSOR6 | 4.2 | 55 | 1.27 | 185 | 2.43 | 270 |
| SENSOR7 | 1.05 | 55 | 0.63 | 200 | 0.87 | 210 |
| SENSOR8 | 3.81 | 50 | 0.55 | 170 | 0.58 | 280 |

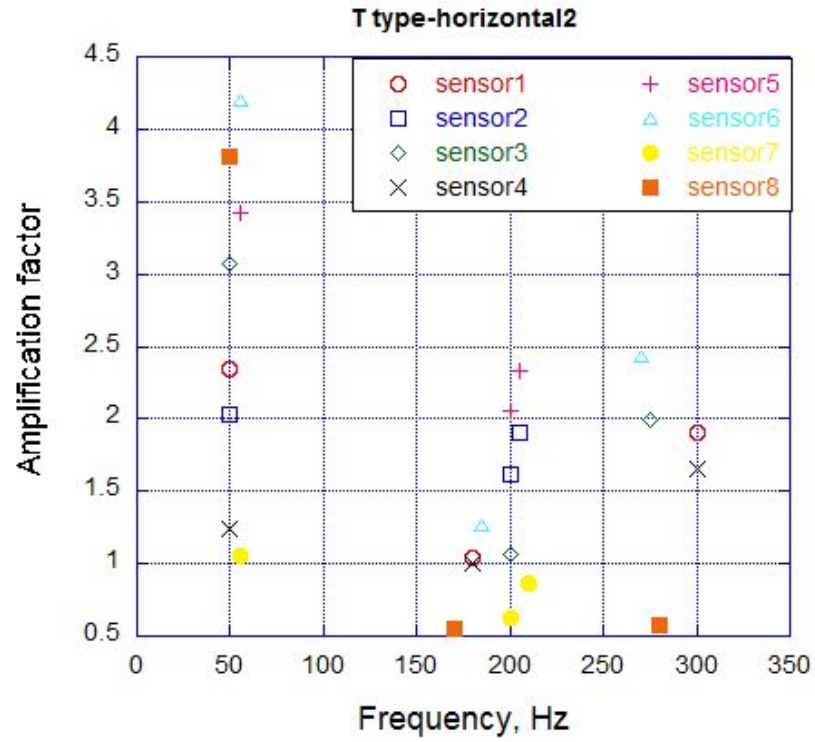


Figure 4.1.3: Peak amplification factor and resonant frequency (T-type, horizontal2).

Table 4.1.9: Peak Amplification factor and Resonant frequency statistics of T-type structure (vertical).

| | 20-100Hz | | 100-200Hz | | 200-300Hz | |
|---------|----------|------------------------|-----------|------------------------|-----------|------------------------|
| | AF | Resonant frequency[Hz] | AF | Resonant frequency[Hz] | AF | Resonant frequency[Hz] |
| SENSOR1 | 0.21 | 50 | 0.7 | 120 | 1.19 | 240 |
| SENSOR2 | 0.28 | 50 | 0.84 | 170 | 1.61 | 270 |
| SENSOR3 | 0.15 | 50 | 1.07 | 200 | 1.59 | 205 |
| SENSOR4 | 0.12 | 45 | 1.31 | 135 | 1.31 | 210 |
| SENSOR5 | 0.15 | 100 | 0.91 | 120 | 0.98 | 205 |
| SENSOR6 | 0.2 | 100 | 0.83 | 200 | 0.77 | 205 |
| SENSOR7 | 0.16 | 35 | 1.52 | 150 | 1.12 | 275 |
| SENSOR8 | 0.19 | 50 | 1.83 | 125 | 1.45 | 205 |

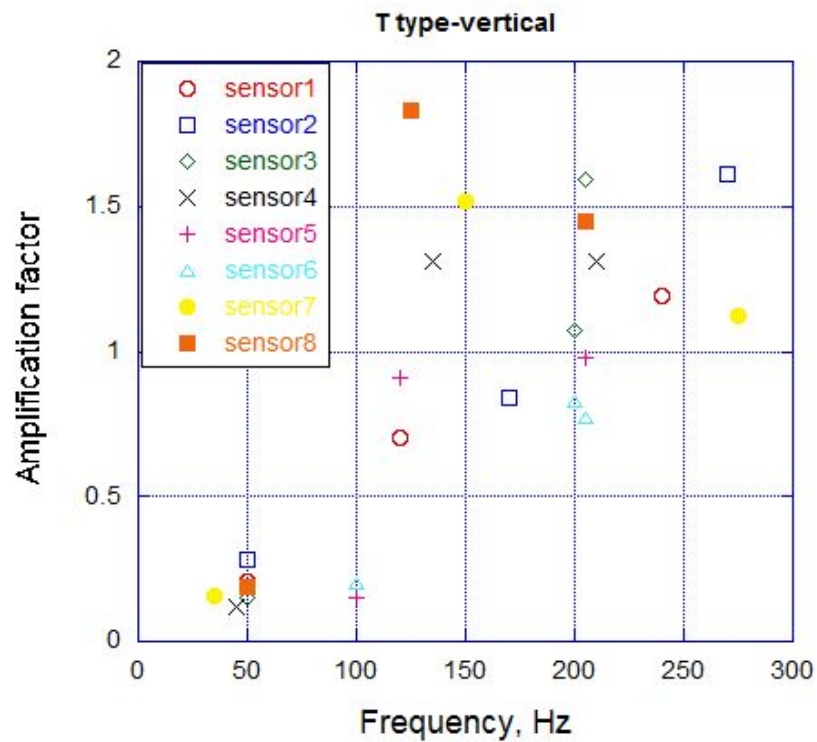


Figure 4.1.4: Peak amplification factor and resonant frequency (T-type, vertical).

Tables 4.1.10-4.1.11 indicate the peak amplification factor and resonant frequency statistics of the Pi-type structure in three different frequency groups and the data are plotted in Figure 4.1.5-4.1.7.

Table 4.1.10: Peak Amplification factor and Resonant frequency statistics of

Pi-type structure (horizontal1).

| | 20-100Hz | | 100-200Hz | | 200-300Hz | |
|---------|----------|------------------------|-----------|------------------------|-----------|------------------------|
| | AF | Resonant frequency[Hz] | AF | Resonant frequency[Hz] | AF | Resonant frequency[Hz] |
| SENSOR1 | 2.13 | 50 | 0.15 | 190 | 0.68 | 255 |
| SENSOR2 | 1.63 | 50 | 0.11 | 155 | 0.79 | 290 |
| SENSOR3 | 1.81 | 50 | 0.22 | 185 | 0.72 | 295 |
| SENSOR4 | 2.00 | 50 | 0.21 | 185 | 0.98 | 255 |
| SENSOR5 | 2.40 | 50 | 0.15 | 145 | 1.13 | 255 |
| SENSOR6 | 2.11 | 50 | 0.15 | 190 | 0.61 | 280 |
| SENSOR7 | 2.03 | 50 | 0.20 | 190 | 0.61 | 260 |
| SENSOR8 | 1.42 | 50 | 0.18 | 190 | 0.42 | 260 |

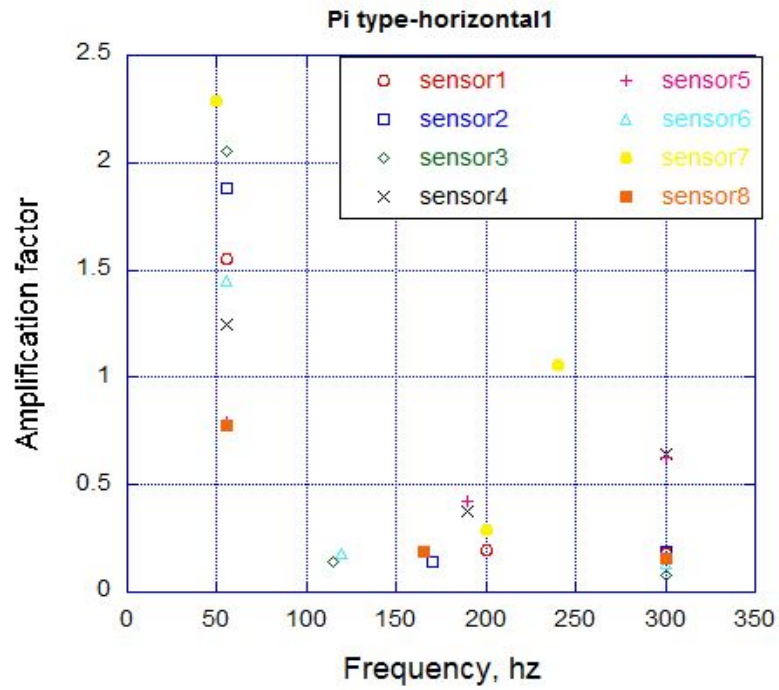


Figure 4.1.5: Peak amplification factor and resonant frequency
(Pi-type, horizontal1).

Table 4.1.11: Peak Amplification factor and Resonant frequency statistics of

Pi-type structure (horizontal2).

| | 20-100Hz | | 100-200Hz | | 200-300Hz | |
|---------|----------|------------------------|-----------|------------------------|-----------|------------------------|
| | AF | Resonant frequency[Hz] | AF | Resonant frequency[Hz] | AF | Resonant frequency[Hz] |
| SENSOR1 | 1.55 | 55 | 0.2 | 200 | 0.18 | 300 |
| SENSOR2 | 1.88 | 55 | 0.14 | 170 | 0.19 | 300 |
| SENSOR3 | 2.05 | 55 | 0.14 | 115 | 0.08 | 300 |
| SENSOR4 | 1.25 | 55 | 0.38 | 190 | 0.64 | 300 |
| SENSOR5 | 0.79 | 55 | 0.42 | 190 | 0.63 | 300 |
| SENSOR6 | 1.45 | 55 | 0.18 | 120 | 0.13 | 300 |
| SENSOR7 | 2.29 | 50 | 0.29 | 200 | 1.06 | 240 |
| SENSOR8 | 0.78 | 55 | 0.19 | 165 | 0.16 | 300 |

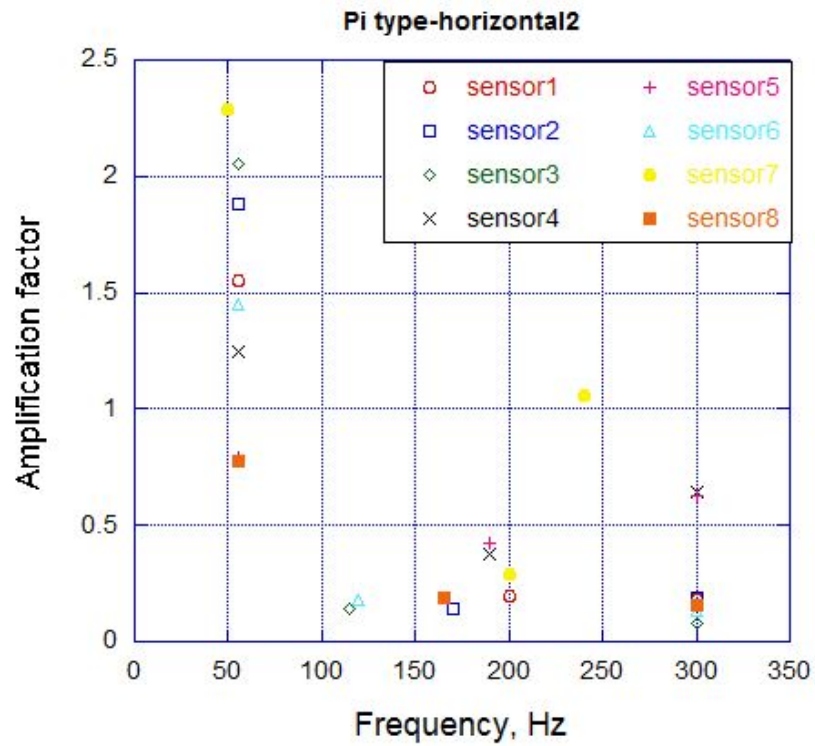


Figure 4.1.6: Peak amplification factor and resonant frequency (Pi-type, horizontal2).

Table 4.1.12: Peak Amplification factor and Resonant frequency statistics of

Pi-type structure (vertical).

| | 20-100Hz | | 100-200Hz | | 200-300Hz | |
|---------|----------|------------------------|-----------|----------------------|-----------|------------------------|
| | AF | Resonant frequency[Hz] | AF | Resonant frequency[H | AF | Resonant frequency[Hz] |
| SENSOR1 | 1.32 | 100 | 6.3 | 190 | 11 | 240 |
| SENSOR2 | 1.21 | 100 | 4.31 | 190 | 6.34 | 240 |
| SENSOR3 | 0.82 | 100 | 1.86 | 190 | 2.87 | 240 |
| SENSOR4 | 0.5 | 100 | 0.92 | 190 | 2.69 | 235 |
| SENSOR5 | 0.8 | 100 | 1.52 | 190 | 2.54 | 235 |
| SENSOR6 | 1.14 | 100 | 2.21 | 185 | 3.62 | 235 |
| SENSOR7 | 1.17 | 100 | 2.92 | 190 | 6.64 | 235 |
| SENSOR8 | 1.23 | 100 | 4.29 | 190 | 8.27 | 240 |

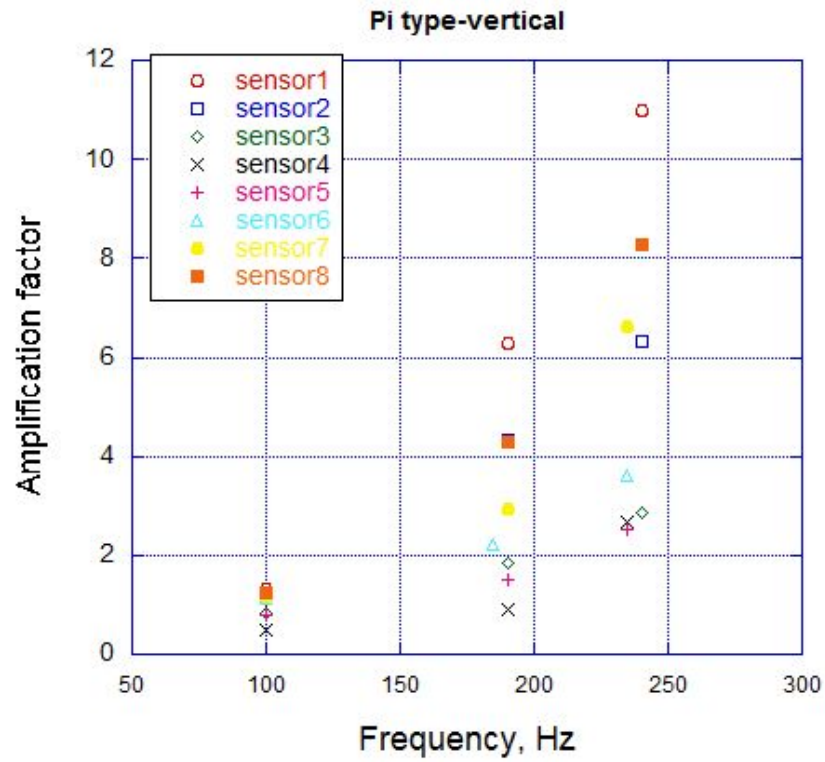


Figure 4.1.7: Peak amplification factor and resonant frequency (Pi-type, vertical).

The analysis result of peak amplification factor and resonant frequency of the virtual sensor at the top corner positions and the statistics of 7 satellites used for whole satellite mode are shown in Table 4.1.13.

Table 4.1.13: Peak Amplification factor and Resonant frequency of top sensor.

| | Model | 20-300Hz | | | | | |
|----------|-----------------------------|--------------------|-------------------|--------------|----------------------|--------------|----------|
| | | Resonant frequency | | | Amplification factor | | |
| | | Horizon tal1, Hz | Horizon tal 2, Hz | Vertical, Hz | Horizon tal1 | Horizon tal2 | Vertical |
| Analysis | Yojo-han | 45 | 40 | 150 | 8.3 | 6.8 | 4.1 |
| | T-type | 55 | 50 | 180 | 6.4 | 5.2 | 3.1 |
| | Pi-type | 55 | 50 | 200 | 4.6 | 3.9 | 4.3 |
| | | | | | | | |
| Test | Satellite-A (center pillar) | 62 | 59 | 165 | 8.2 | 10.4 | 8.0 |
| | Satellite-B (Pi type) | 56.3 | 43.8 | 165.6 | 4.21 | 5.18 | 5.86 |
| | Satellite-C (T-type) | 48.8 | 44.6 | 186 | 6.52 | 5.75 | 7.56 |
| | Satellite-D (T-type) | 44.6 | 40.9 | 144 | 7.31 | 7.27 | 5.05 |
| | Satellite-E (T-type) | 61 | 61 | 208 | 5.73 | 6.92 | 3.39 |
| | Satellite-F (yojohan) | 32.3 | 29.3 | 144 | 6.78 | 5.19 | 3.27 |
| | Satellite-G (Pi type) | 70 | 65 | 190 | - | - | - |

Each satellite has different resonance and amplification as shown in Tables 2.4.11-2.4.12. The table shows analysis result of maximum amplification factor and resonant frequency in the range 20-300Hz for dummy satellite model, T and Pi type model. If we compare these values to the real satellites measurement data, we could see similar results but not uniformly same. Because, these structure models are generic types of micro/nano satellite structures with same materials, components and sizes etc. Those 7 satellites have

different internal structure, some satellites are similar to Pi type such as Satellite-B and G, Satellite-A has center pillar internal structure, some of them are similar internal panel of T-type i.e Satellites C-E, and satellite F is same internal structure as yojo-han structure model. Although these satellites have similar internal panel structures to the analyzed models, the materials, panel connections, component masses and positions are different from the analyzed models. These are the reasons of some small differences for resonant frequencies and amplification factors between real satellites and analyzed data.

4.2 Derivation of unit QT conditions

Derivation of unit QT based on the analysis results to cover any type of satellite structure. The same statistical method was used as experiment data. The average value, Standard deviation, Lower and upper value of resonant frequency range were estimated based on the analysis data as listed in Table 4.2.1-4.2.6.

Table 4.2.1~Table 4.2.6 are based on the virtual sensors placed inside a satellite. The unit QT derived by the experiment used the sensor at the top corner of the satellite in the range 20-300Hz. For the range 300-2000Hz, the Unit QT used the sensors placed inside the satellites. The best way to define the unit QT level is to use existing real satellite vibration test data. If we had internal panel sensor data of those 7 satellites, we did not have to limit up to 300Hz. But unfortunately, the author did not measure inside of those satellites, for these various satellites, the author had only vibration test data of top position on external panel. That is why inside measurement data was needed. These internal sensors information is more important because the author is deriving Unit QT

level. The units are mostly placed at internal panels. In external panel data, the amplification and the resonant frequency can be seen in the range 20-300Hz.

Table 4.2.1: Resonant frequency range of dummy satellite model (20-300Hz).

| | Resonant frequency [Hz] | | |
|--------------------|-------------------------|----------------|--------------|
| | T1(horizontal) | T3(horizontal) | T2(vertical) |
| Average | 41.9 | 42.5 | 135.6 |
| Standard deviation | 10.2 | 10.3 | 47.9 |
| Lower value | 36.9 | 37.4 | 111.7 |
| Upper value | 47.0 | 47.6 | 159.4 |

Table 4.2.2: Normal tolerance limit of amplification factor of dummy satellite model, 20-300Hz (log values are shown in bracket).

| | Amplification Factor | | |
|--------------------|----------------------|----------------|-------------------|
| | T1(horizontal) | T3(horizontal) | T2(vertical) |
| Average | 5.5(0.71) | 4.9(0.69) | 3.3(0.52) |
| Standard deviation | 1.4(0.15) | 1.41(0.15) | 1.12(0.05) |
| NTL(min) | 2.88(0.46) | 2.75(0.44) | 2.69(0.43) |
| NTL(max) | 9.12(0.96) | 8.71(0.94) | 3.98(0.6) |

Table 4.2.3: Resonant frequency range of T-type ,20-300Hz.

| | Resonant frequency [Hz] | | |
|--------------------|-------------------------|----------------|--------------|
| | T1(horizontal) | T3(horizontal) | T2(vertical) |
| Average | 50.6 | 51.9 | 200.6 |
| Standard deviation | 2.3 | 6.6 | 99.3 |
| Lower value | 48.7 | 46.5 | 119.8 |
| Upper value | 52.5 | 57.3 | 281.4 |

Table 4.2.4: Normal tolerance limit of amplification factor of T type, 20-300Hz

(log values are shown in bracket).

| | Amplification Factor | | |
|--------------------|----------------------|----------------|---------------------|
| | T1(horizontal) | T3(horizontal) | T2(vertical) |
| Average | 3.80(0.58) | 2.45 (0.39) | 1.32 (0.12) |
| Standard deviation | 1.32(0.12) | 1.58 (0.20) | 1.32 (0.12) |
| NTL(min) | 2.40(0.38) | 1.17(0.07) | 0.85 (-0.07) |
| NTL(max) | 5.89(0.77) | 5.25 (0.72) | 2.04 (0.31) |

Table 4.2.5: Resonant frequency range of Pi-type.(20-300Hz).

| | Resonant frequency [Hz] | | |
|--------------------|-------------------------|----------------|---------------|
| | T1(horizontal) | T3(horizontal) | T2(vertical) |
| Average | 50.00 | 55.00 | 237.50 |
| Standard deviation | 0.00 | 0.00 | 2.67 |
| Lower value | 50.00 | 55.00 | 235.33 |
| Upper value | 50.00 | 55.00 | 239.67 |

Table 4.2.7 lists the overall value of the log normal limit of the peak amplification factor and resonant frequency range deduced both from the statistics of the three satellite structures.

The estimated range of resonant frequency and the Normal tolerance limit in the frequency range 20-300Hz shows that the minimum normal tolerance limit of the amplification factors of the T-type and Pi-type structure are lower than the amplification of the dummy satellite. That means the Unit QT level derived from the experiment results (i.e. Figure 2.4.7) is applicable.

Table 4.2.6: Normal tolerance limit of amplification factor of Pi type, 20-300Hz

(log values are shown in bracket).

| | Amplification factor | | |
|--------------------|----------------------|----------------|-------------------|
| | T1(horizontal) | T3(horizontal) | T2(vertical) |
| Average | 1.91(0.28) | 0.19 (-0.72) | 4.79 (0.68) |
| Standard deviation | 1.17 (0.07) | 1.51 (0.18) | 1.79 (0.25) |
| NTL(min) | 1.48 (0.17) | 0.10 (-1.00) | 1.93(0.29) |
| NTL(max) | 2.51 (0.40) | 0.36 (-0.44) | 11.84(1.07) |

The statistical results shown in Table 4.2.4 and Table 4.2.6 express that the minimum log normal tolerance limit of the amplification factors are lower than the amplification factor that was derived from the experiment data. From the statistical results of dummy satellite, T and Pi type structure, the following notices can be stated. There are several peaks in the frequency range, depending on the vibration direction. We took maximum value of minimum amplification factors in perpendicular to the axial direction (i.e. horizontal (T1)) for each satellite for further verification. For Pi type and T type structure, 1.93 and 2.4 were obtained for the verification of the minimum test level in the range 20-300Hz while 2.88 is obtained from the statistics from the dummy satellite analysis data. Taking into consideration of satellite to satellite variation, we had to choose the maximum value (i.e. 4.2) among dummy satellite experiment data, Pi and T-type structure analysis data.

Table 4.2.7: Overall statistics of experiment and analysis

| | Horizontal | | Vertical | |
|---|--------------------------------------|---------------------------|--------------------------------------|---------------------------|
| | Resonant frequency (horizontal) [Hz] | Peak amplification factor | Resonant frequency (horizontal) [Hz] | Peak amplification factor |
| Experiment (Statistics of 7 satellites using the sensor at the top corner) | 20~101 | 4.2 | 101~270 | 2.6 |
| Experiment (Yojyo-han, i.e. Dummy satellite) statistics of the internal sensors | 300~1000 1000~2000 | 1.15 1 | 300-1000 1000-2000 | 1 1 |
| Experiment (Yojyohan, 20-300Hz) | 20-89.7 | 2.88 | 20-302.1 | 2.45 |
| Analysis (Yojyo-han) statistics of the internal sensors | 37-48 | 2.9 | 112-159 | 2.6 |
| Analysis (T-type) statistics of the internal sensors | 49-57 | 2.4 | 120-281 | 0.85 |
| Analysis (Pi-type) statistics of the internal sensors | 50-55 | 1.48 | 235-240 | 1.93 |

5. Conclusions and Future work

5.1 Conclusions

The author aimed to propose the minimum guarantee that a given unit sold as “a satellite unit” has a certain level of tolerance against space environment. In order to determine unit QT level a series of random vibration test were conducted up to 2,000Hz. Two test articles were used. They represent 50cm class satellites. The author noticed two vibration modes, “whole satellite mode” and “local vibration mode”. The first one corresponds to the whole satellite mode and the second and third ones correspond to the local vibration mode. The peak amplification factors and resonant frequencies were deduced within those three ranges. Based on statistical analysis, the author defined the range of resonant frequencies and the log normal tolerance limit of the peak amplification factors. The maximum value in the lower limits of the peak amplification among the three excited vibration directions was proposed as the unit QT level test.

In order to cover wide range of structural styles expected in micro/nano satellites, structural analysis was carried out using a finite element analysis (FEA) software. In the analysis, the acceleration inside various types of satellites i.e yojo-han, T-type and Pi type was calculated. The results are used to update the unit QT level proposed before.

Based on the experiment and analysis results, the following specific conclusions can be drawn:

1. This work presents extrapolation to T-type and Pi type FEM where the numerical model was used to predict vibration acceleration response at specific points inside the satellite models. The vibration amplification waveforms generated by dummy satellite model is investigated and verified by comparing the analysis results with the experimental data.
2. The experimental and numerical analyses of this work have both indicated that there are several vibration modes for the satellites and that are mainly associated with the internal panel structure of the satellites.
3. The finite element modal analysis of the simplified model based on the original CAD drawings of the dummy satellite has introduced amplification peaks and their resonant frequencies, both of which are close to the experimental ones. That is expected, the Unit QT level derived from the experiment results is applicable, especially at lower frequency modes. However, the FE modal analysis may introduce errors if it is used to investigate vibration acceleration response and resonant frequencies associated with higher and most local vibration modes beyond 200Hz of the satellites.
4. Knowing the problem at resonant frequencies that can cause higher acceleration at specific points at internal panels where units or components are mounted to the micro/nano satellites, it may become possible to propose a solution to avoid the resonance in satellites by introducing vibration distribution study of the tested and analyzed structures.

5. From the analysis results it can be concluded that the unit QT level derived from the experiment is acceptable for the various types of micro/nano satellite structures.

5.2 Future works

The overall research was extensive. But all of the main objectives were achieved. Nevertheless, there are some aspects that may still be studied further and improved. We would like to give some suggestions and directions for additional work which may be developed in future.

The real test model (dummy satellite) with flight quality is one of the main contributors to the achievement of the study. For the presented study the dummy satellite which has flight quality was tested to develop the Unit QT level. The dummy satellite is already equipped with dummy masses heater inside and satellite main components such as PCU, RF, OBC and Battery. We may need dummy satellite of other type of satellites to confirm the analysis results by comparing analysis and real experimental results.

The simplified model of the dummy satellite is still good when FEA methods are used for analysis. But when small parts are simulated then the performance could not be optimal. In fact, modelling of every small parts are still important. We may need to model real 3D CAD model of other types of satellites.

Another drawback of having not good agreement of the resonant frequency and amplification in higher frequency may be represented by the non-linearity of the model in higher vibration acceleration. One suggestion would be to study a non-linear analysis for FEM models and which may cover a wider range of vibration level as possible.

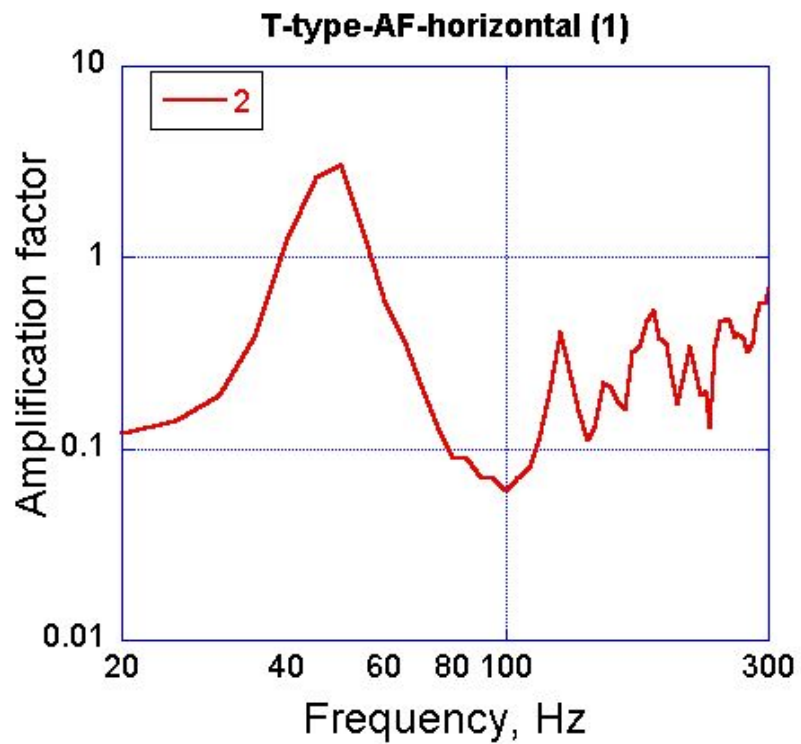
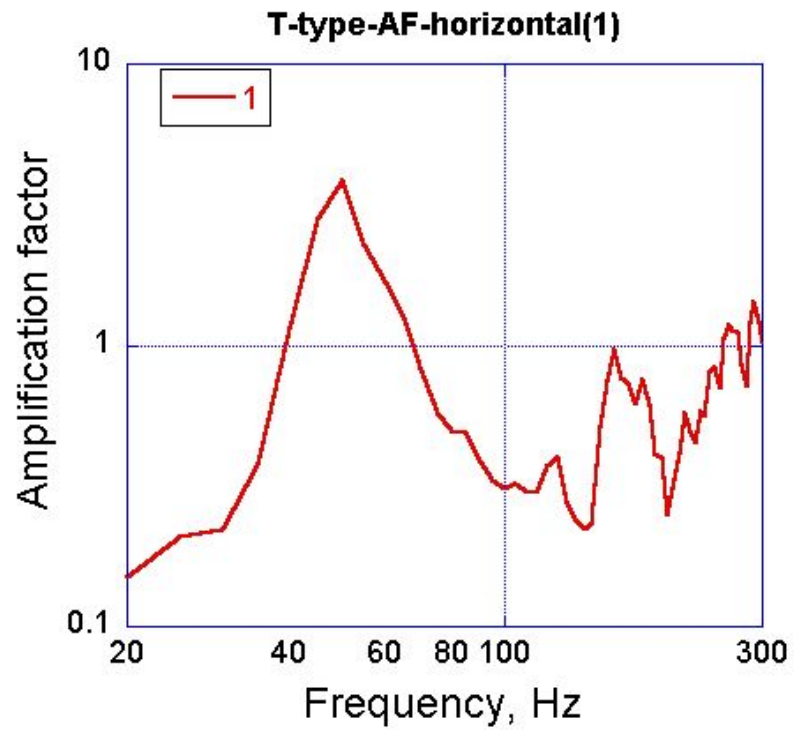
References

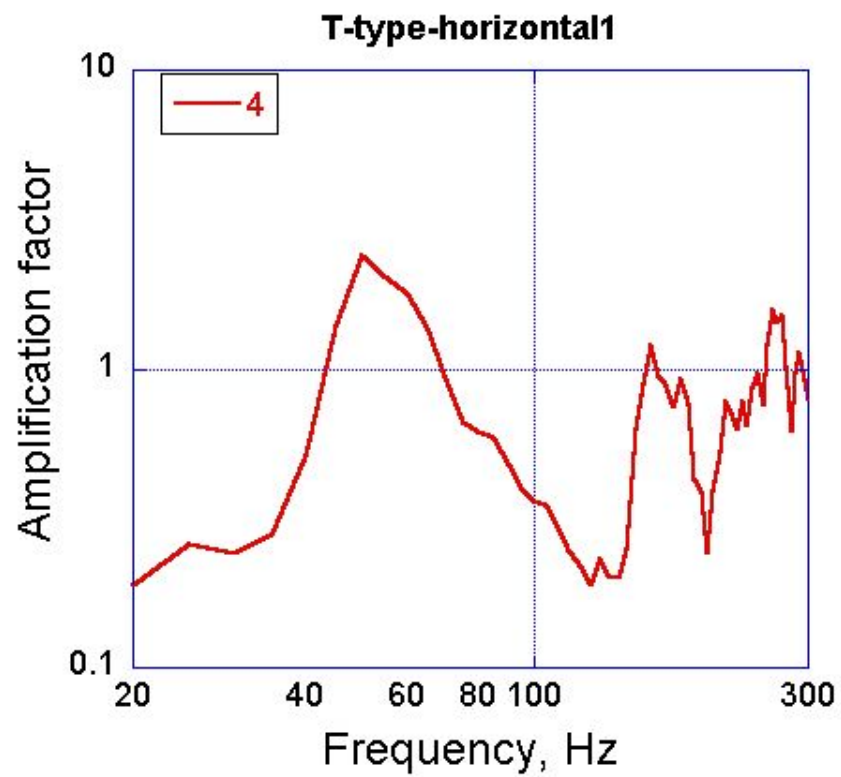
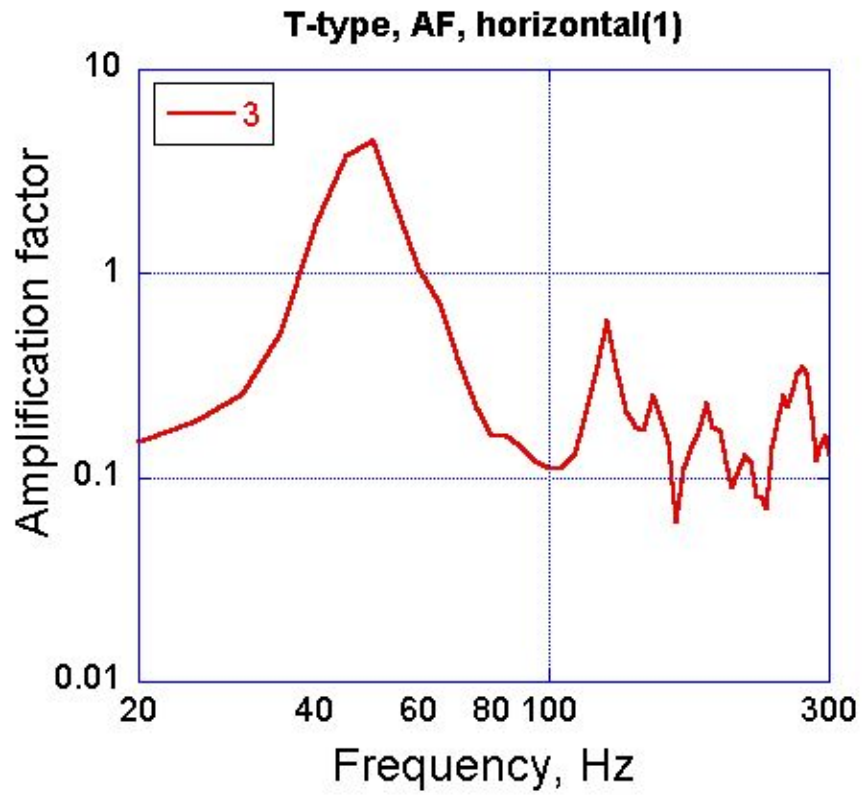
1. Cho, M., Date, K., Horii, S. and Obata, S.: Introduction of Nanosatellite Environment Test Standardization (NETS) Project, Background and Objectives, Joint-Conference on Space Technology and Science, 2011, JSASS-2011-4424.
2. NASA Technical Standard NASA-STD-7001, Payload Vibroacoustic Test Criteria.
3. K J Bathe Finite Element Procedures in Engineering Analysis Prentice Hall, New Jersey, 1982
4. B M Irons, S Ahmad Techniques of Finite Elements Ellis Horwood, Chichester, 1980
5. MSC/NASTRAN Handbook for Numerical Methods ,The MacNeal-Schwendler Corporation, Los Angeles, 1990
6. NAFEMS A Finite Element Primer ,National Agency for Finite Element Methods and Standards, 1986
7. O C Zienkiewicz, R L Taylor The Finite Element Method, Vol. 1
8. NASA Handbook NASA-HDBK-7005, March 13, 2001
9. Michael Yang, Paul Blelloch., “Estimation of Maximum Principal Stress from Random Analysis”, Proceeding of Spacecraft and Launch Vehicle Workshop, June 4-6, 2013
10. Chung, Y. T., and Foist, B. L., “Prediction of Payload Random Vibration Loads”, *Proc. 13th Intern. Modal Analysis Conf.*, pp 934-9940, Feb. 1995.
11. Condos, F. M., and Butler, W. L., "A Critical Analysis of Vibration Prediction Techniques," *Proc., Inst. Envir. Sc.*, pp 321-326, 1963.

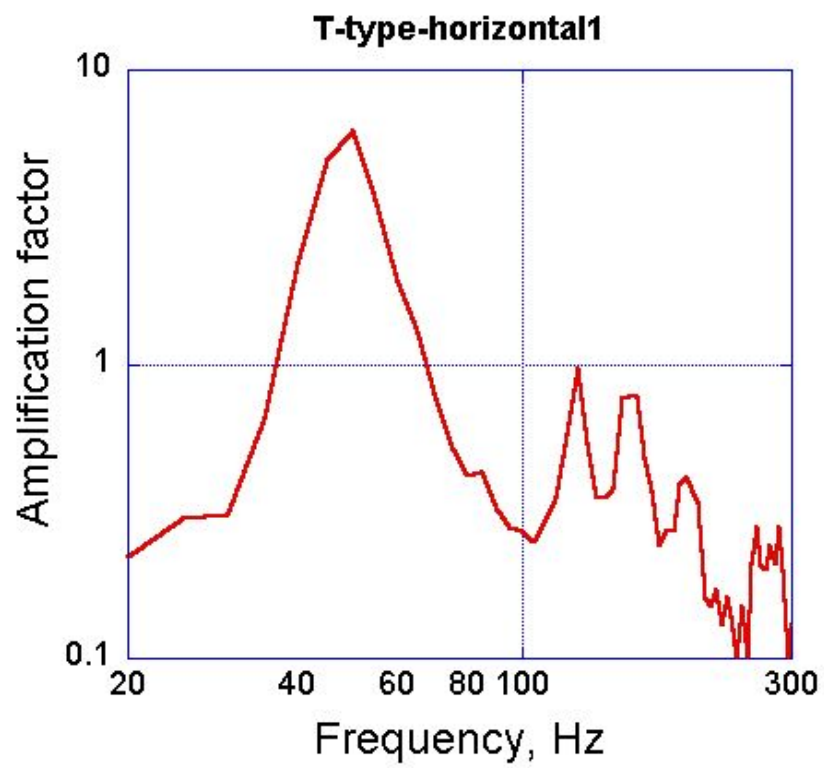
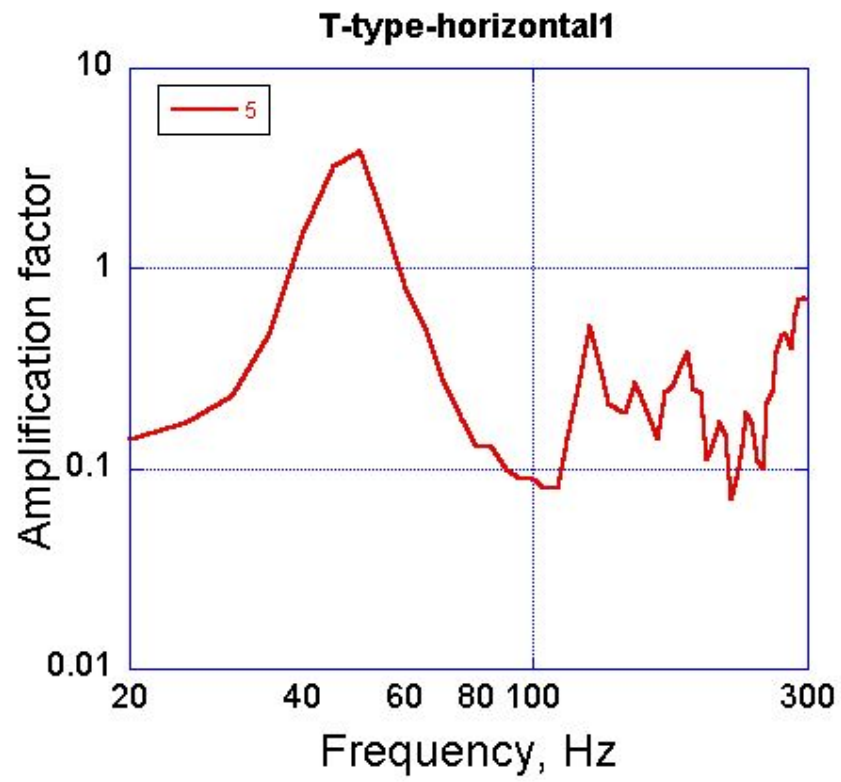
12. Piersol, A. G., "Procedures to Compute Maximum Structural Responses from Predictions or Measurements at Selected Points," Shock and Vibration. Vol. 3, No. 3, pp.211-221, 1996.
13. Barrett, R. E., "Statistical Techniques for Describing Localized Vibration Environments of Rocket Vehicles," NASA TN D-2158, July 1964.
14. Anon., "Procedures Utilized in Developing All-Random Vibration Test Specifications for Titan III," BBN Rep. No. 1083, Bolt Beranek and Newman, Canoga Park, CA, 1964.
15. SMC Standard SMC-S-016, 13 June 2008
16. Batsuren, A., Tomida, K., Hatamura, T., Masui, H. and Cho, M.: Laboratory Tests to standardize Environment Test Conditions of Micro/Nano Satellite Units, Trans JSASS Aerospace Tech Japan, Vol. 12, No. 12, pp. Pf_1-Pf_10, 2014.
17. Tomida, K., Batsuren, A., Hatamura, T., Masui, H. and Cho, M.: Basic Research on Vibration Test Level for Nanosatellite Components, 29th International Symposium on Space Technology and Science, 2013, 2013-f-26.
18. G W Snedecor, W G Cochran, Statistical Methods, Eighth Edition, 1989

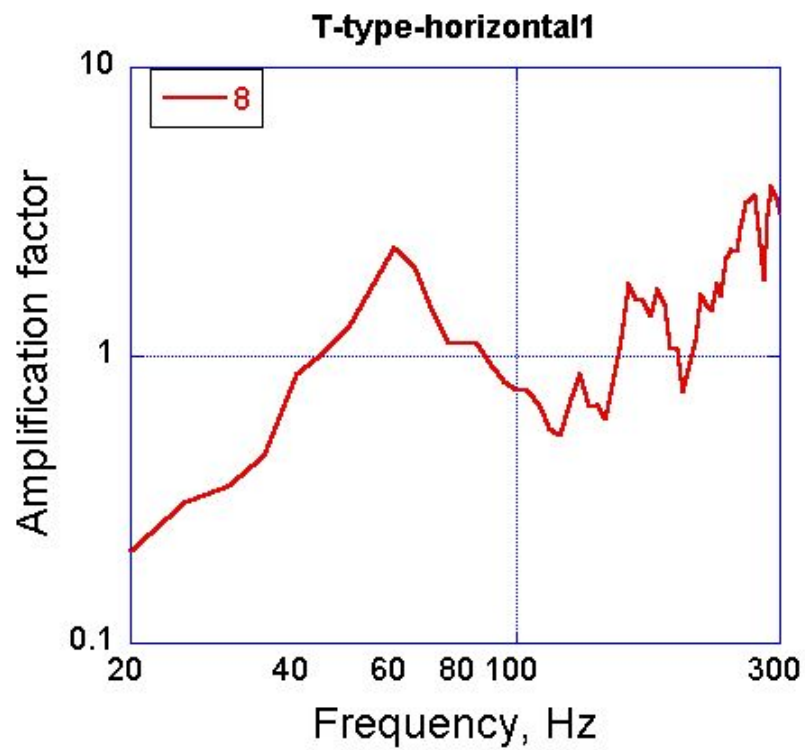
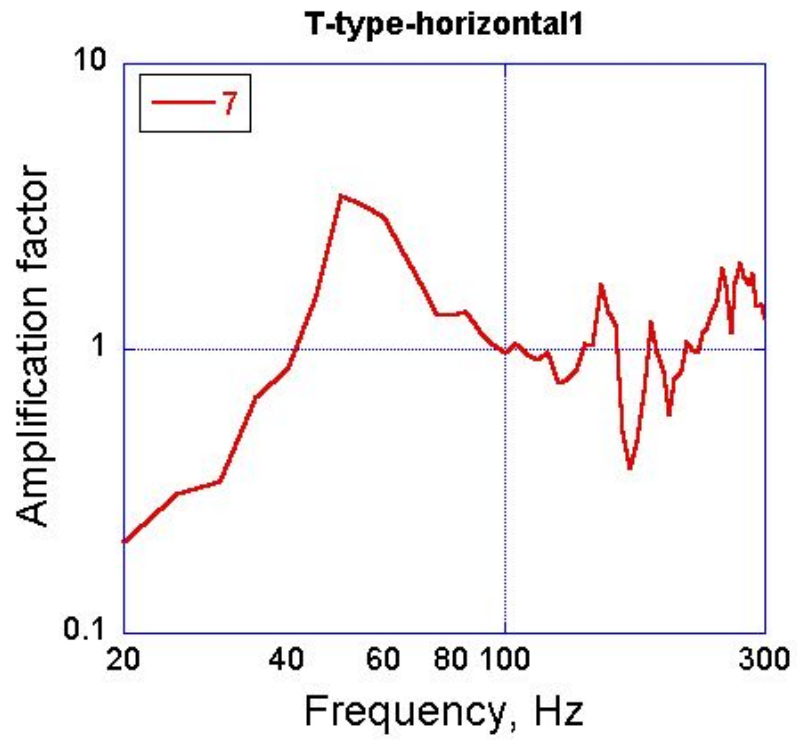
Appendix

Amplification factor. T-Type. Horizontal direction(1)

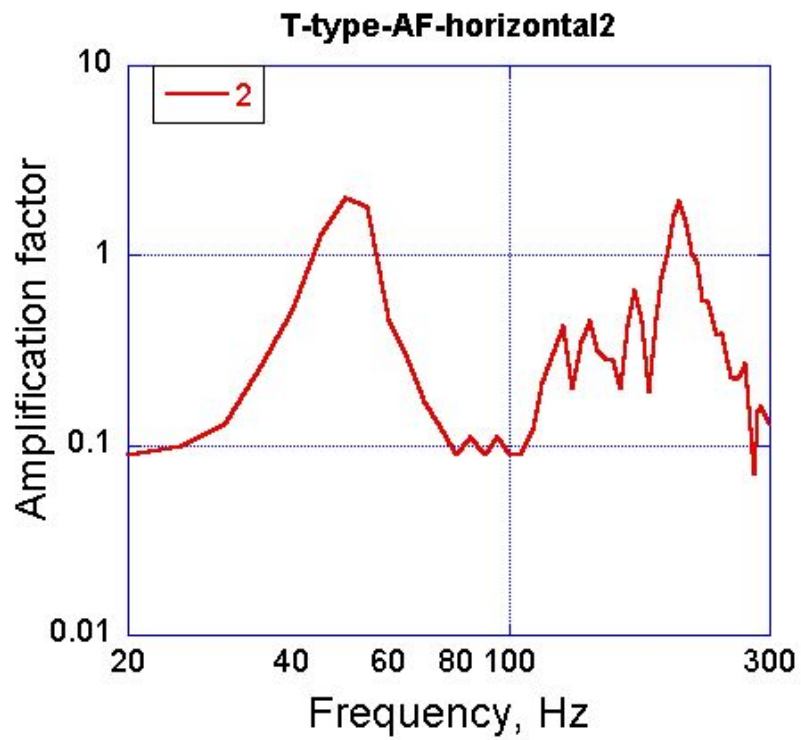
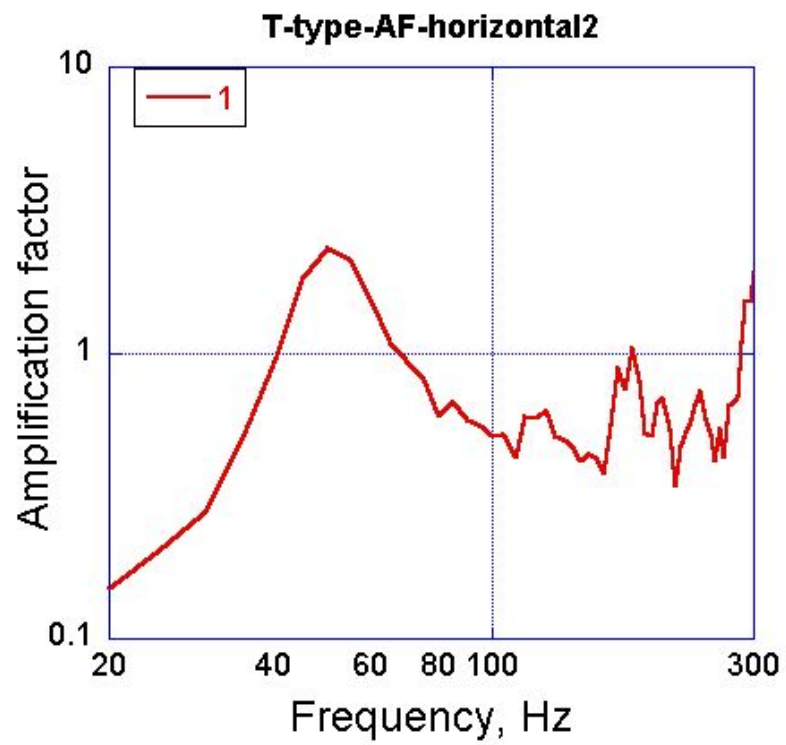


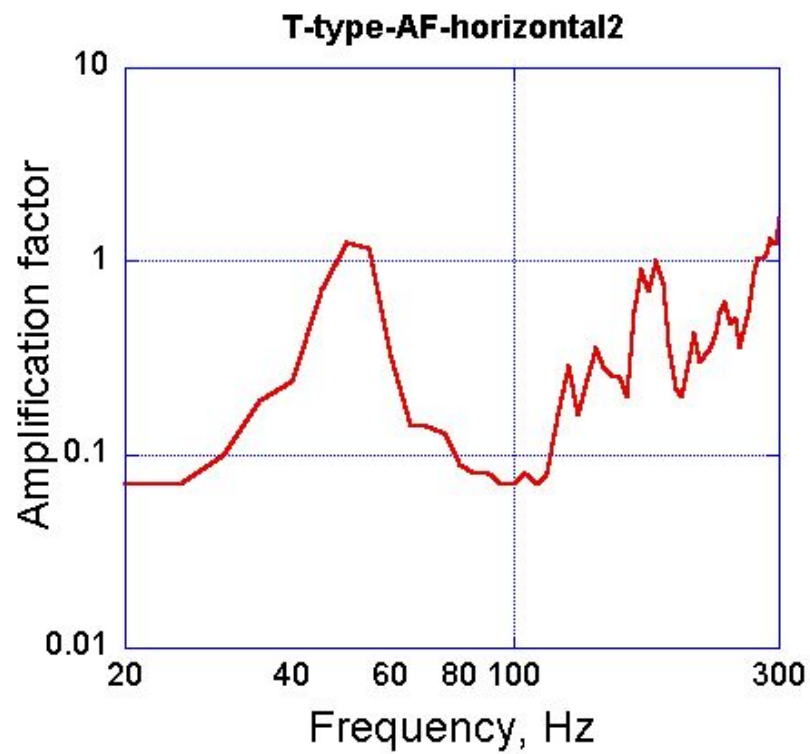
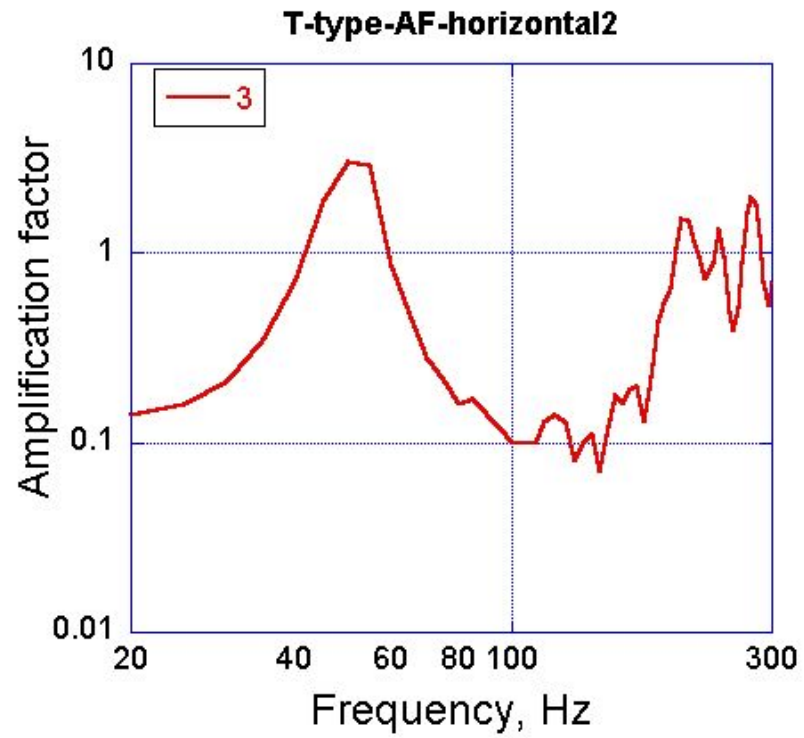


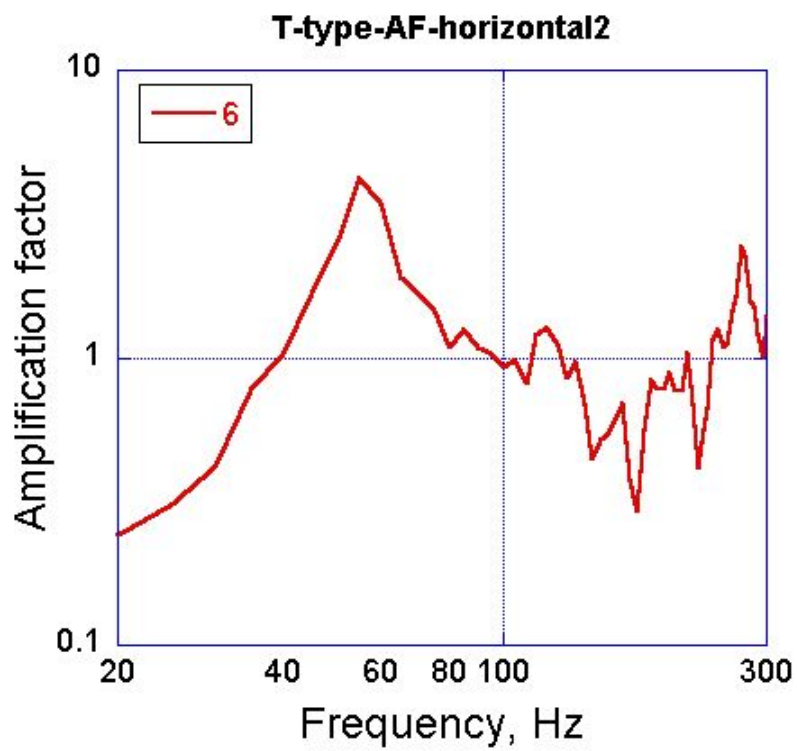
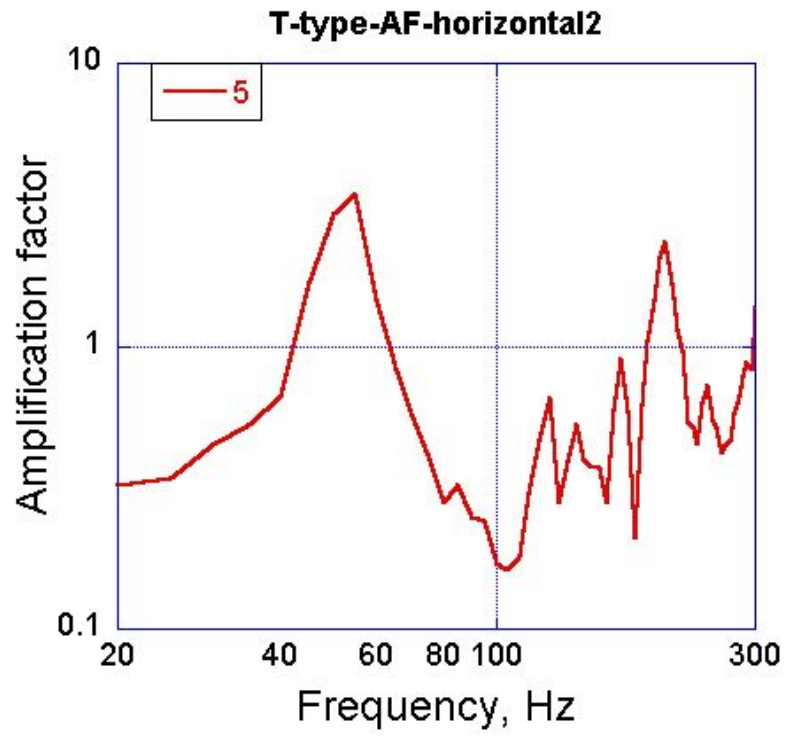


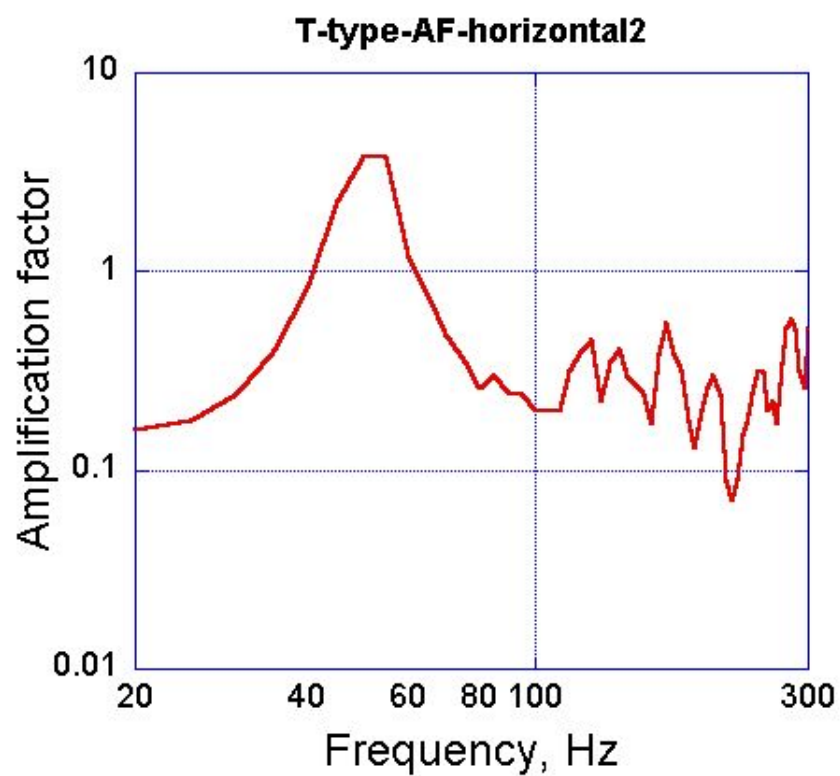
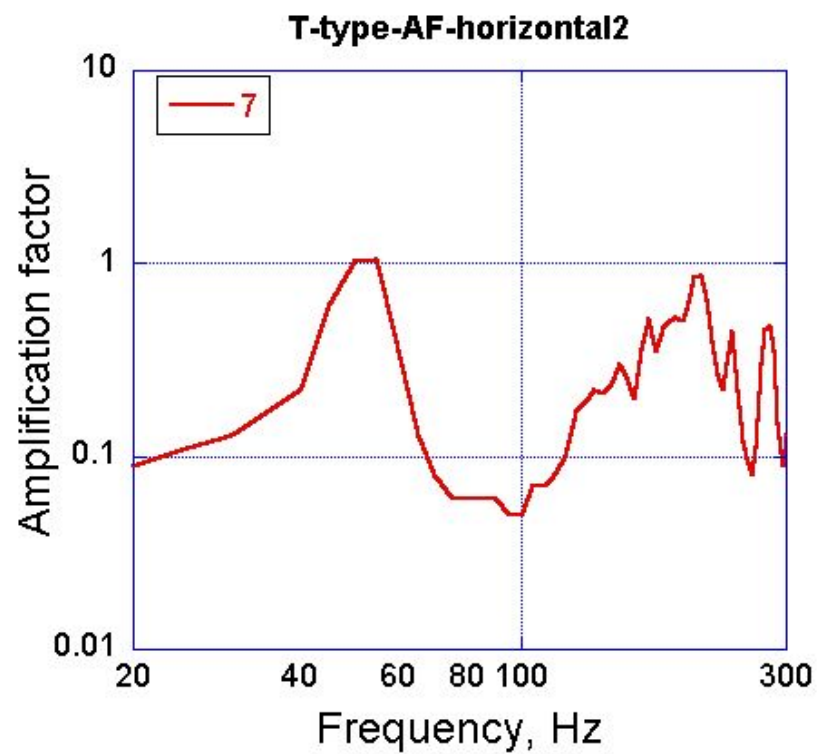


Amplification factor. T-Type. Horizontal direction(2)

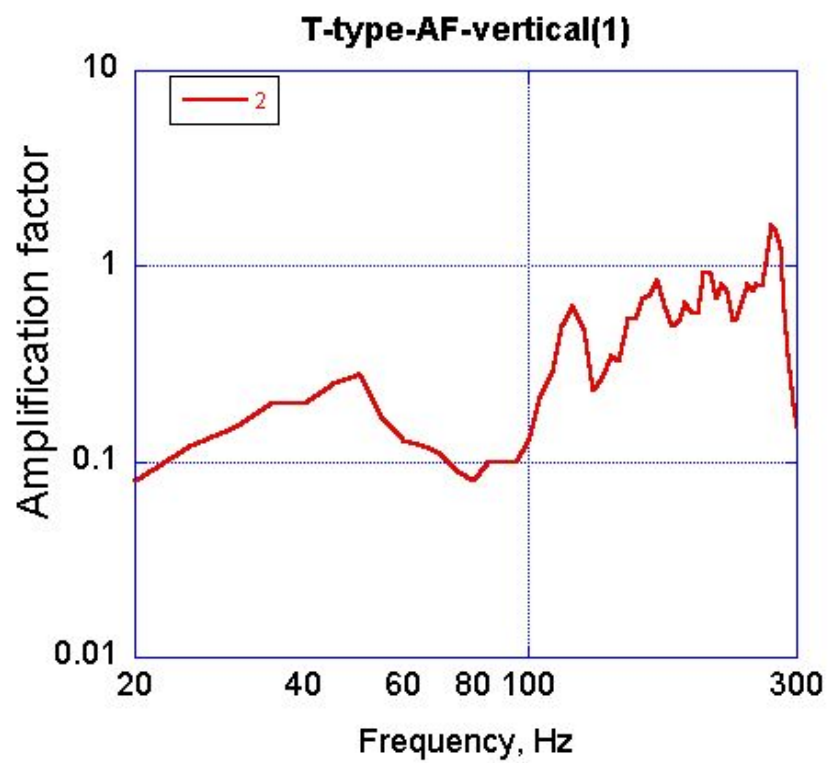
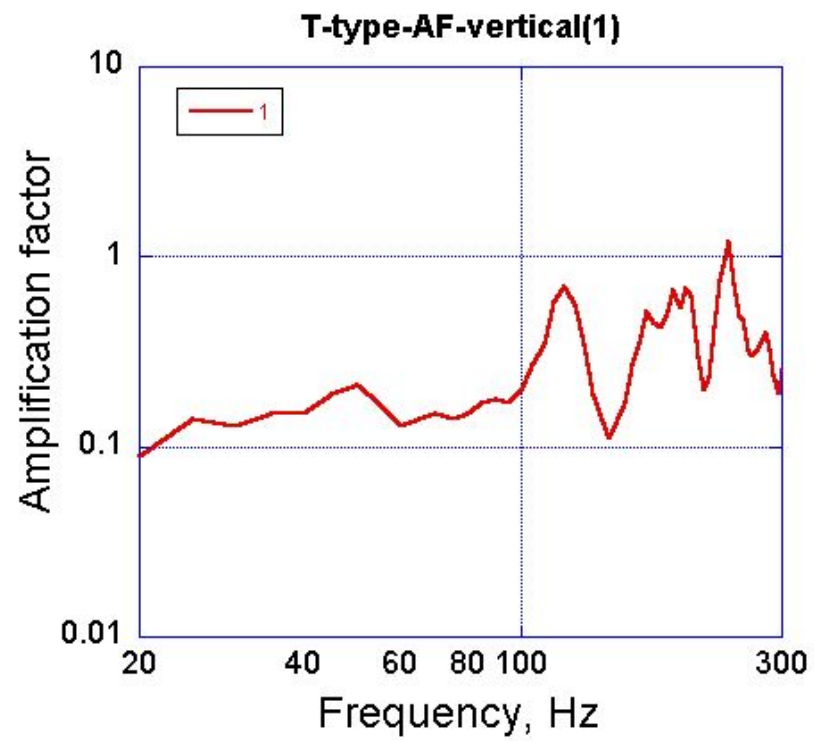


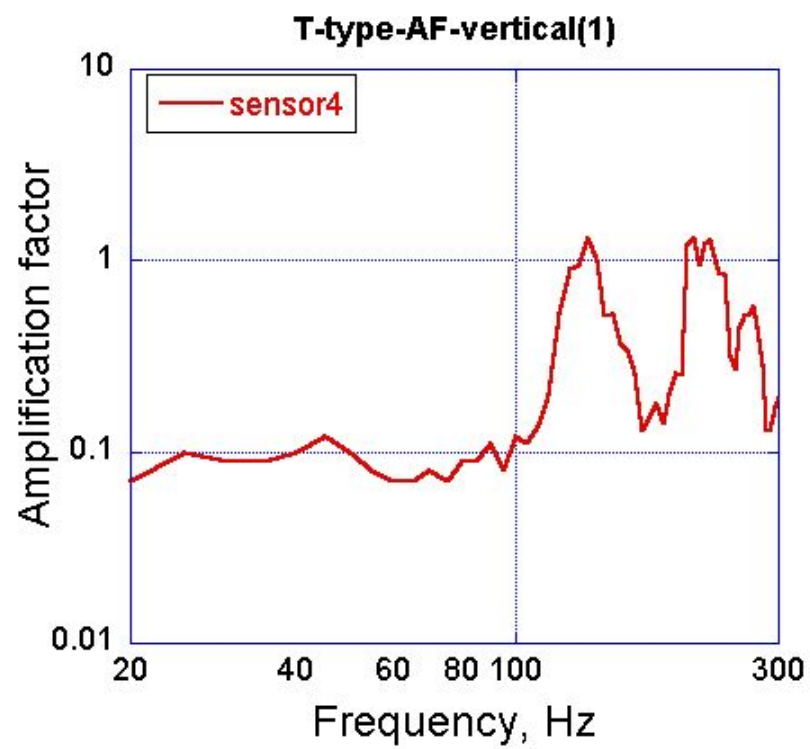
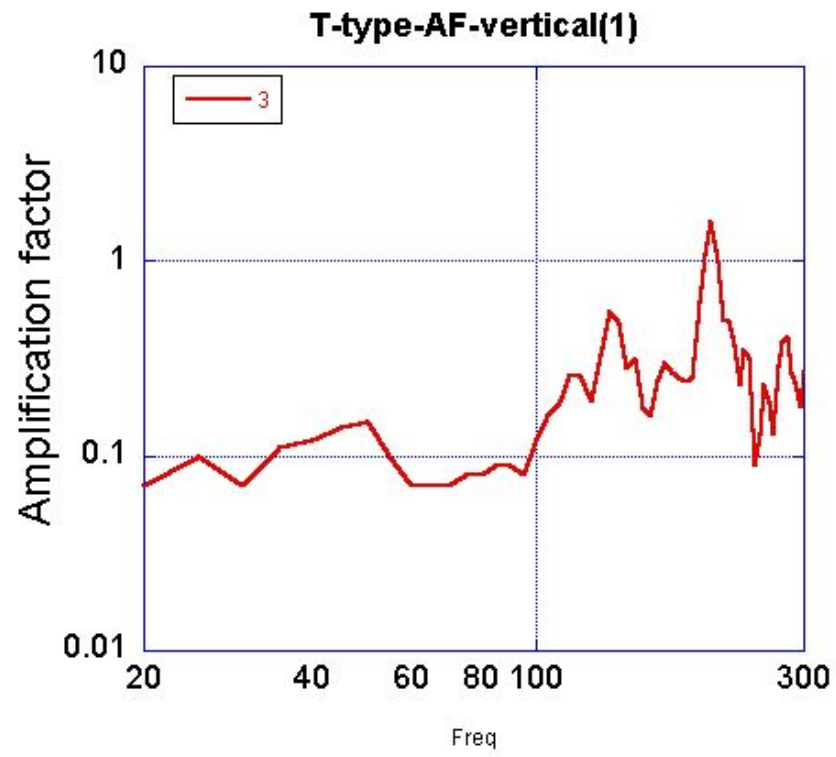


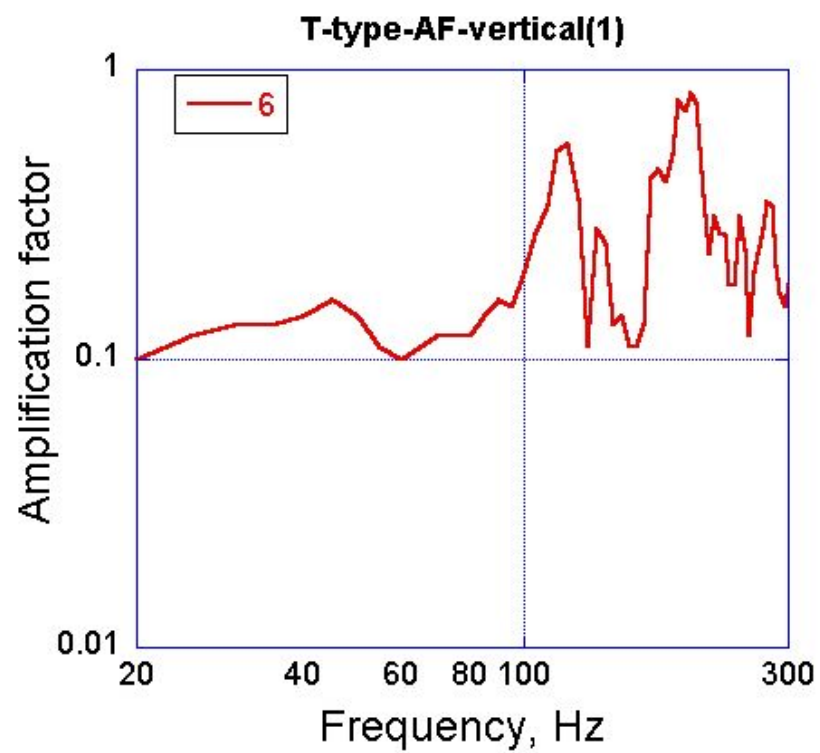
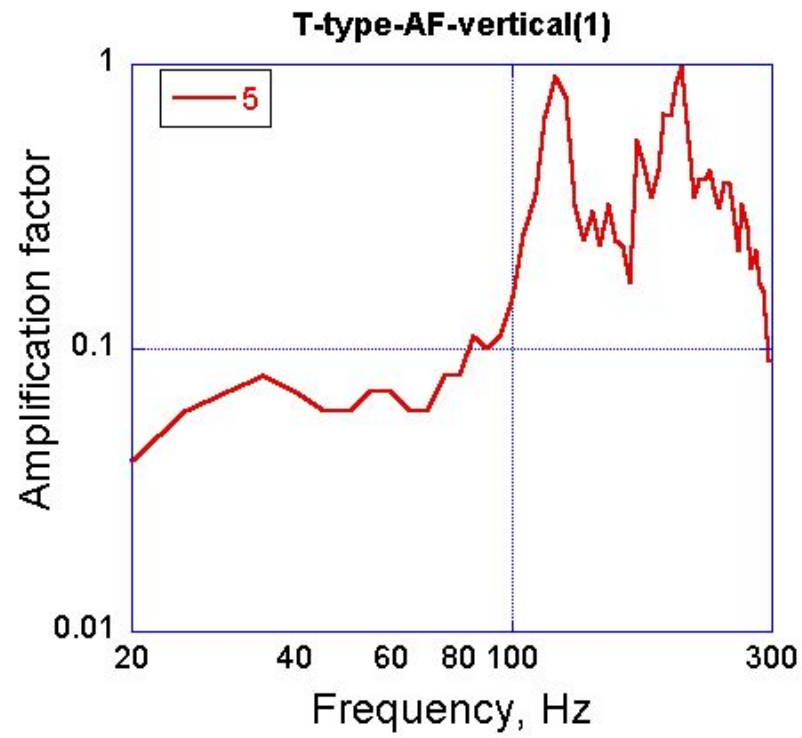


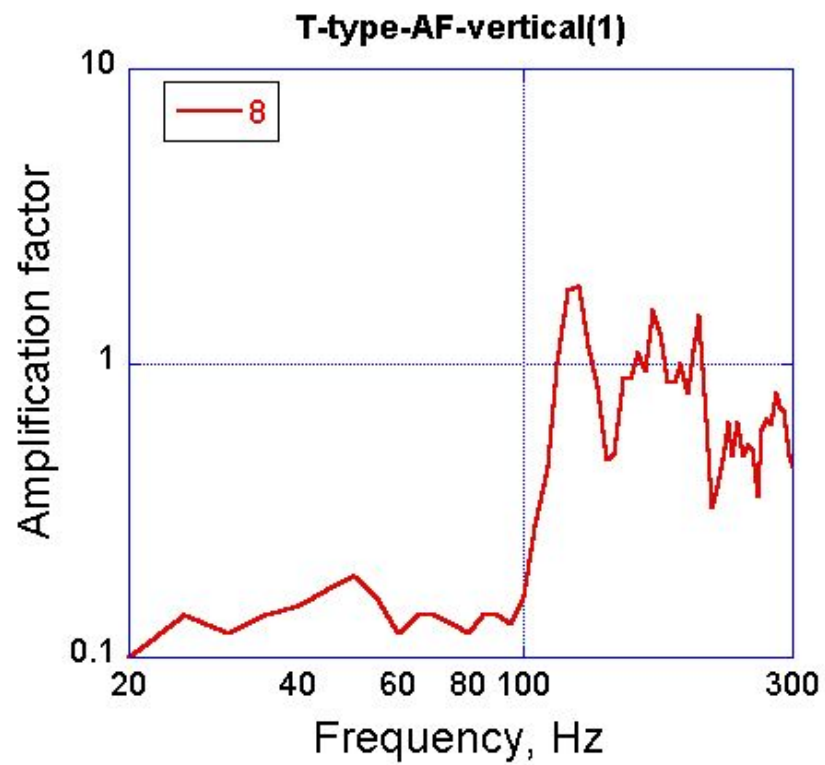
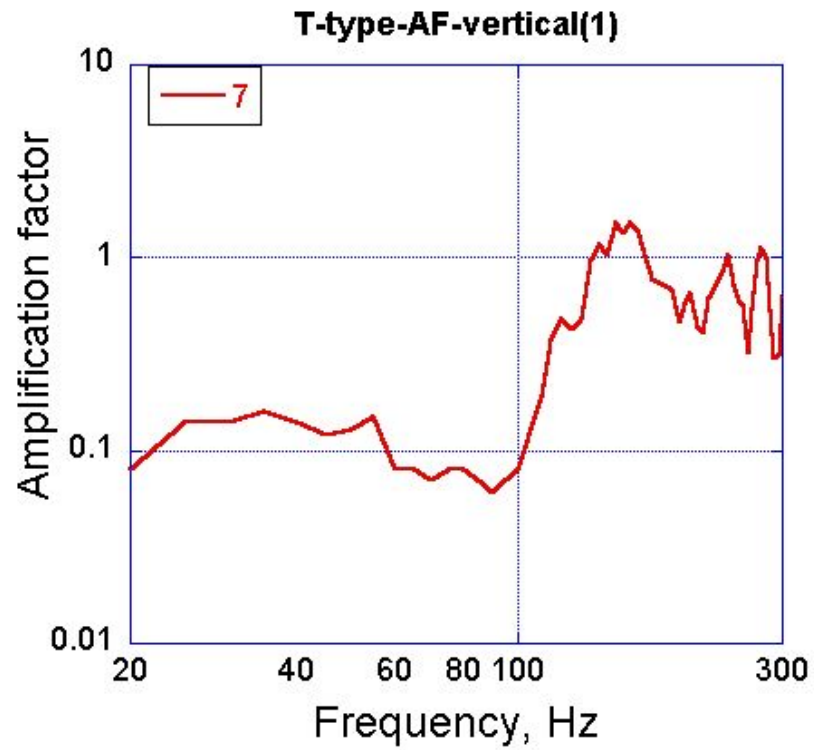


Amplification Factor. T-Type. Vertical direction

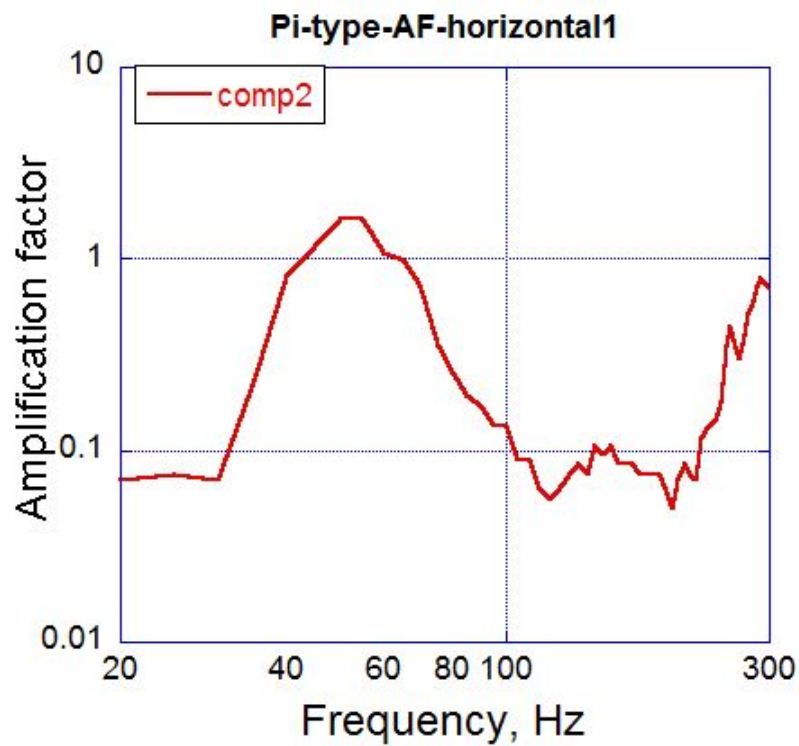
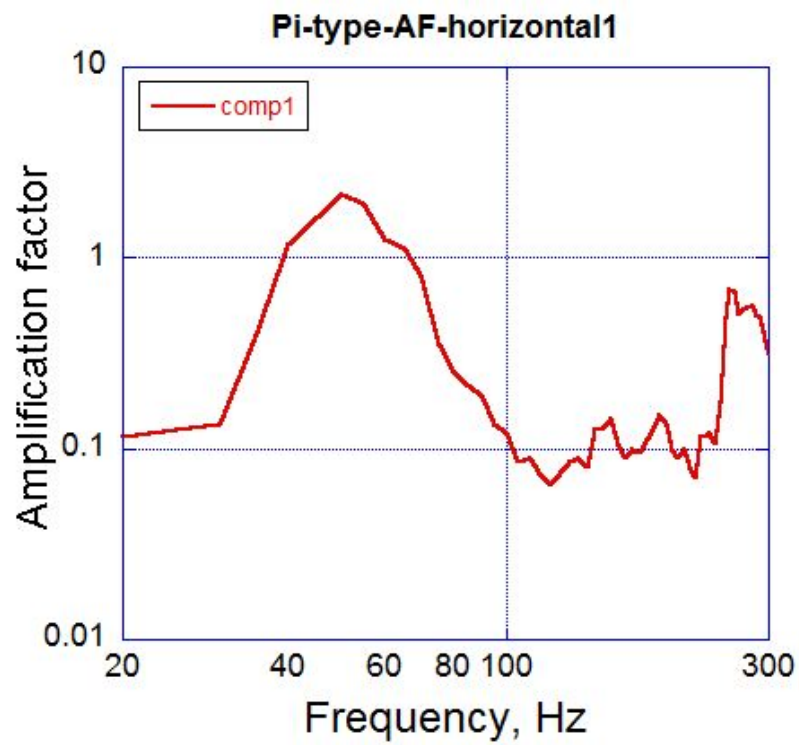


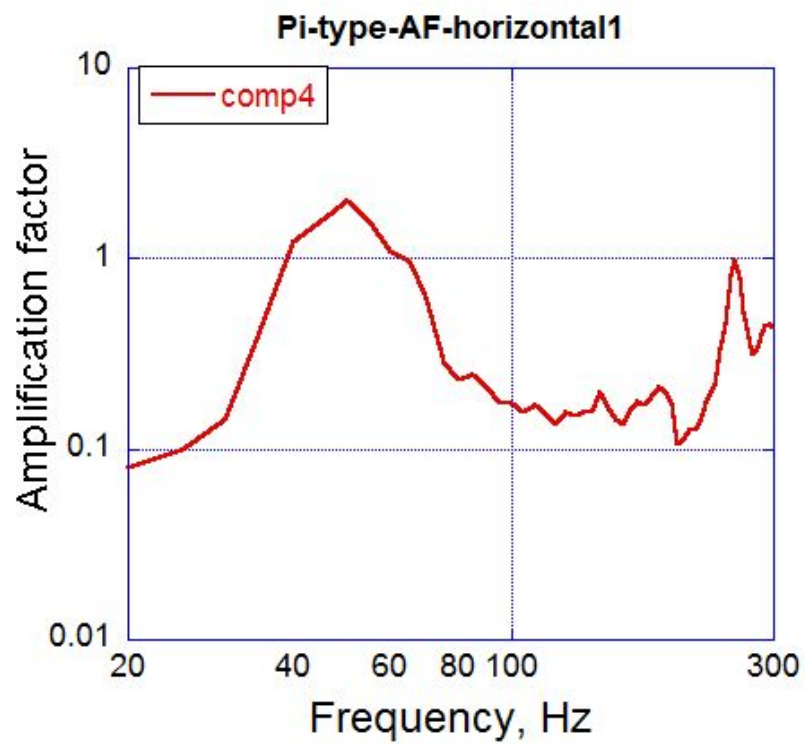
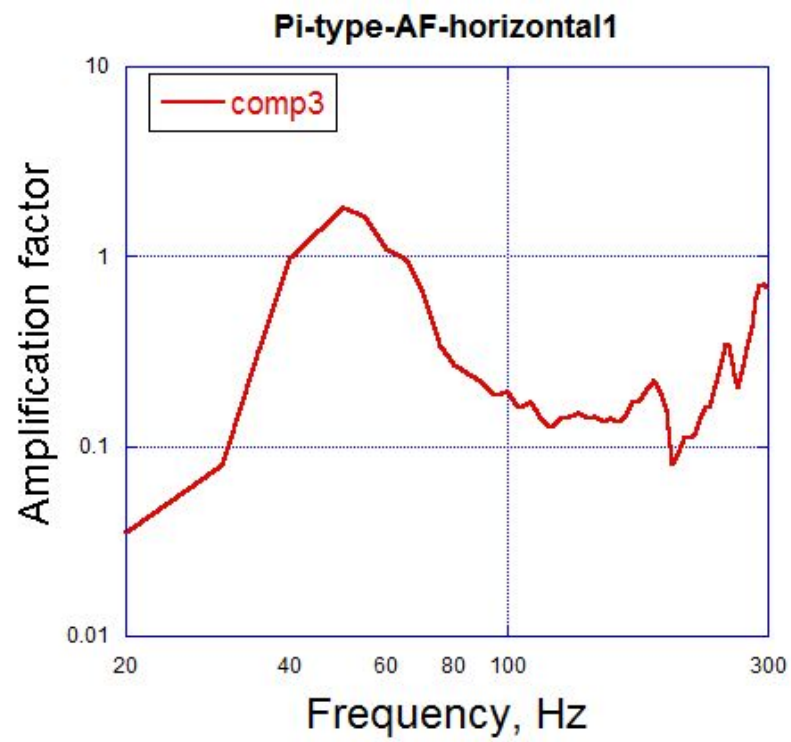


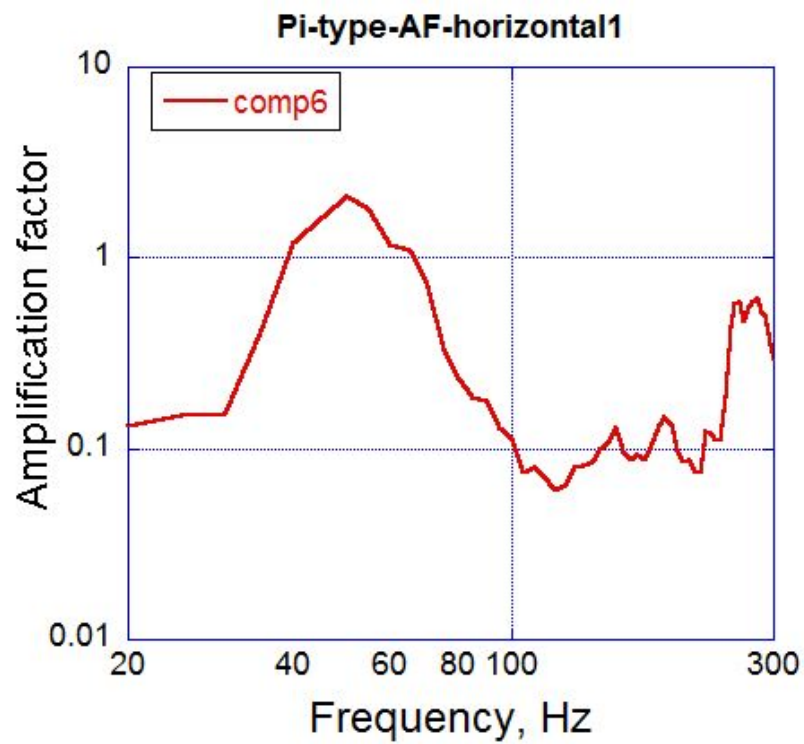
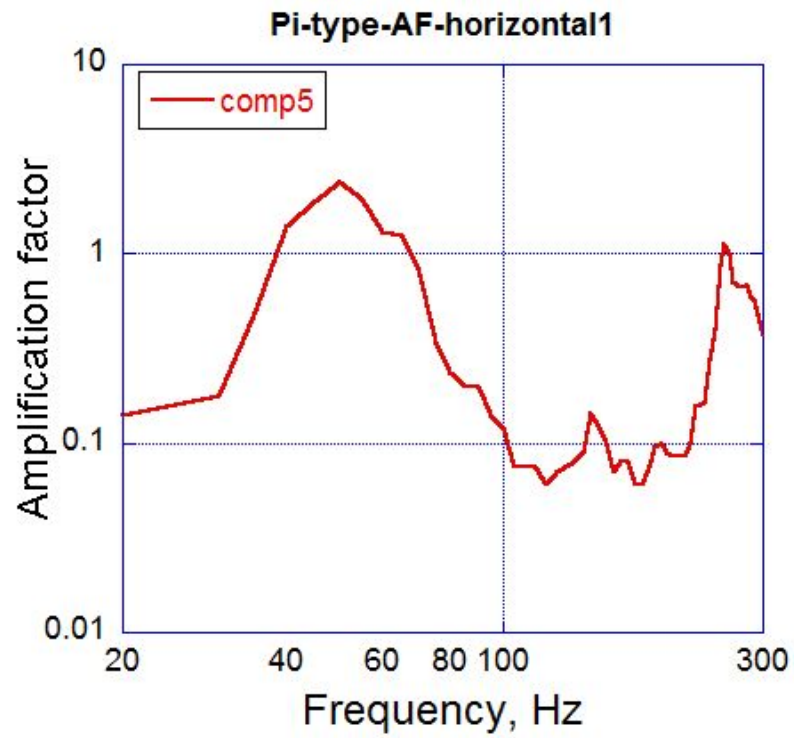


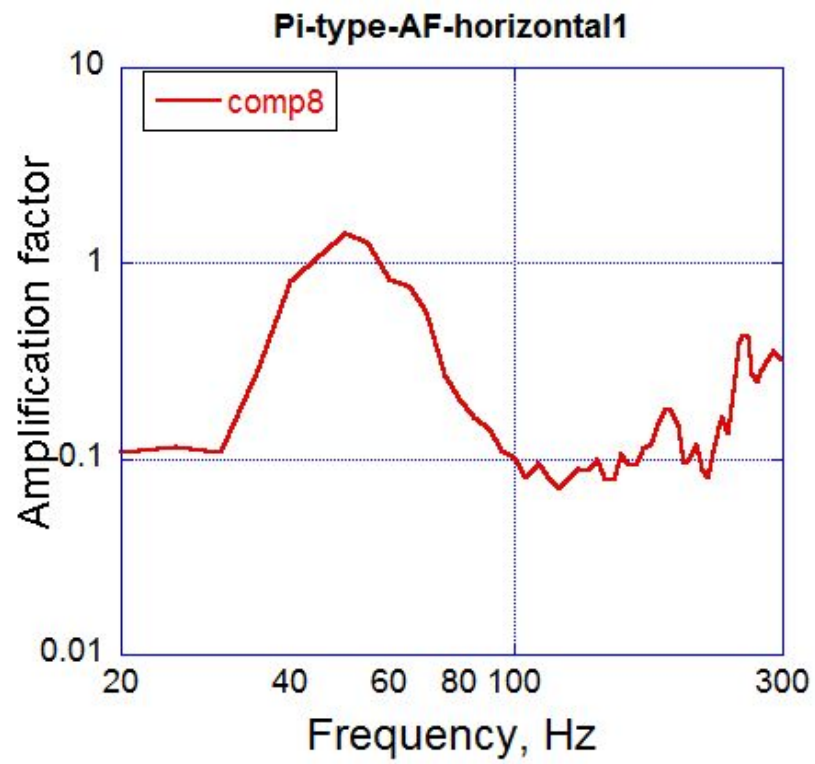
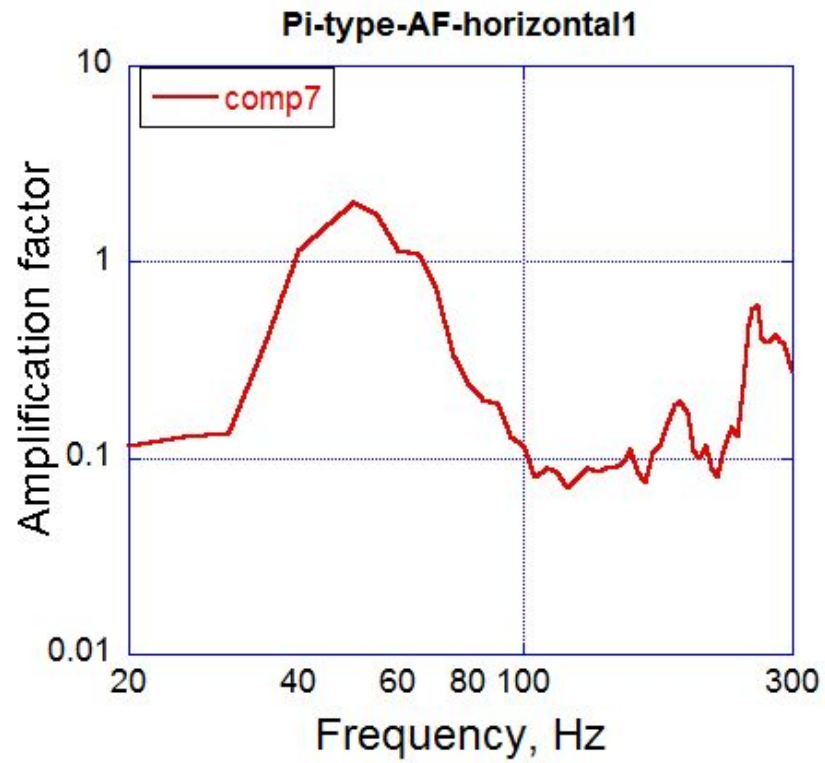


Amplification Factor. Pi-Type. Horizontal direction(1)

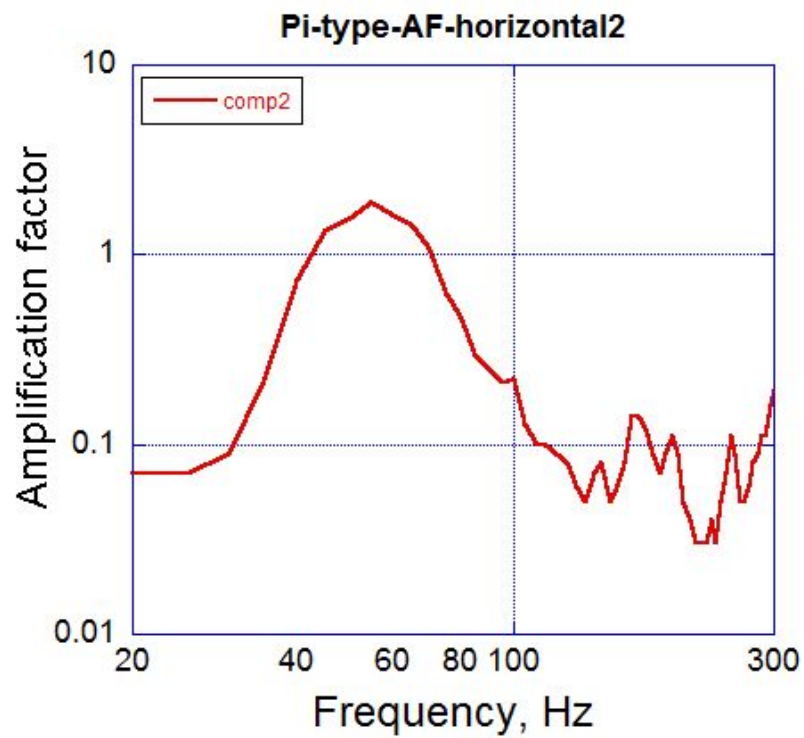
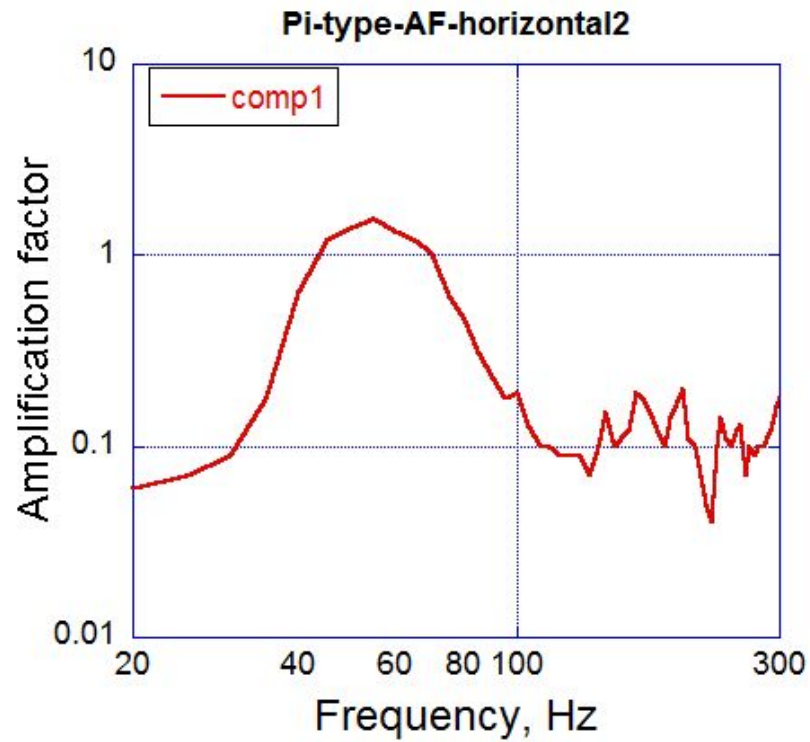


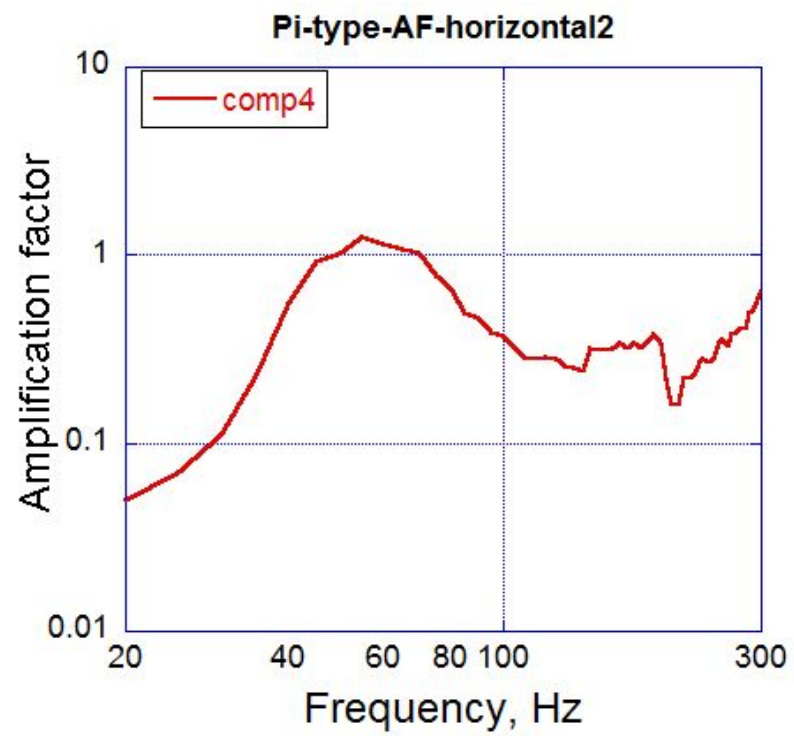
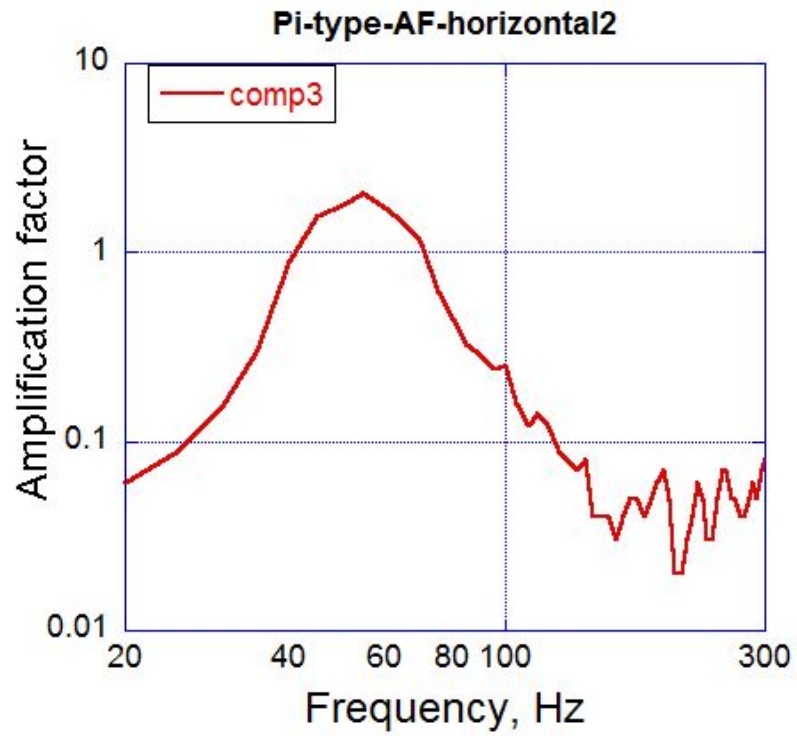


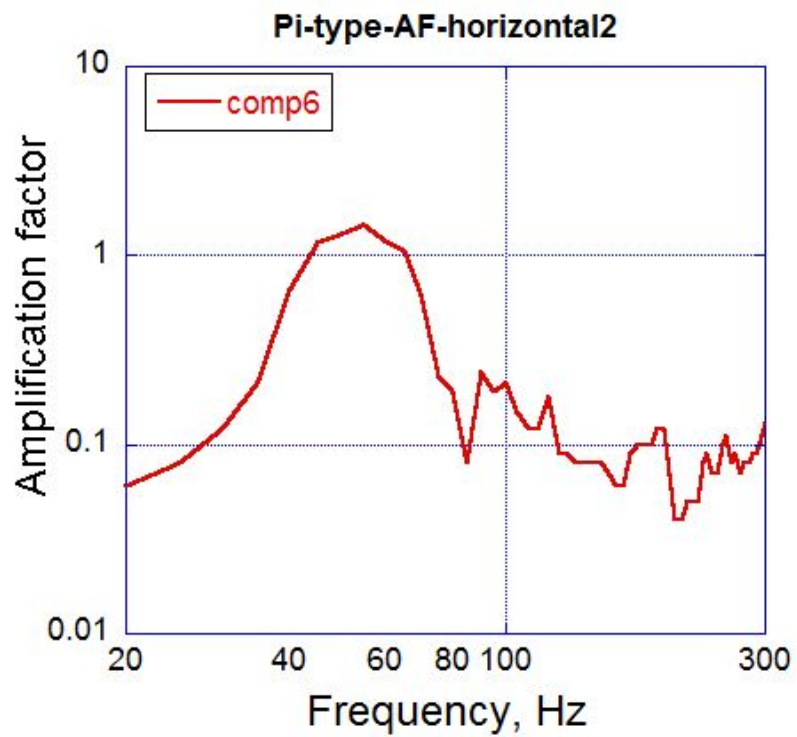
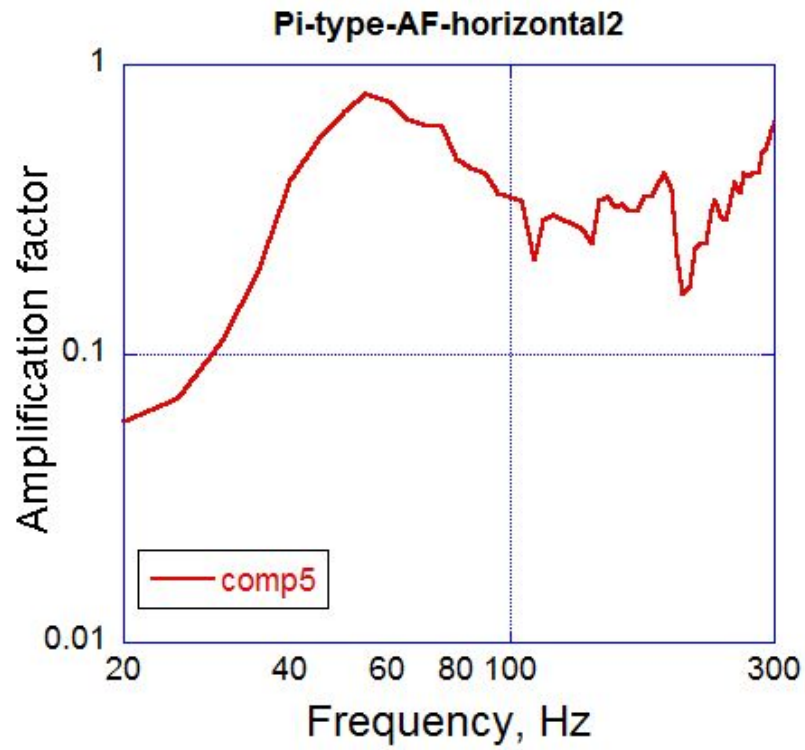


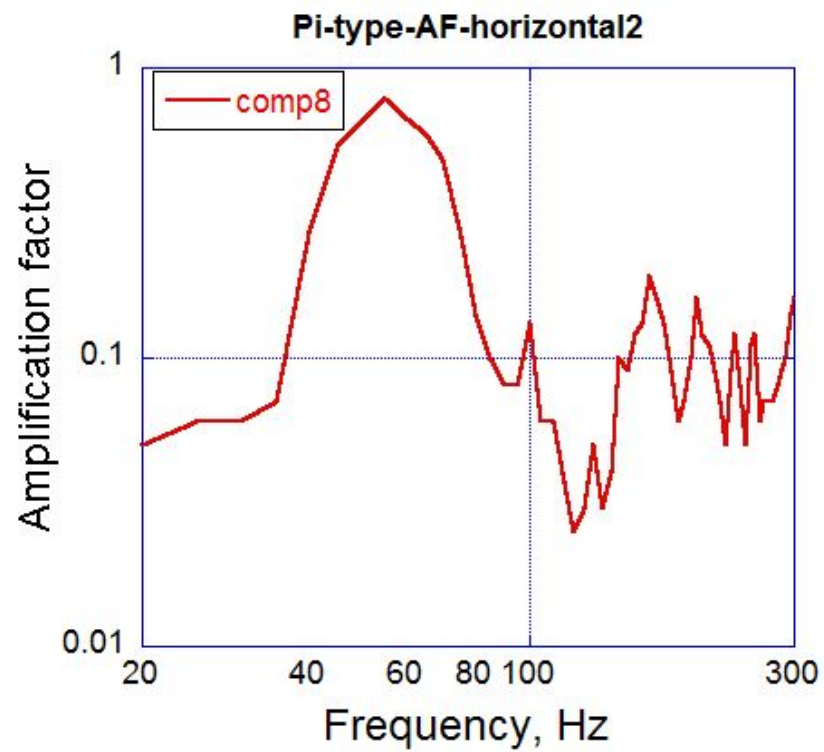
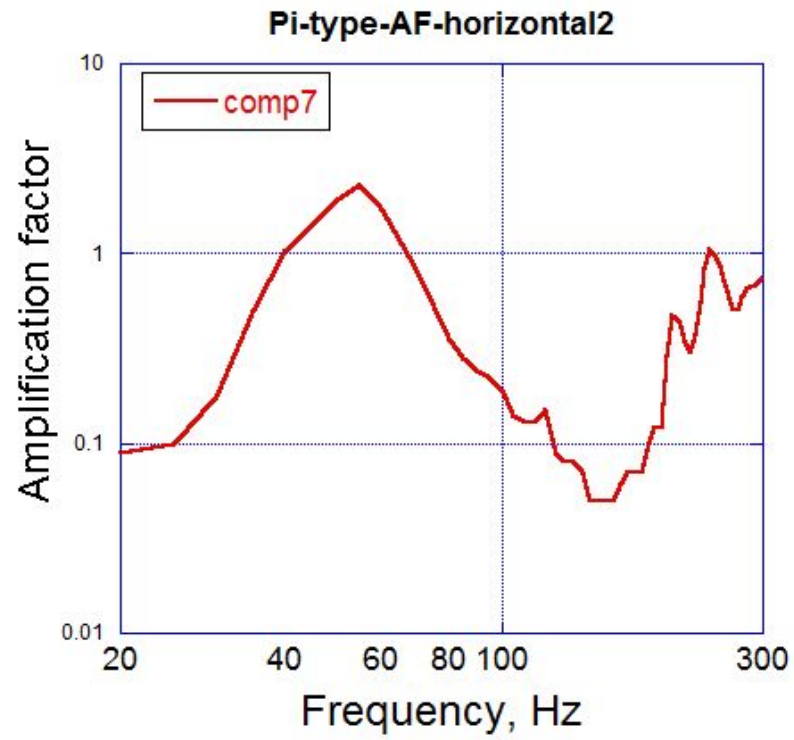


Amplification Factor. Pi-Type. Horizontal direction(3)

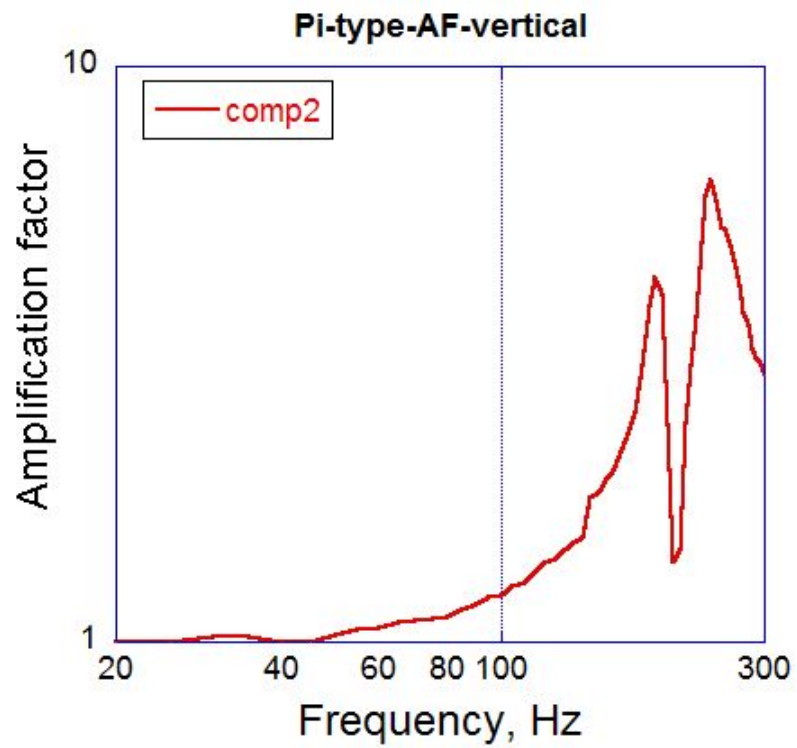
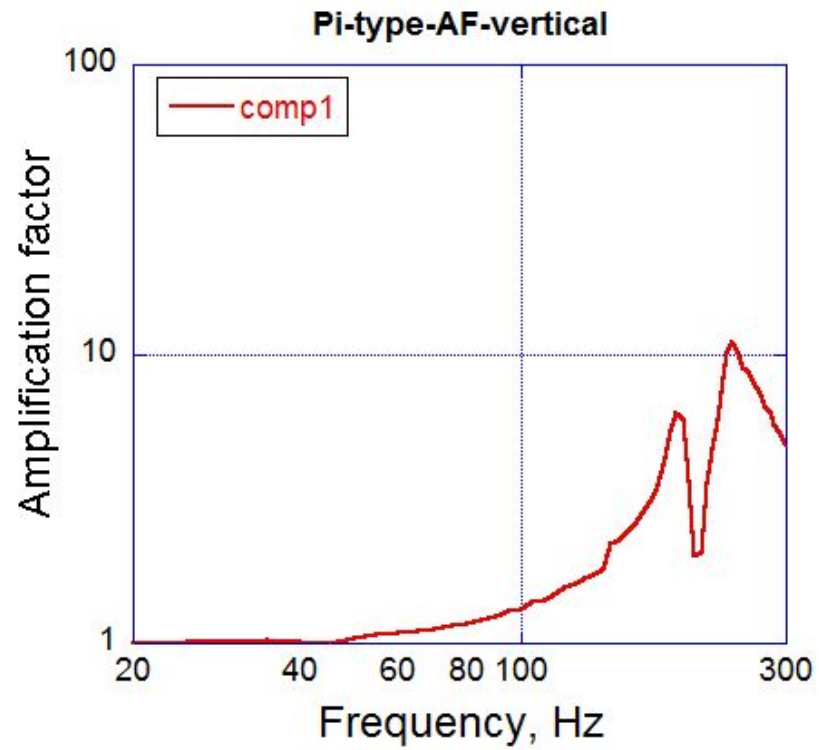


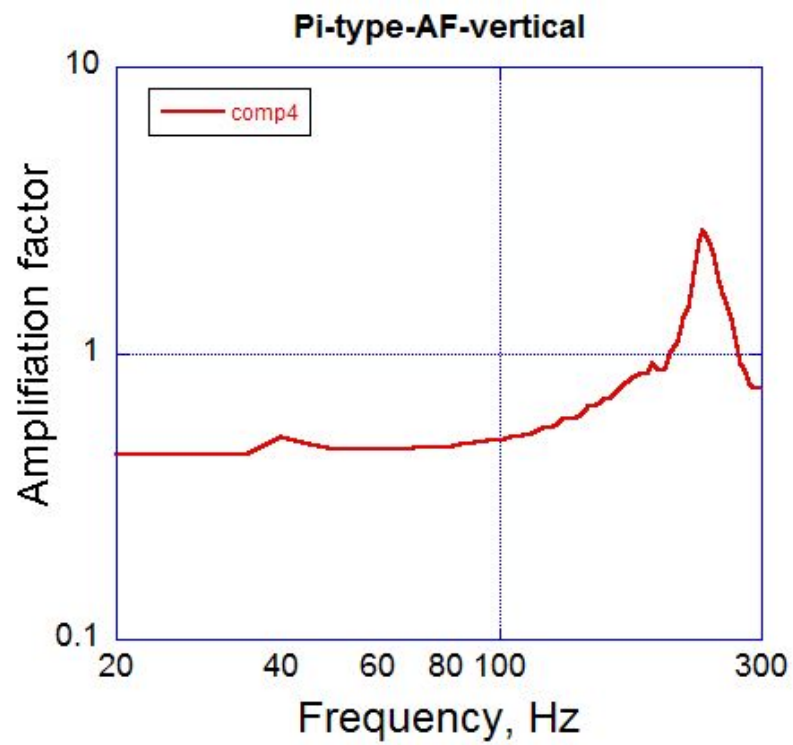
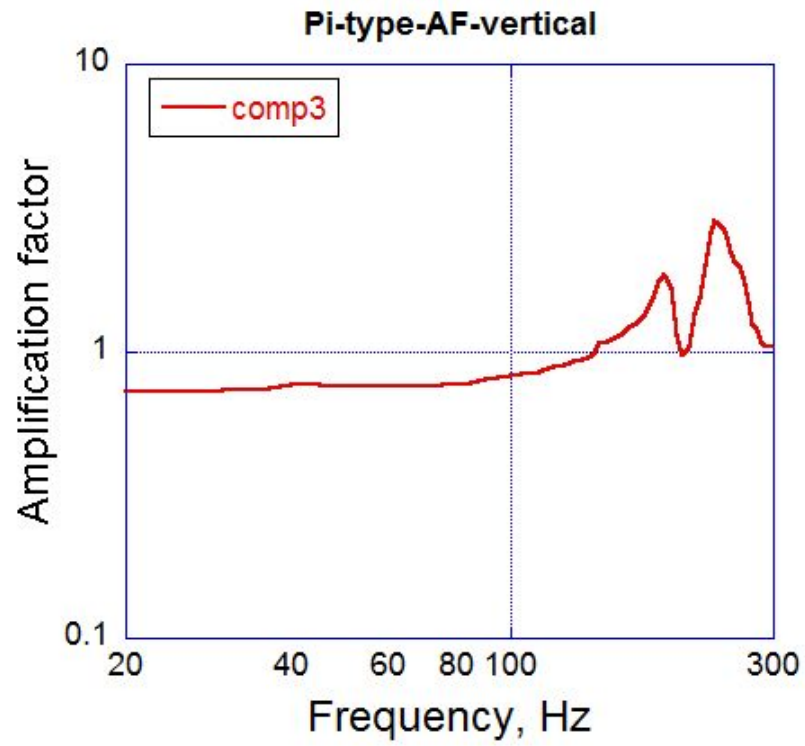


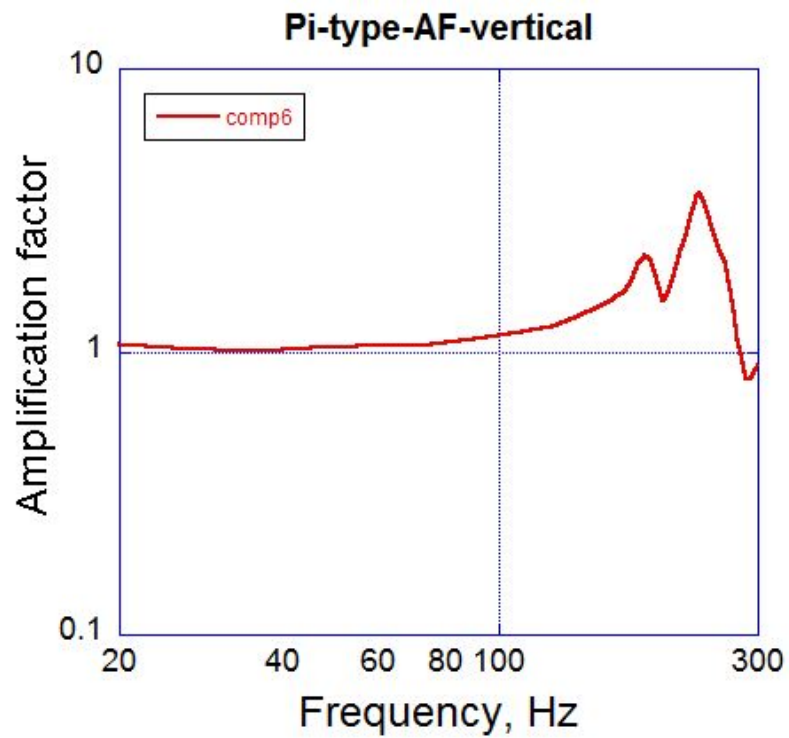
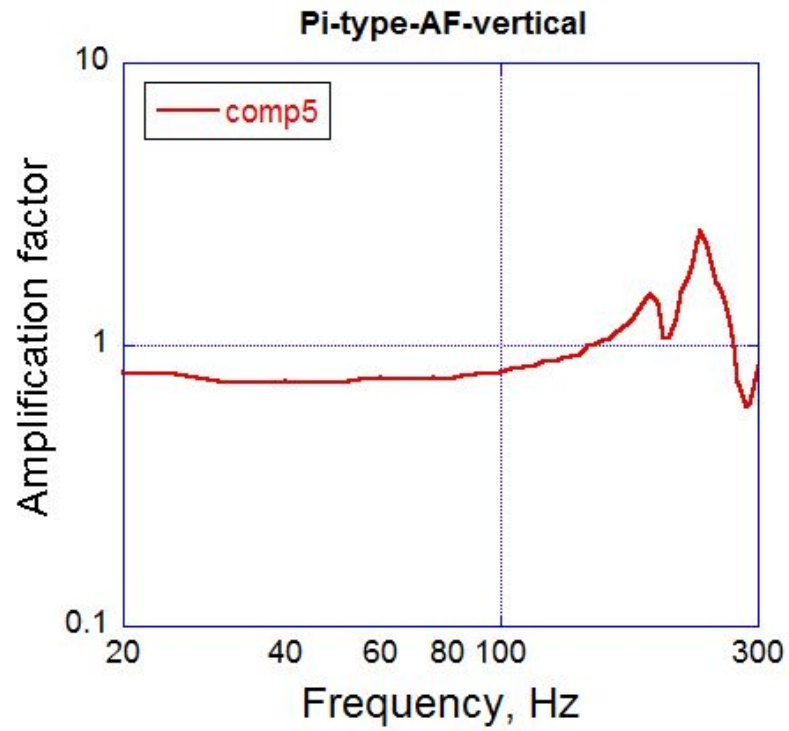


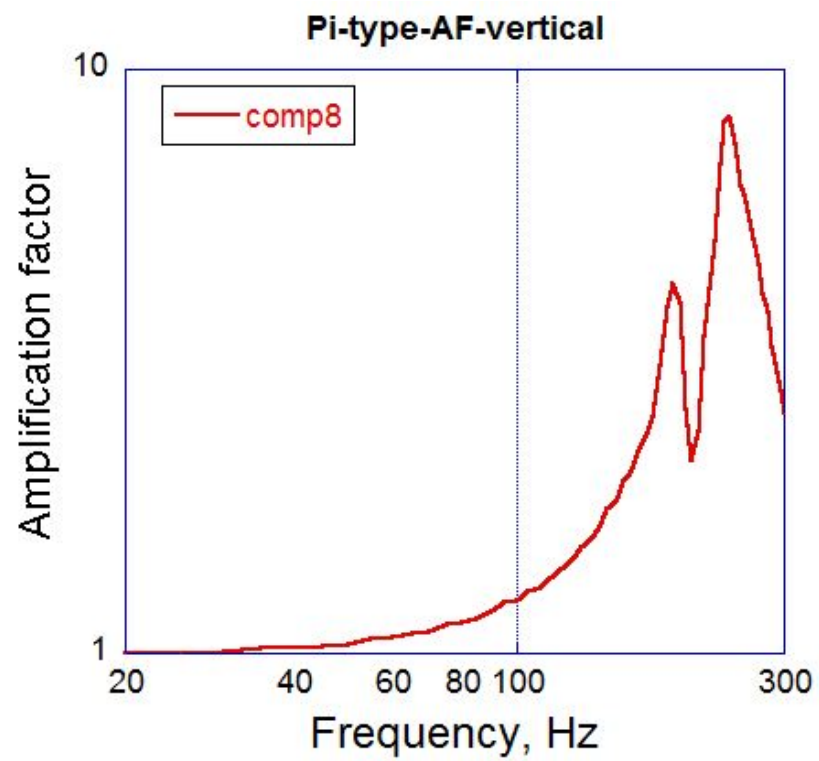
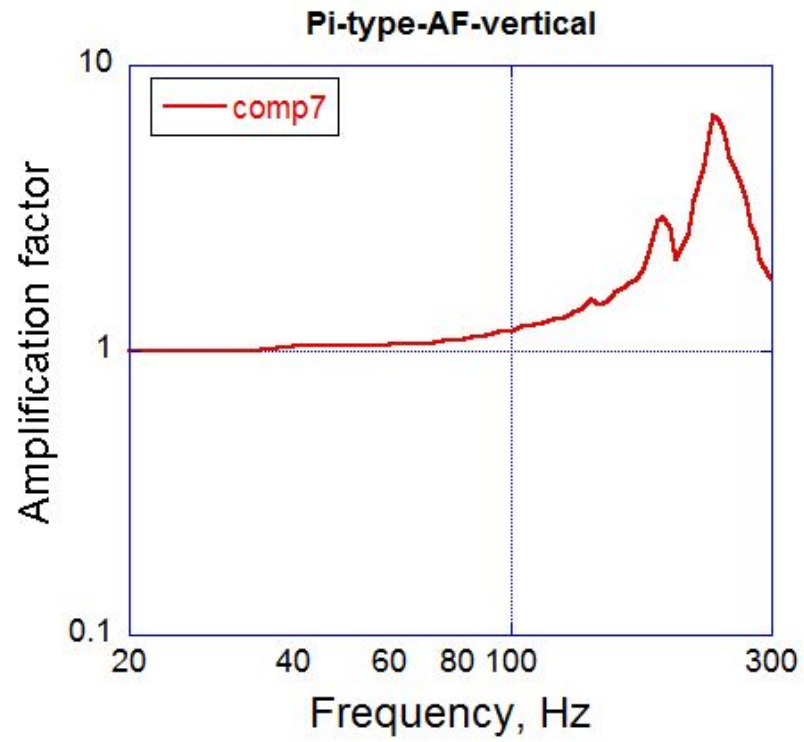


Amplification Factor. Pi-Type. Vertical direction









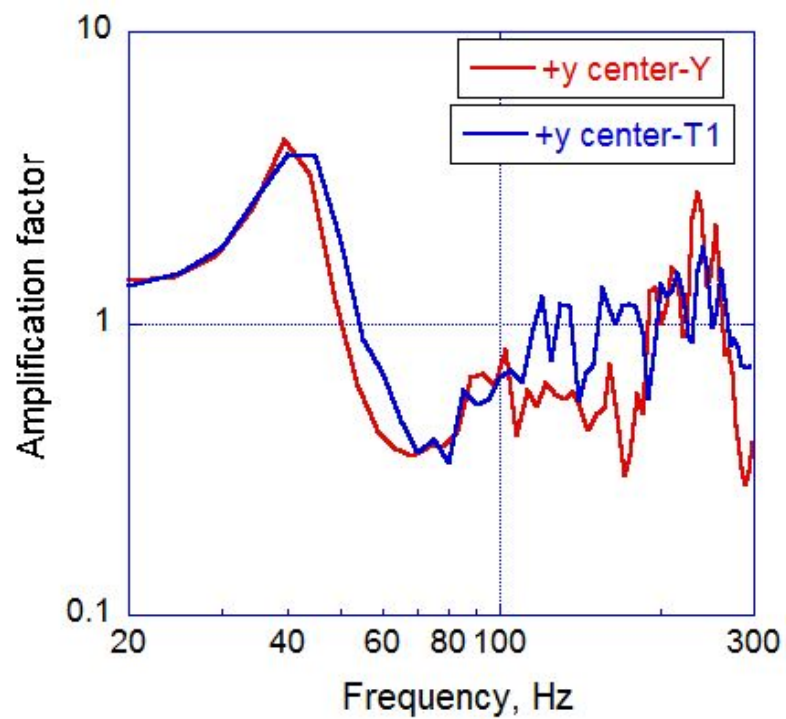
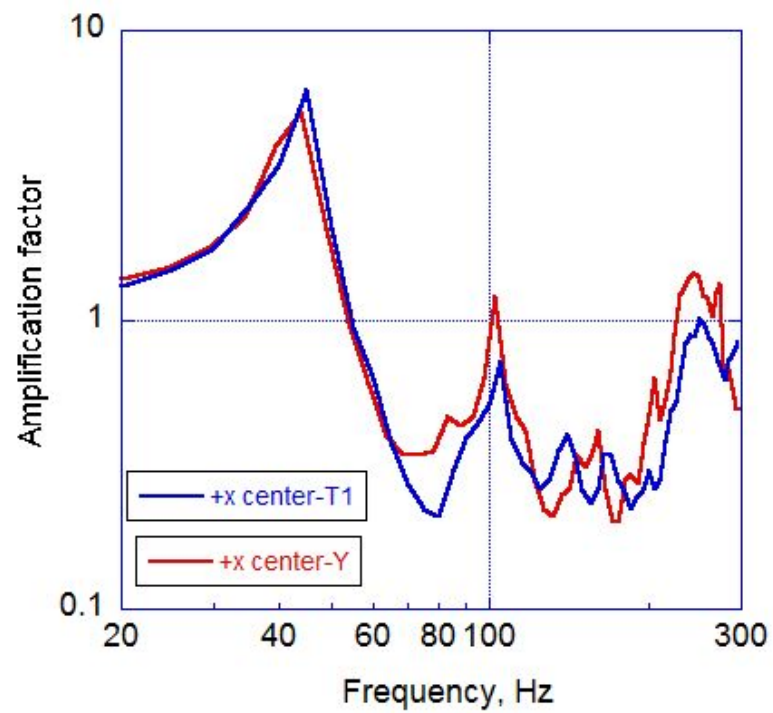
Resonant frequency statistics of dummy satellite
(experiment, 20-300Hz).

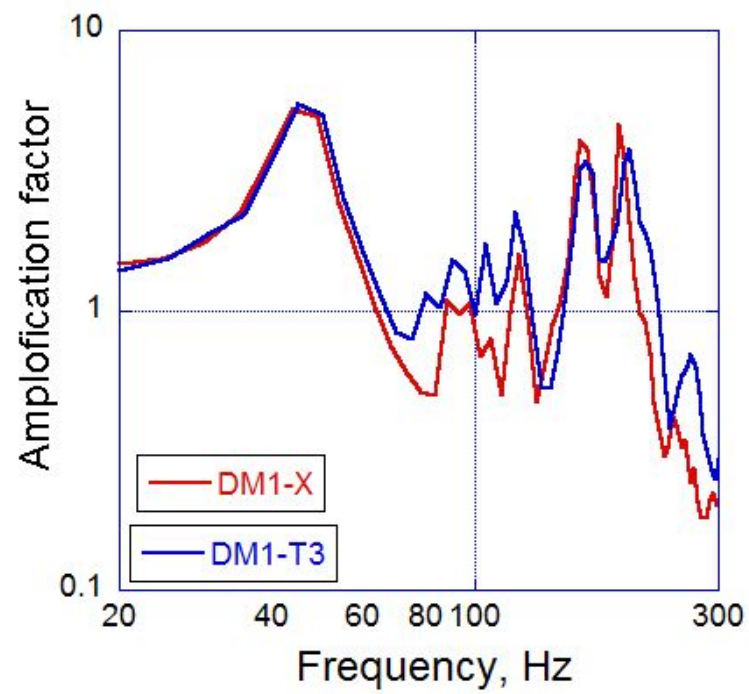
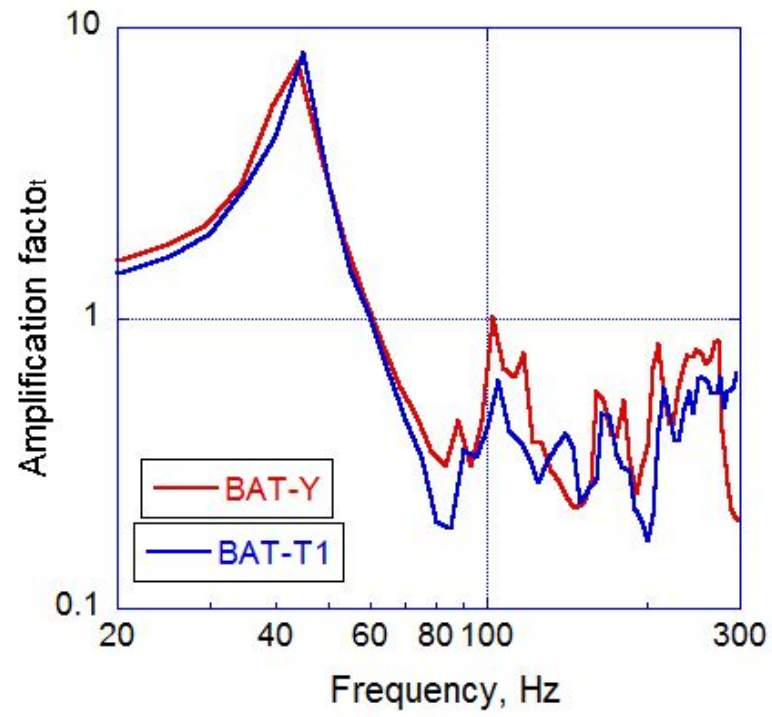
| | Resonant Frequency | | |
|-----------|-------------------------------|-------------------------------|--------------------|
| | Perpendicular to the axial(x) | Perpendicular to the axial(y) | Axial direction(z) |
| DM1 | 43.9 | 43.9 | 141.6 |
| PCU | 39.1 | 39.1 | 141.6 |
| BATTERY | 43.9 | 43.9 | 141.6 |
| +X CENTER | 43.9 | 39.1 | 141.6 |
| DM6 | 39.1 | 39.1 | 170.9 |
| OBC | 39.1 | 34.2 | 170.9 |
| RF | 39.1 | 39.1 | 170.9 |
| +Y CENTER | 39.1 | 39.1 | 170.9 |
| DM4 | 39.1 | 34.2 | 166.0 |
| DM2 | 87.9 | 34.2 | 83.0 |
| DM5 | 117.2 | 34.2 | 166.0 |
| -X CENTER | 39.1 | 34.2 | 83.0 |
| DM3 | 39.1 | 34.2 | 83.0 |
| DM9 | 39.1 | 39.1 | 170.9 |
| DM7 | 39.1 | 78.1 | 170.9 |
| DM10 | 39.1 | 39.1 | 107.4 |
| -Y CENTER | 39.1 | 34.2 | 170.9 |
| DM8 | 39.1 | 34.2 | 107.4 |

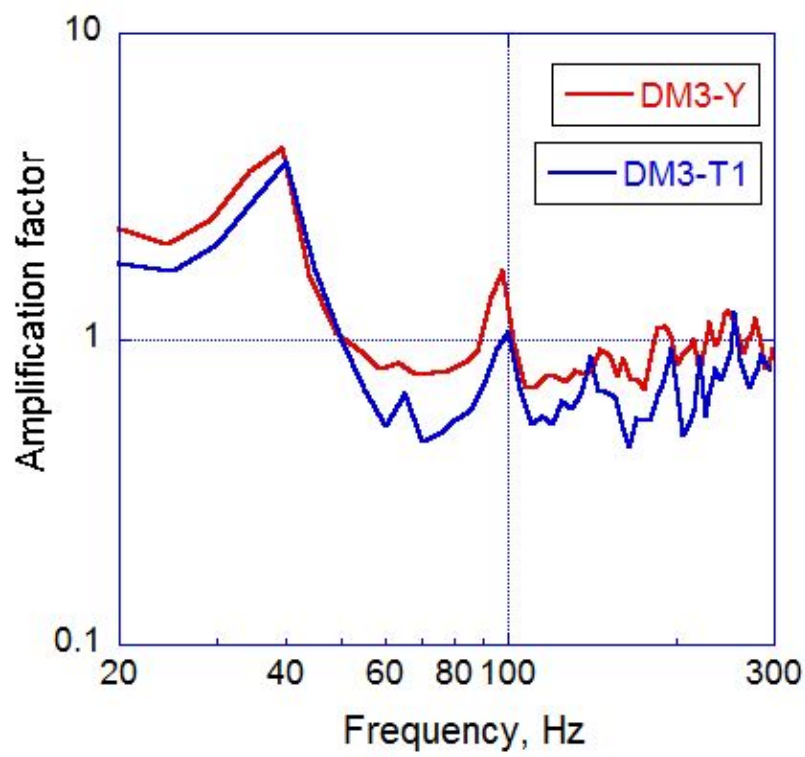
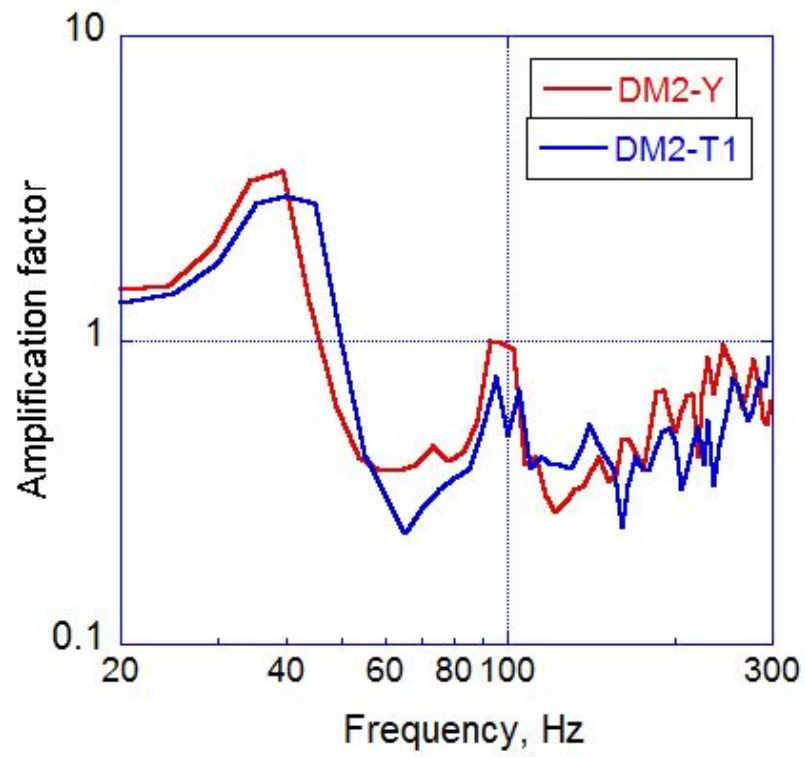
Peak value of amplification factor of dummy satellite(experiment, 20-300Hz).

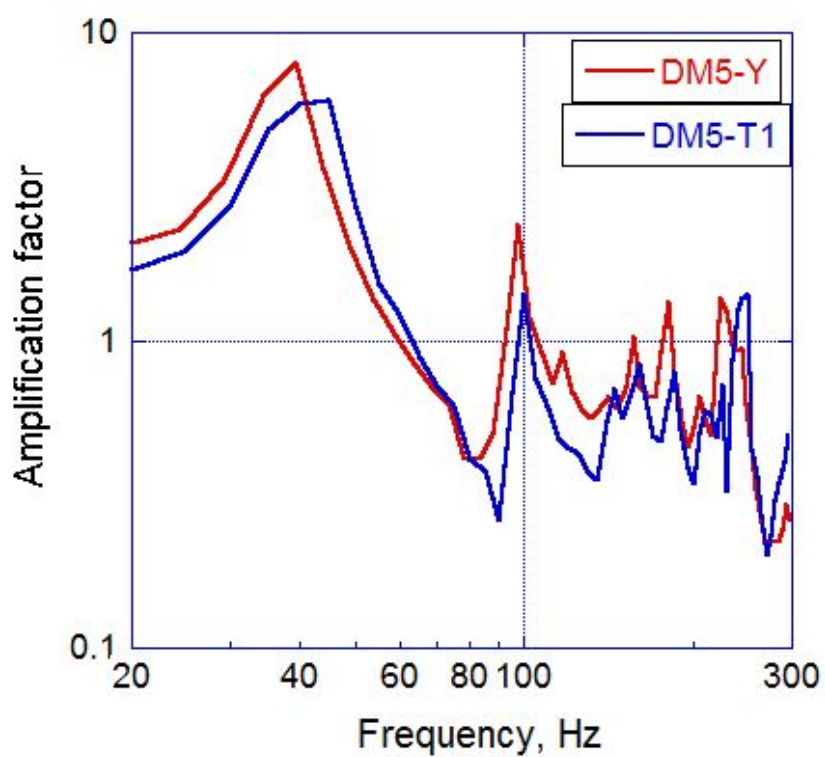
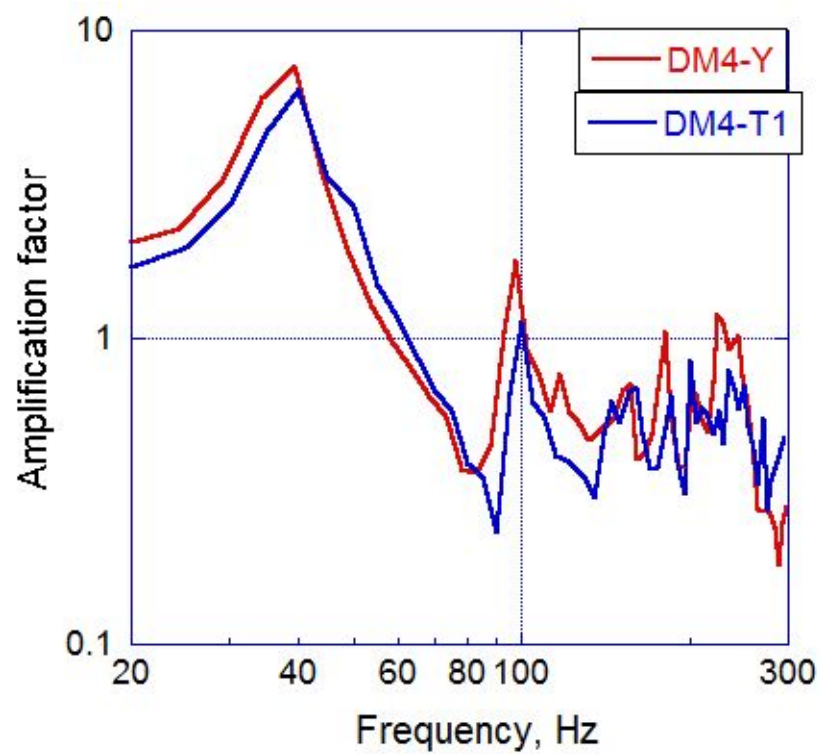
| | Amplification factor | | |
|-----------|-------------------------------|-------------------------------|--------------------|
| | Perpendicular to the axial(x) | Perpendicular to the axial(y) | Axial direction(z) |
| DM1 | 5.18 | 4.43 | 2.86 |
| PCU | 9.18 | 2.4 | 3.41 |
| BATTERY | 6.00 | 5.27 | 4.02 |
| +X CENTER | 3.98 | 3.87 | 3.12 |
| DM6 | 5.24 | 6.9 | 3.54 |
| OBC | 2.55 | 9.36 | 3.8 |
| RF | 4.97 | 5.62 | 5.58 |
| +Y CENTER | 3.92 | 3.98 | 4.26 |
| DM4 | 7.45 | 6.83 | 3.23 |
| DM2 | 13.8 | 3.77 | 4.03 |
| DM5 | 11.2 | 7.21 | 3.46 |
| -X CENTER | 4.02 | 4.24 | 3.19 |
| DM3 | 4.47 | 4.93 | 3.14 |
| DM9 | 6.17 | 8.76 | 2.89 |
| DM7 | 3.67 | 8.41 | 2.8 |
| DM10 | 6.59 | 7.73 | 2.73 |
| -Y CENTER | 4.05 | 4.33 | 2.69 |
| DM8 | 3.45 | 4.9 | 2.8 |

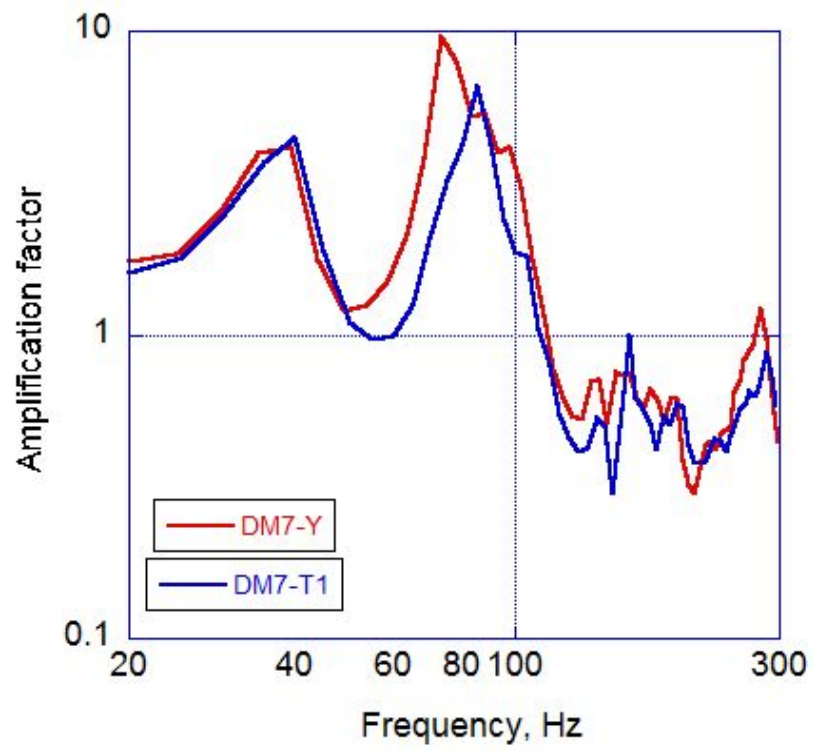
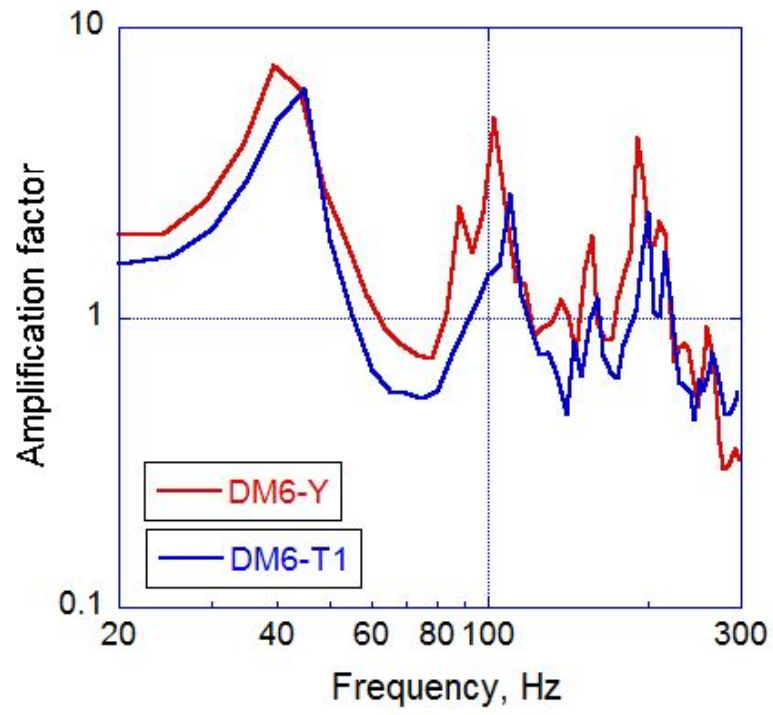
Test and analysis comparison (dummy, horizontal1)

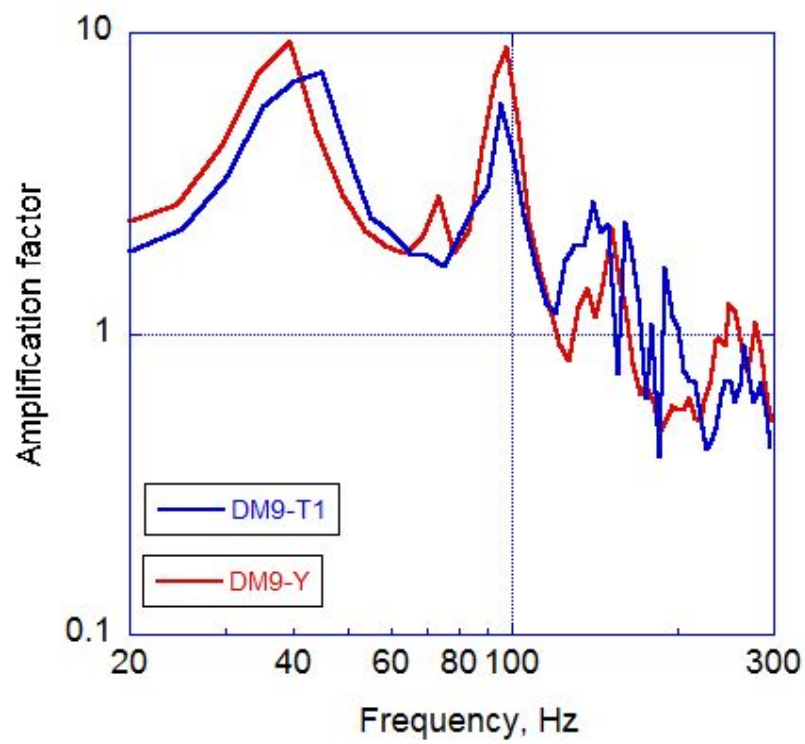
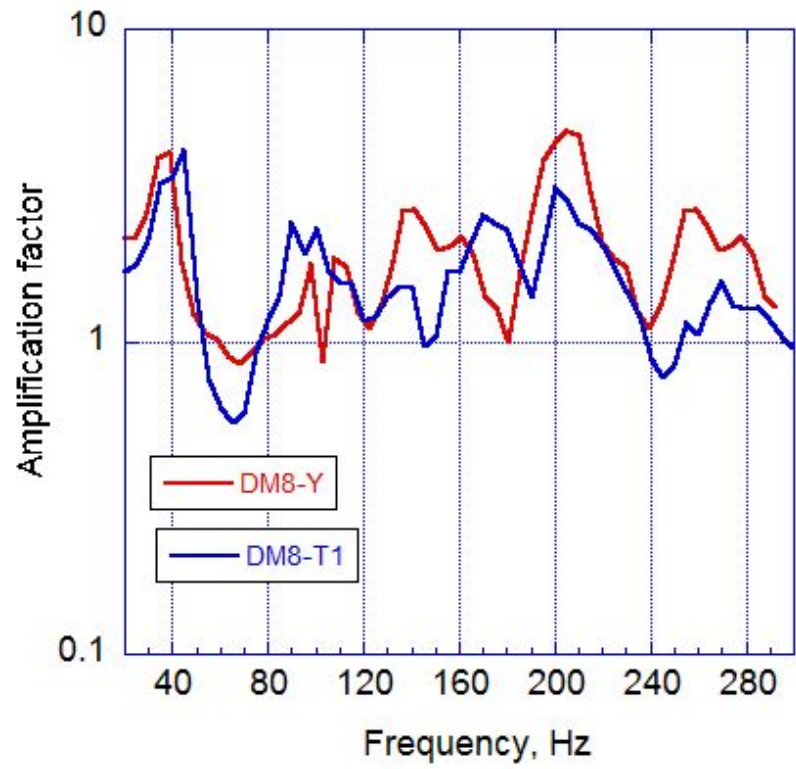


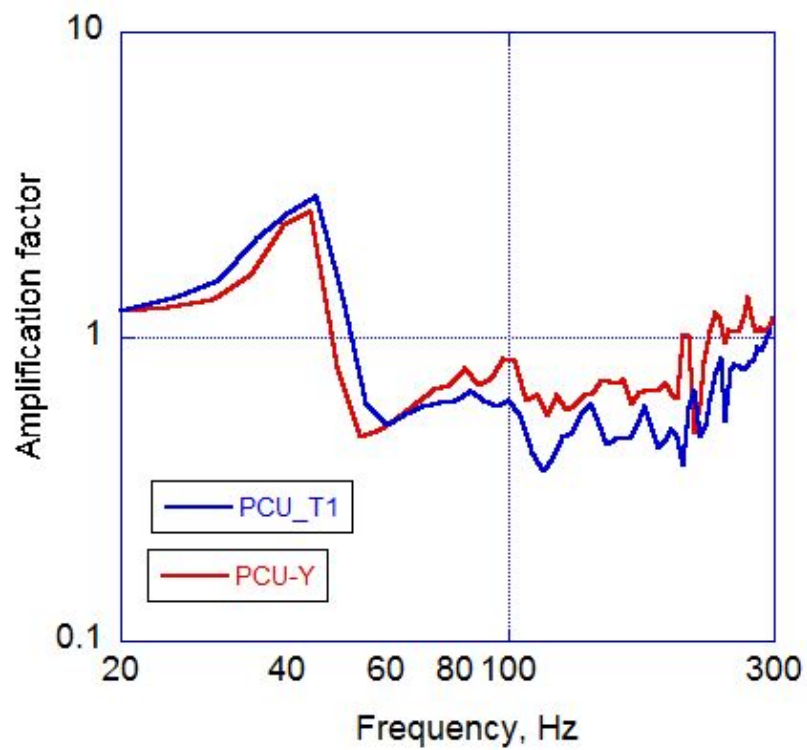
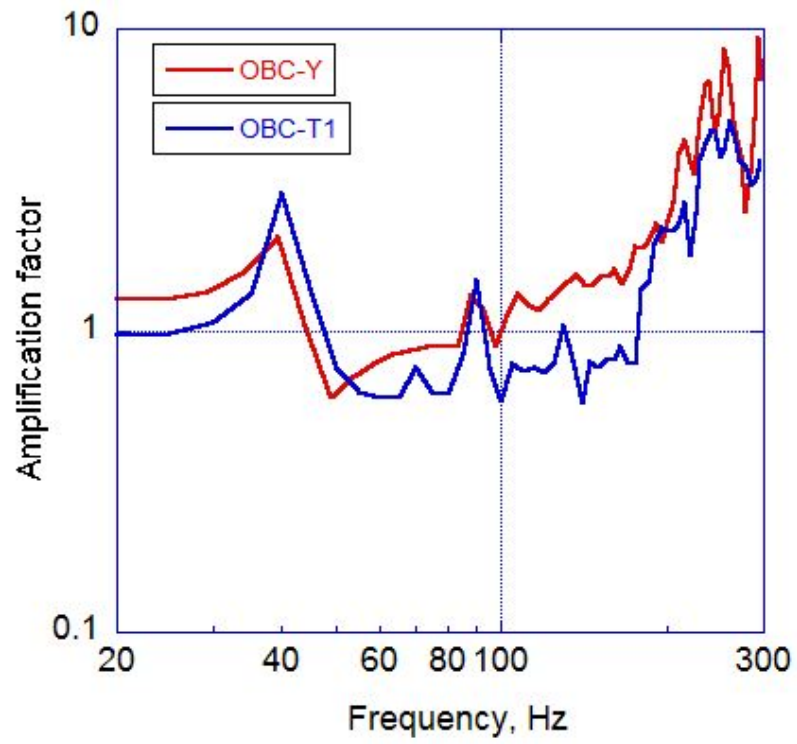


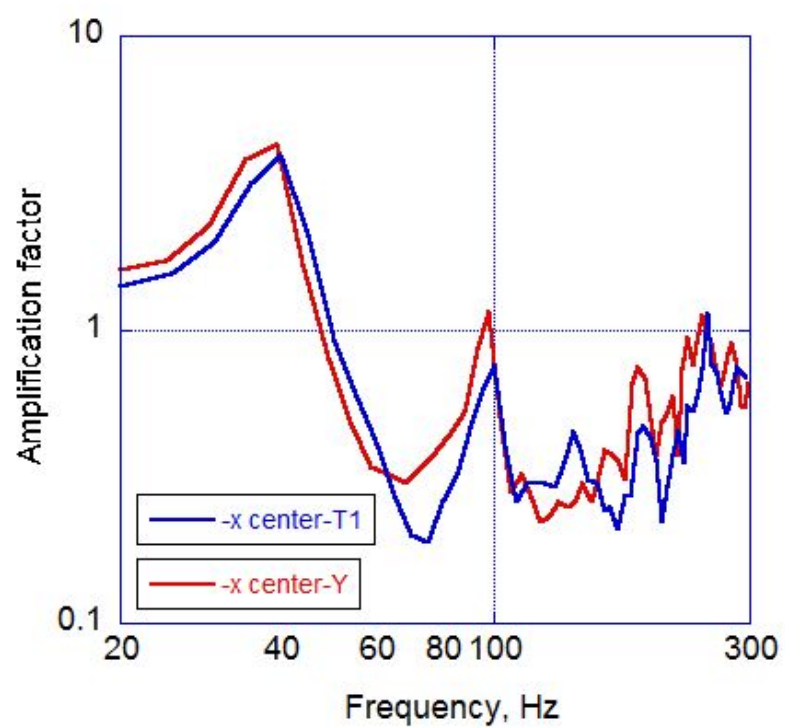
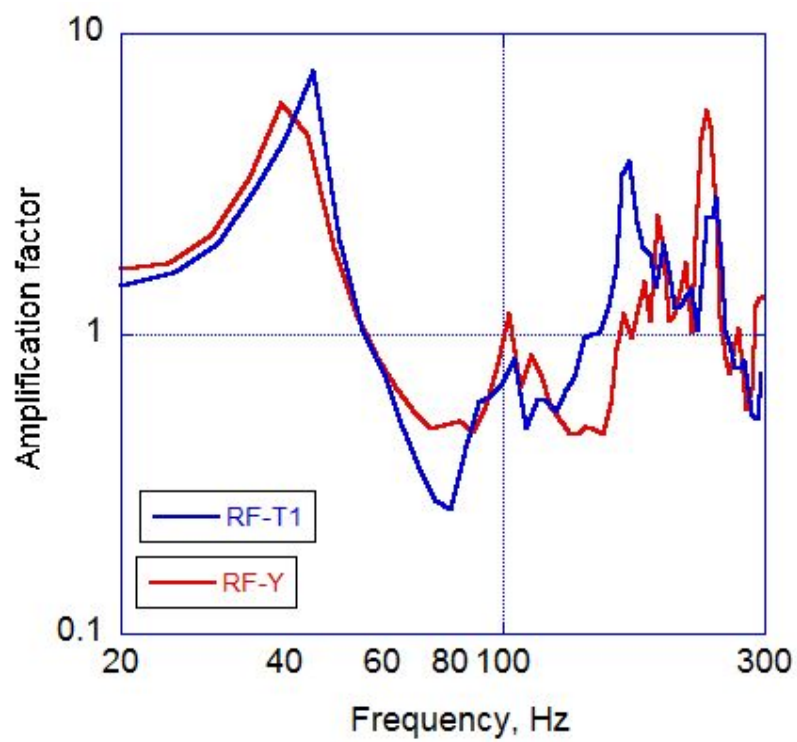


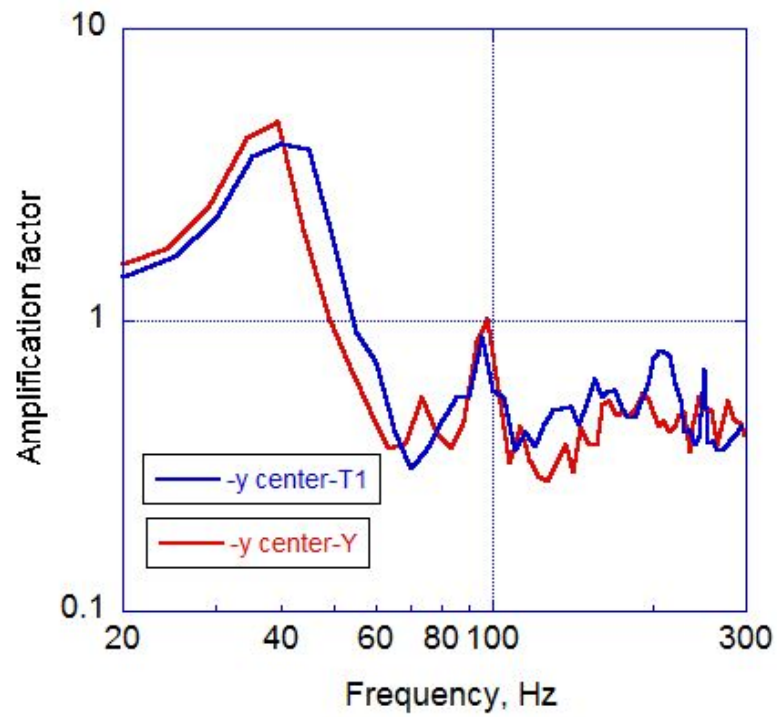




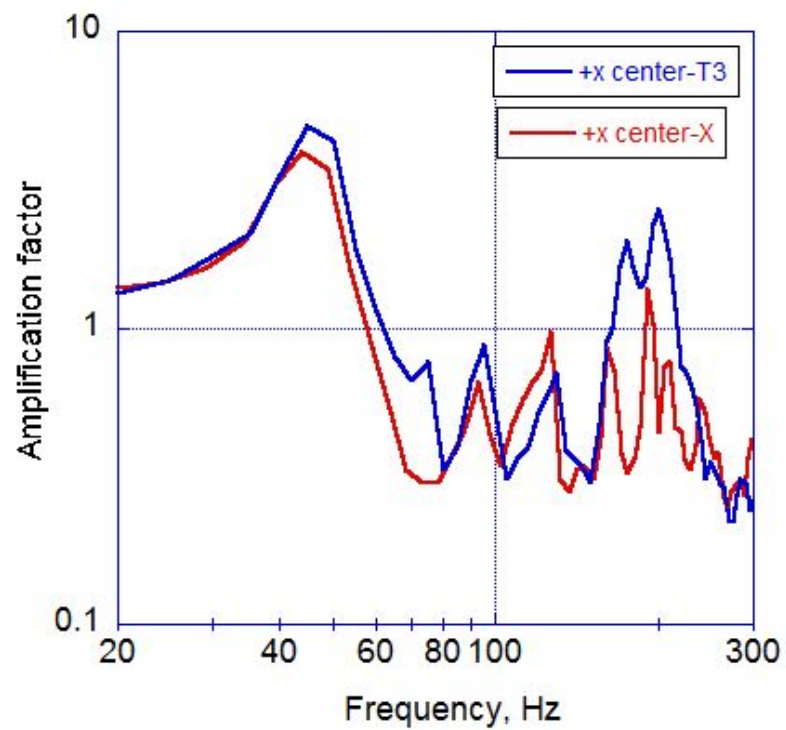


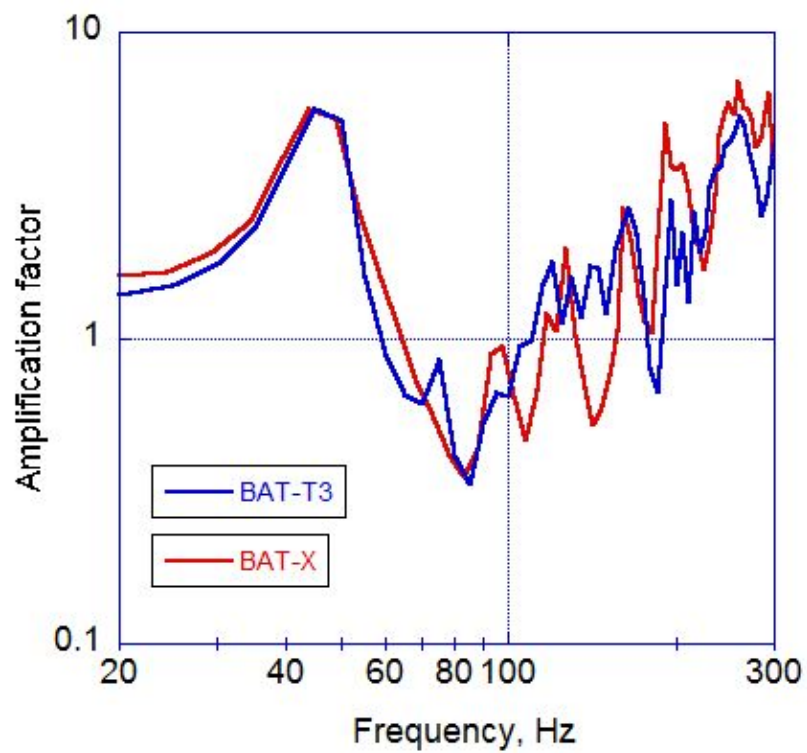
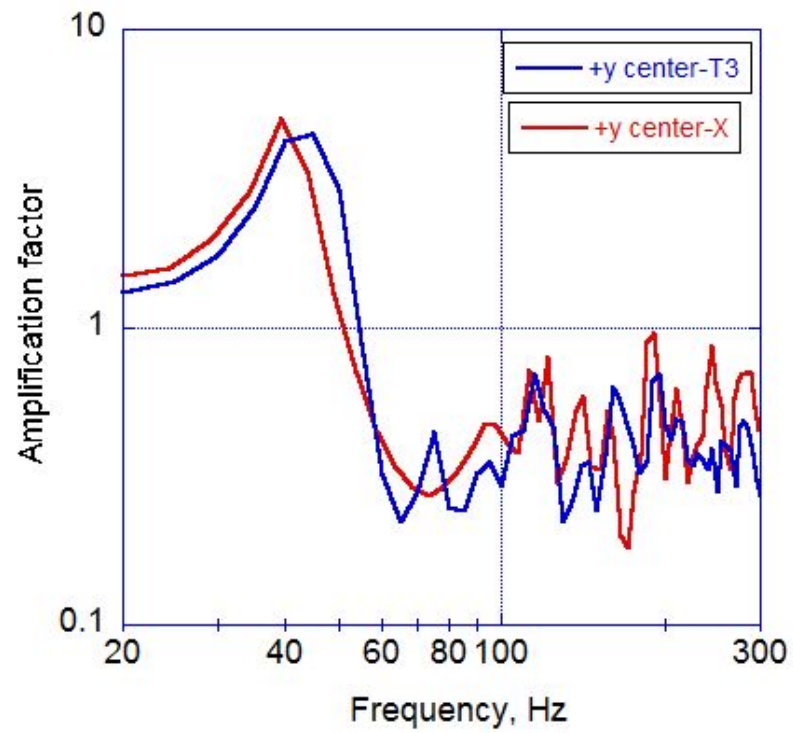


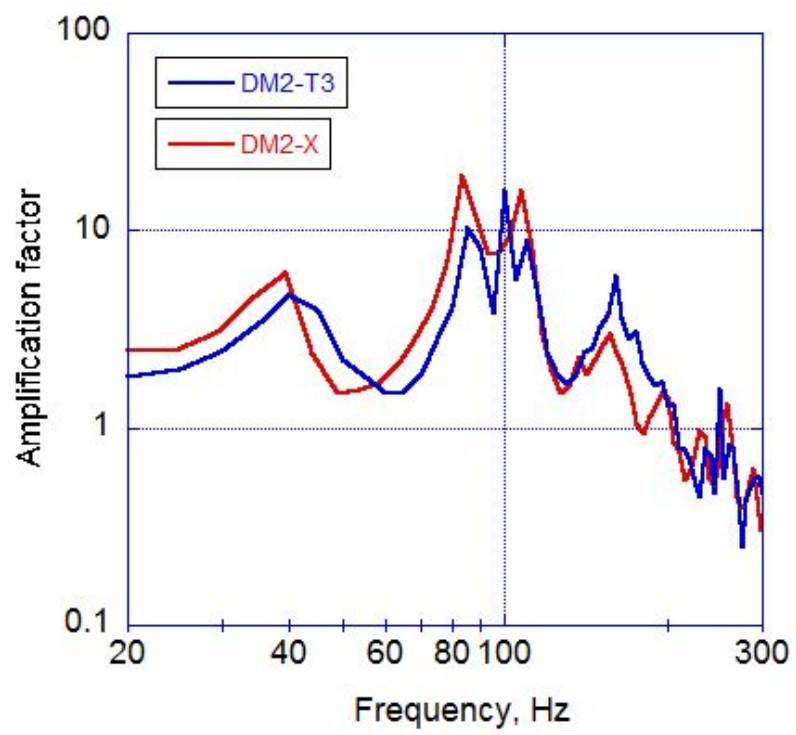
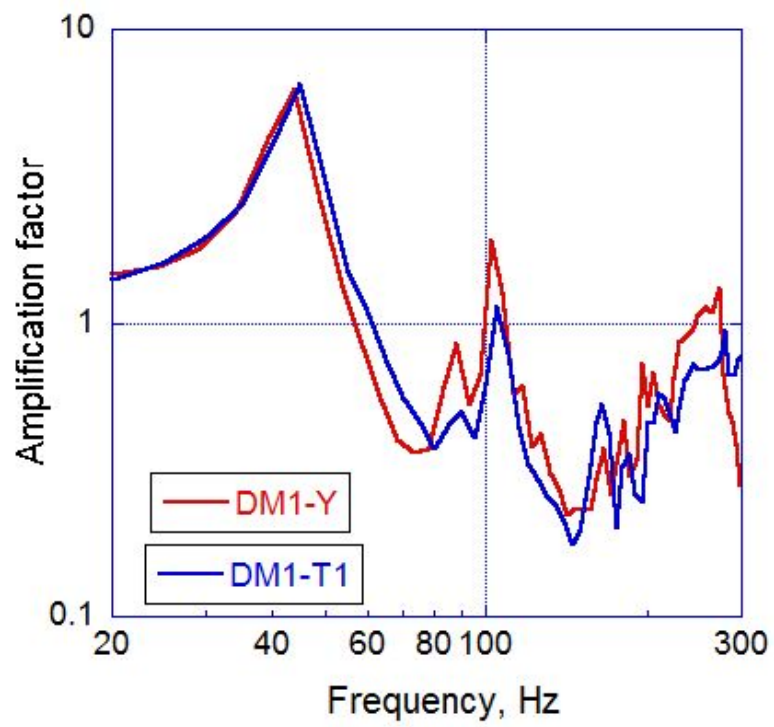


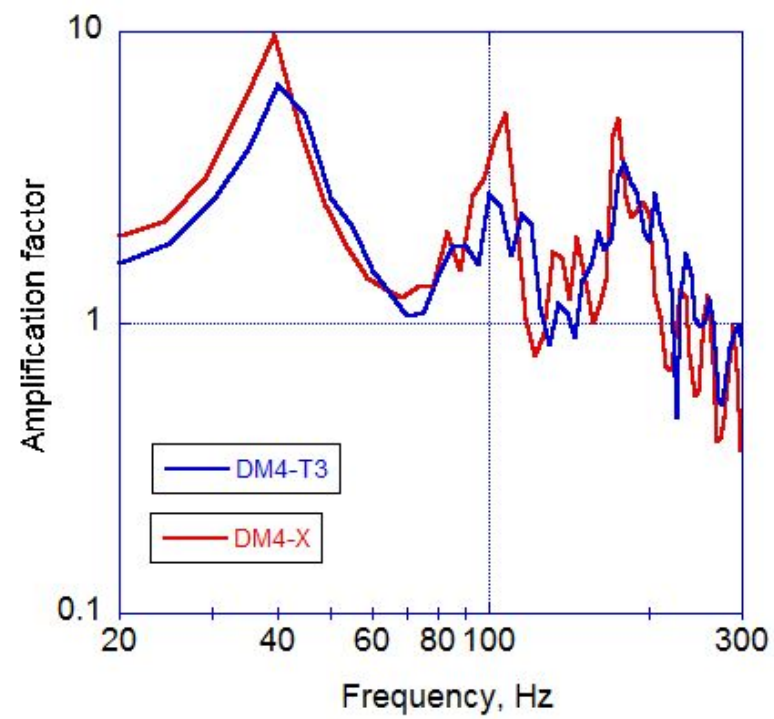
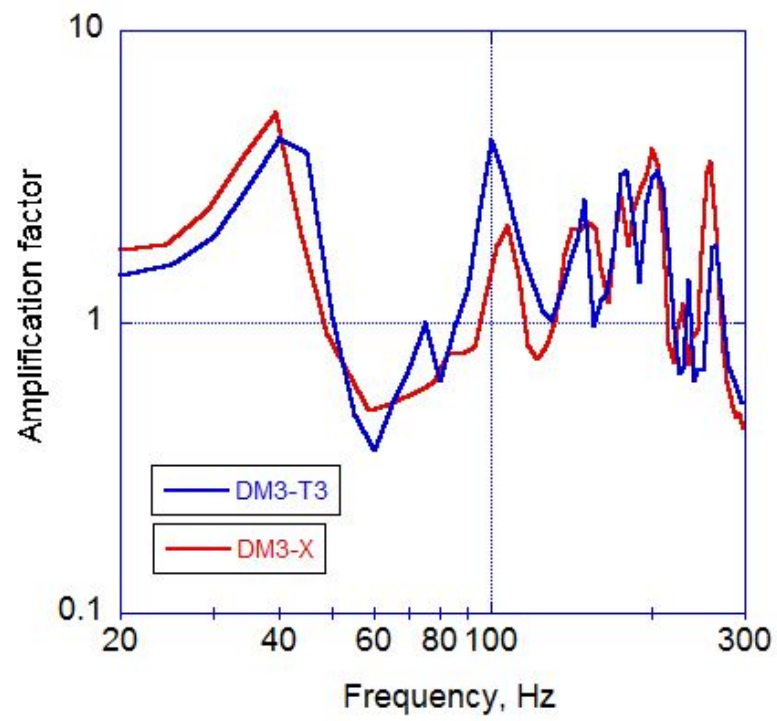


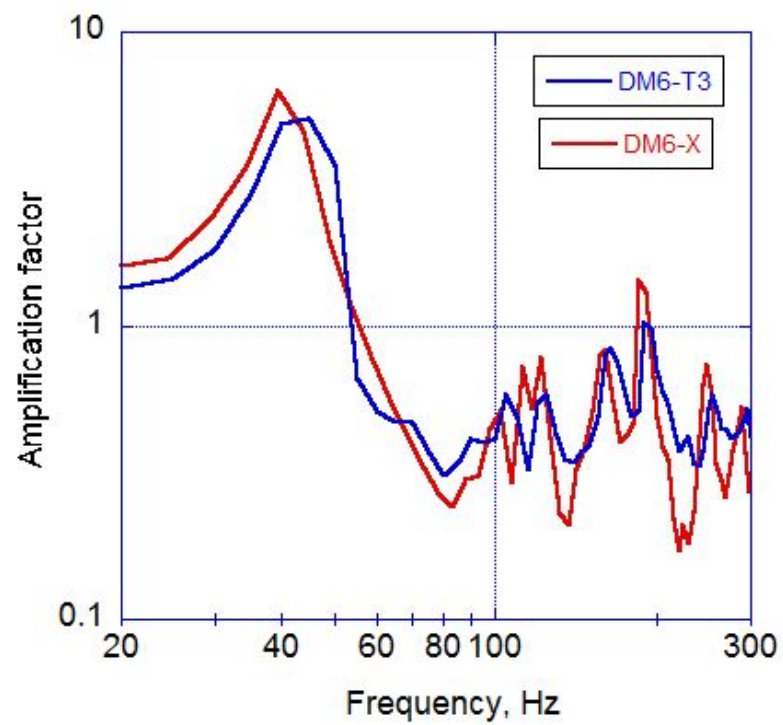
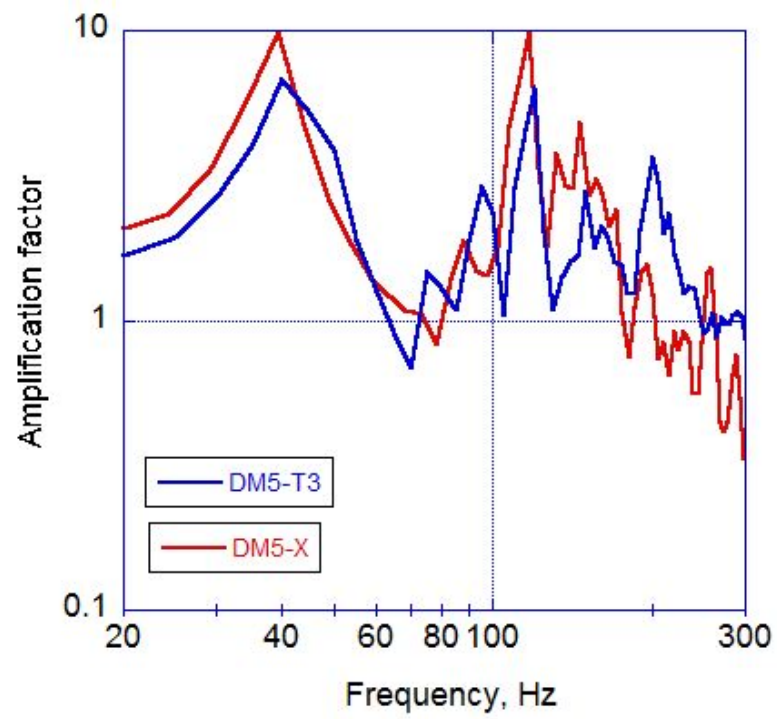
Test and analysis comparison (dummy, horizontal2)

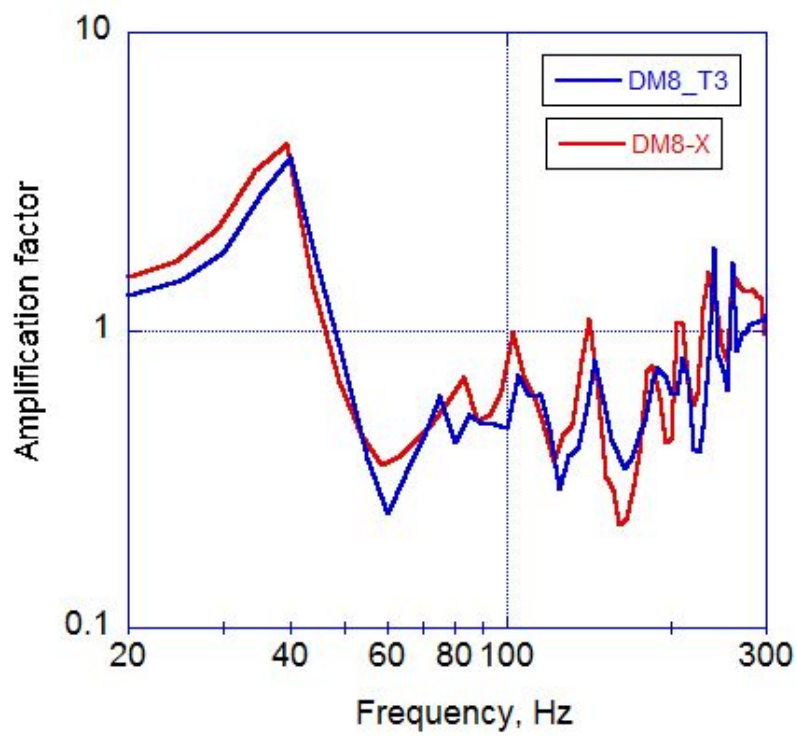
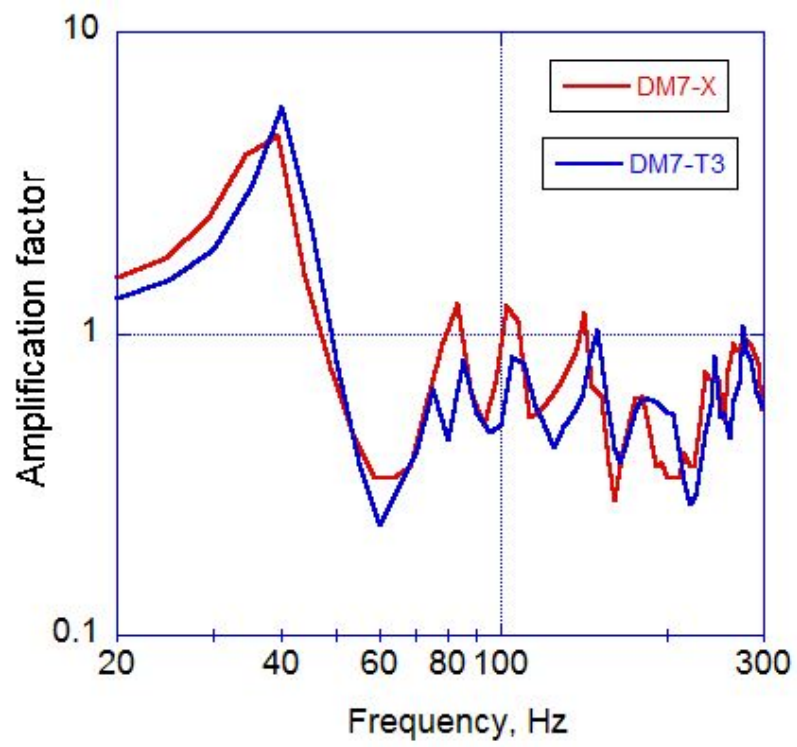


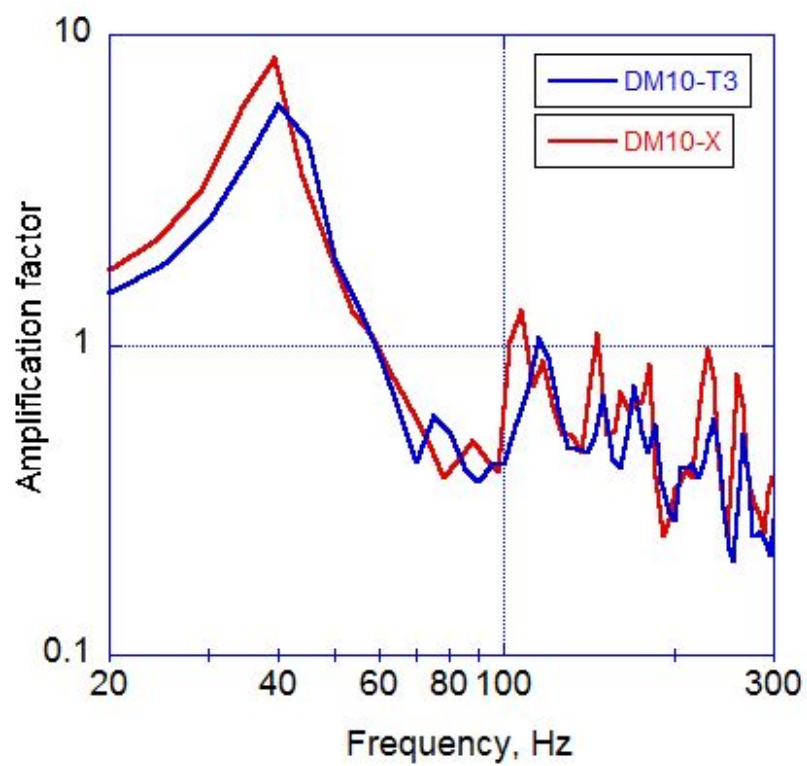
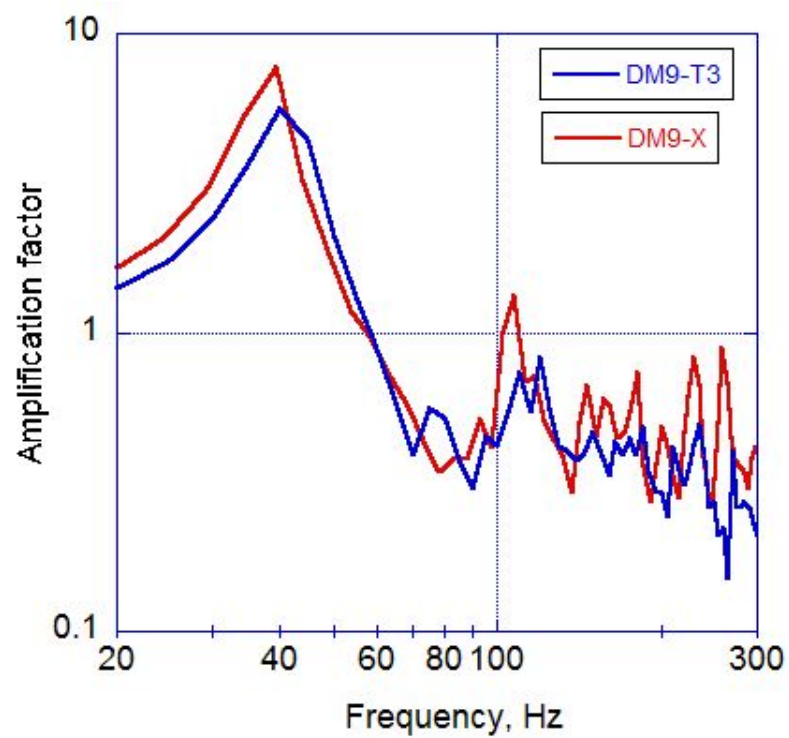


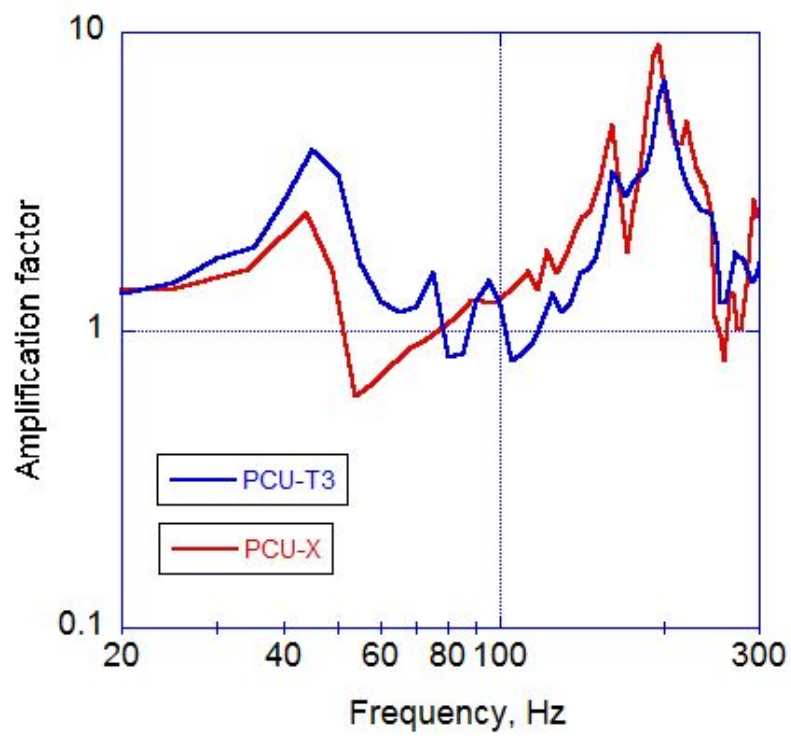
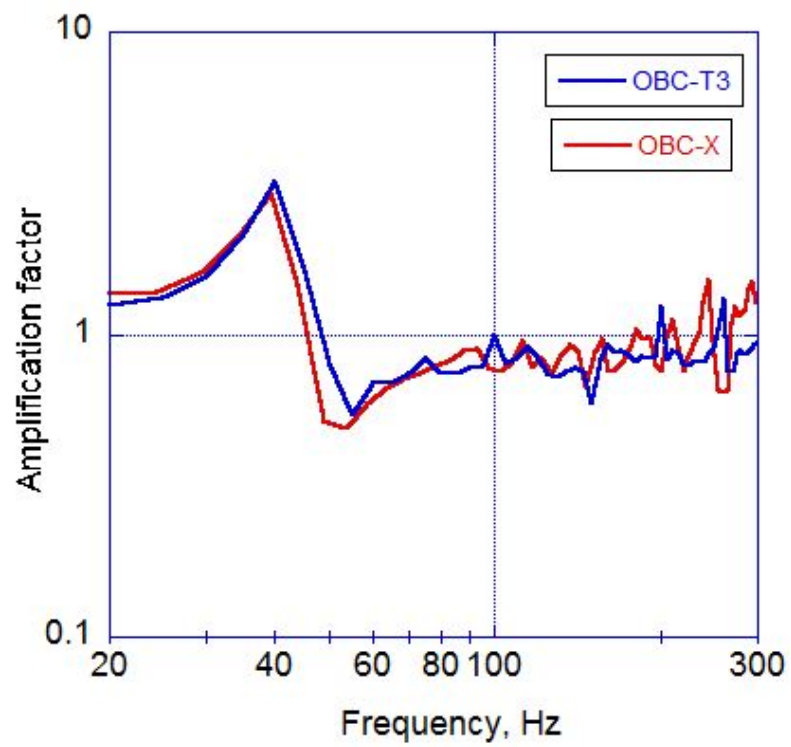


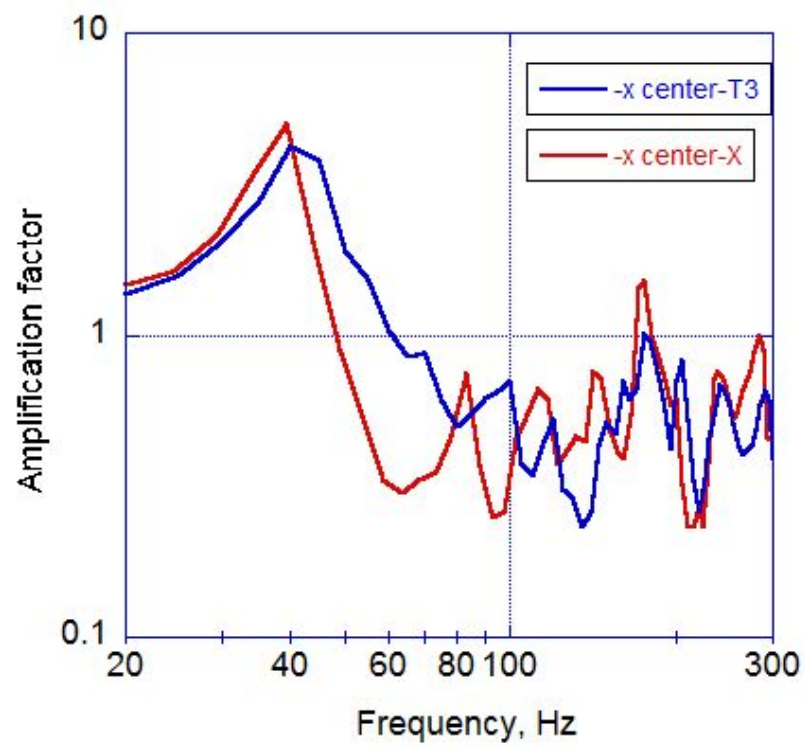
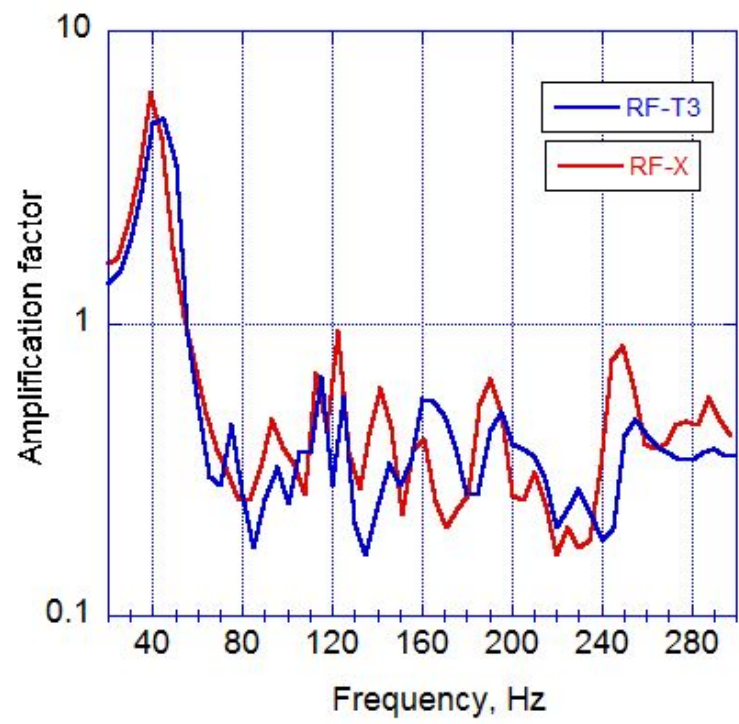


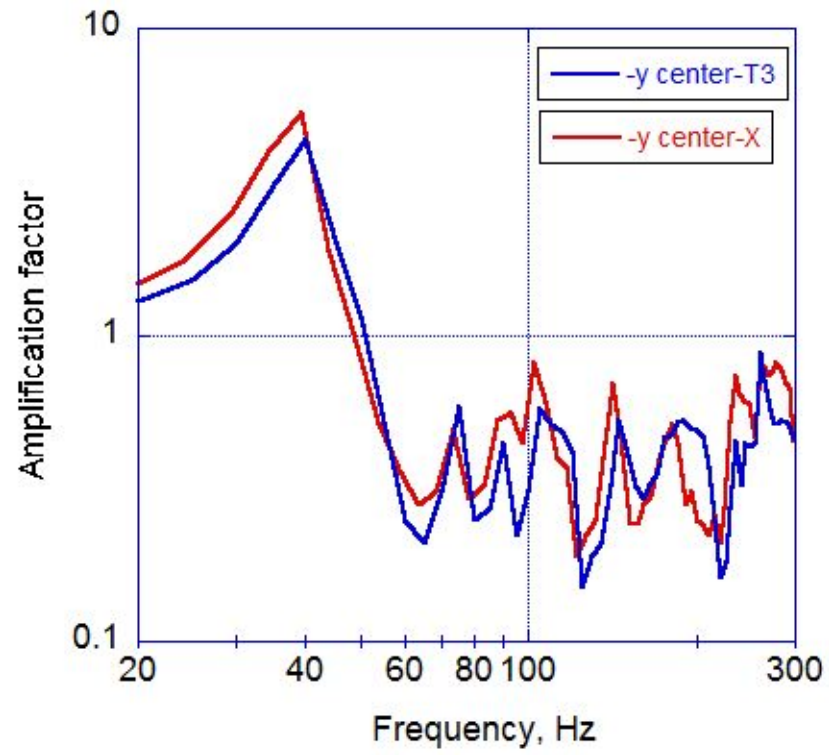












Test and analysis comparison (dummy, vertical)

